# The Role of Transmembrane Domain Helix-Helix Interactions in the Function of Pentameric Ligand-Gated Ion Channels

James Patrick Daniel Therien

A Thesis Submitted to the Faculty of Graduate and Postdoctoral Studies in partial fulfillment of the requirements for the M.Sc. degree in Biochemistry.

Department of Biochemistry, Microbiology, and Immunology

Faculty of Medicine

University of Ottawa

**Abstract**

The pentameric ligand gated ion channel super family plays a central role in fast synaptic communication between neurons and at the neuromuscular junction. Extensive studies on the prototypic pLGIC, the *Torpedo* nicotinic acetylcholine receptor (nAChR) have revealed an exquisite lipid sensitivity, with the nAChR adopting a novel uncoupled conformation in membranes lacking activating anionic and neutral lipids. The lipid-exposed transmembrane $\alpha$-helix, M4, in each homologous subunit likely acts as a lipid sensor. One model proposes that activating lipids promote M4 "binding" to the adjacent $\alpha$-helices, M1 and M3, to enhance interactions between the M4 C-terminus and the Cys-loop of the agonist-binding domain, with such interactions promoting coupling between the agonist site and channel gate. The first part of my thesis indirectly tests this hypothesis by exploring the effects of membrane hydrophobic thickness on nAChR function. Specifically, I tested the hypothesis that thicker membranes, which should promote alignment of M4 parallel to M1/M3 and thus helix-helix interactions, favor a coupled conformation. Although I found that the nAChR is uncoupled in all membranes tested, regardless of hydrophobic thickness, thicker membranes promote transitions from uncoupled to ultimately the desensitized state over the minutes to hours time frame. In contrast to anionic lipids, which influence function primarily via a conformational selection mechanism, membrane hydrophobic thickness influences function via a kinetic mechanism - thick membranes lower the activation energy between uncoupled and coupled conformations to promote conformational transitions. In the second part of my thesis, I used the two prokaryotic homologs, GLIC and ELIC, to explore how amino acid interactions at the interface between M4 and M1/M3 influence channel activity. Alanine scanning mutagenesis of this interface shows that disruption of almost any interaction in GLIC leads to a loss of folding and/or function, while

analogous mutations in ELIC typically lead to no change or produce gains in function. Sequence comparisons with other members of the pLGIC superfamily suggest that the transmembrane domains of GLIC and ELIC represent two distinct archetypes. Each archetype may strike a different balance between the need for strong M4 binding to M1/M3 to promote folding and pentamer assembly, and the need for weaker interactions that allow for greater conformational flexibility during function.

**Acknowledgments**

First and foremost, I wish to thank my supervisor Dr. John Baenziger. Your mentorship over the years has helped me develop both personally and professionally. You have provided me with some amazing opportunities. Thank you for everything.

I would also like to thank the members of my thesis advisory committee, Dr. Roberto Chica and Dr. Mary Hefford for their insightful comments.

To the members of the Baenziger lab over the years: Camille Hénault, Dr. Casey Carswell, Claire Edrington, Daniel Giguere, Jaimee Domville, Jiayin Sun, Jon Labriola, Dr. Julian Surujballi, Matthew Vincent, Nishaan Brar, and Dr. Peter Juranka. It has been an amazing opportunity to work alongside everyone over the years. All of our adventures and discussions have made my experiences here unforgettable.

To all the graduate students that I have had the pleasure of meeting during my studies, I wish you all the best in your future studies.

And lastly to all my friends and family, thank you for your encouragement and support.

**Table of Contents**

## List of Abbreviations

| | |
|---|---|
| $^{1}H$ | Hydrogen |
| $^{2}H$ | Deuterium |
| $^{2}H_2O$ | Deuterium Oxide |
| $\alpha$-BTX | $\alpha$-Bungarotoxin |
| Å | Angstrom |
| ABD | Agonist Binding Domain |
| ACh | Acetylcholine |
| AChBP | Acetylcholine Binding Protein |
| Aso | Asolectin |
| ATP | Adenosine Triphosphate |
| au | Arbitrary Units |
| C-terminal M4 | C-Terminus of the nAChR Transmembrane $\alpha$-helix 4 |
| $Ca^{2+}$ | Calcium Ion |
| Carb | Carbamylcholine Chloride |
| CD | Cytoplasmic Domain |
| Chol | Cholesterol |
| CMS | Congenital Myasthenic Syndrome |
| CNS | Central Nervous System |
| cRNA | Clonal Ribonucleic Acid |
| cryo-EM | Cryo-Electron Microscopy |
| Da | Dalton |
| DAG | Diacylglycerol |
| Dib | Dibucaine |
| EthBr | Ethidium Bromide |
| $GABA_A$ | $\gamma$-Aminobutyric Acid Receptor |
| GLIC | *Gloeobacter* Ligand-Gated Ion Channel |
| GlyR | Glycine Receptor |
| $EC_{50}$ | Concentration at Half Maximal Activity |
| ELIC | *Erwinia* Ligand-Gated Ion Channel |
| FTIR | Fourier Transform Infrared Spectroscopy |
| GluCl | Glutamate-Gated Chloride Channel |
| $K^+$ | Potassium Ion |
| $K_d$ | Dissociation Constant |
| kDa | KiloDalton |

| | |
|---|---|
| M1 | nAChR Transmembrane $\alpha$-helix 1 |
| M2 | nAChR Transmembrane $\alpha$-helix 2 |
| M3 | nAChR Transmembrane $\alpha$-helix 3 |
| M4 | nAChR Transmembrane $\alpha$-helix 4 |
| mRNA | Messenger Ribonucleic Acid |
| N-$^{1}$H | Peptide Hydrogen |
| N-$^{2}$H | Peptide Deuterium |
| $Na^{+}$ | Sodium Ion |
| nAChR | Nicotinic Acetylcholine Receptor |
| PA | Phosphatidic Acid |
| PC | Phosphatidylcholine |
| PE | Phosphatidylethanolamine |
| PDB | Protein Data Bank |
| PI | Phosphatidylinositol |
| PNS | Peripheral Nervous System |
| PS | Phosphatidylserine |
| pLGIC | Pentameric Ligand Gated Ion Channel |
| rapsyn | Receptor-Associated Protein of the Synapse |
| SDS-PAGE | Sodium Dodecyl Sulfate Polyacrylamide Gel Electrophoresis |
| TEVC | Two-Electrode Voltage Clamp |
| TLC | Thin Layer Chromatography |
| TMD | Transmembrane Domain |

## List of Figures

## List of Tables

# Chapter 1

## Introduction

## 1.1 The Nervous System

The nervous system plays a fundamental role in life and is responsible for many higher cognitive functions, such as reading, writing, and learning. On a molecular level, cell-to-cell communication allows us to complete a variety of tasks, such as making complex decisions, learning, adapting, and ultimately surviving. Specialized cells within the nervous system form a highly complex network that have the capacity to integrate large volumes of information and execute a variety of functions. The complexity of the nervous system makes it of particular interest to study and understand how communication between cells may lead to both our consciousness and disease.

The nervous system is divided into two categories, the central nervous system (CNS) and the peripheral nervous system (PNS). The CNS is confined to the head and spinal cord of the body and is responsible for receiving and integrating signals received from the body, while also conveying both information and commands to targeted locations within the body. The PNS simply acts as an extension of the CNS innervating most of the body relaying signals to and from the CNS.

A number of different cell types exist within the nervous system, each with their own specialized function. The two main types of cells are neurons and glial cells. In the human body, it is estimated that there are over 100 billion neurons, each with the capacity to form thousands of connections to other nerve cells. Neurons have two main mechanisms for communication; they use electrical signals to carry a message along the cell, while a chemical signal is typically used to communicate between adjacent cells. Glial cells, which are also found within the nervous system, serve to support the neurons.

The anatomy of the neuron can be divided into four segments (Figure 1.1). The

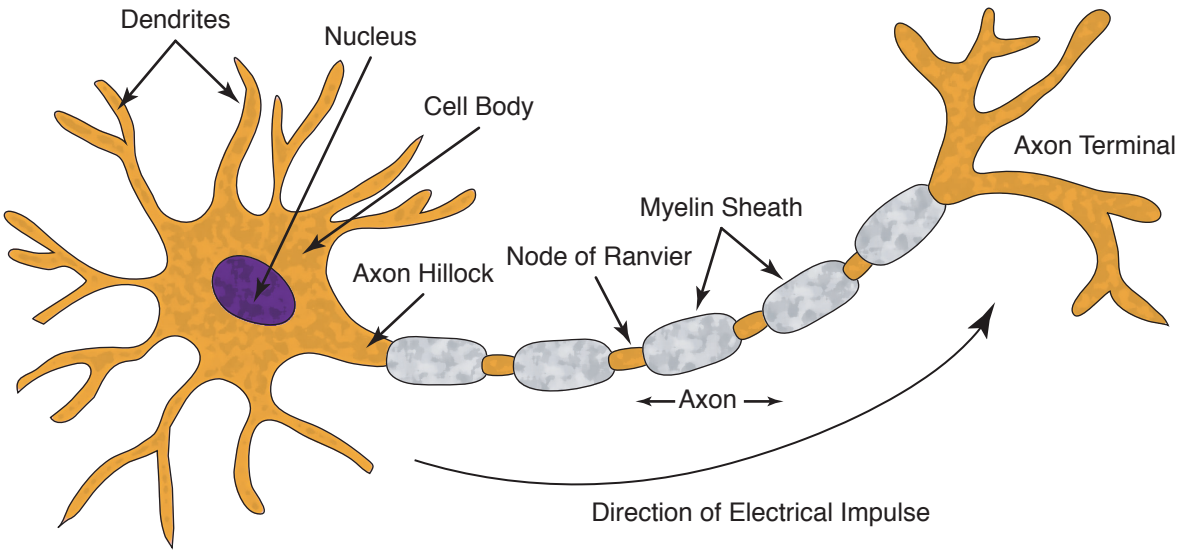


**Figure 1.1: Schematic Diagram of a Neuron's Anatomy.** A representative figure showing a multipolar neuron identifying different structural features: dendrites, nucleus, cell body, axon hillock, axon, myelin sheath, and axon terminal. The direction of electrical signal represents the traveling direction of an action potential traveling through the axon.

dendrites of the neuron serve as branched projections that receive inhibitory or excitatory stimuli from other neurons. The soma (cell body) acts as the core of the cell, containing the nucleus and most of the cellular organelle. The axon is a long projection of the neuron that conducts electrical impulses away from the cell body. The axon terminal allows the neuron to make connections to other neurons (or muscle fibers), and thus propagate the neuronal signal.

## 1.2 Neuronal Communication

### 1.2.1 The Neuronal Plasma Membrane

The plasma membrane of a cell serves as a barrier between the internal and external cellular environment; it is composed of both lipid and protein. Phospholipids are the major lipids found in the plasma membrane and they are typically made up of two hydrocarbon chains and a phosphate head group. In aqueous solution, these lipids spontaneously form two leaflets of laterally arranged phospholipids; the hydrophobic hydrocarbon chains forming the core, and the polar phosphate head groups facing the solvent on either side. The rapid movement of small ions across a lipid bilayer is restricted as the bilayer is essentially impermeable to these ions.

### 1.2.2 The Resting Membrane Potential

Cells are capable of producing an electric potential across their cellular membrane due to an imbalance of ion concentrations in the internal and external cellular environments. These ion gradients are generated primarily by the sodium-potassium ATPase, which is a pump that catalyzes the movement of ions against their electrochemical gradients using energy in the form of ATP hydrolysis. Cells expend a large amount of energy pumping sodium ions out and potassium ions

into the cell through the pump, which as a result produces a greater potassium concentration in the intracellular environment and a greater sodium concentration in the extracellular environment. However, due to a high number of potassium leak channels in the lipid membrane, potassium ions diffuse out of the cell down their concentration gradient leaving unpaired negative charges in the intracellular environment. The growing intracellular negative charge will counteract the driving force of the potassium concentration gradient, thus creating an equal flow of potassium ions in both directions across the membrane. Thus, at steady state conditions the resting membrane potential is almost equal to the potassium equilibrium potential (the membrane potential at which the net flow of potassium ions across the membrane is 0) between -70 mV and -100 mV.

### 1.2.3 The Action Potential

Neurons conduct electrical impulses along the axon, called action potentials, to transmit signals (Figure 1.2). Action potentials are all or nothing events initiated at the axon hillock when depolarization of the membrane potential from stimuli reaches roughly -55 mV. Once the threshold is attained, voltage sensitive sodium channels activate by opening a channel pore allowing the flow of sodium ions into the cell down their electrochemical gradient leading to a membrane depolarization to between +50 mV and +100 mV. Sodium ions rapidly diffuse along the axon down their concentration gradient. This leads to the depolarization of sites that are distal to the axon hillock, causing the activation of neighboring voltage-gated sodium channels within the uninsulated nodes found between myelin sheaths. This process occurs repetitively allowing action potentials to propagate along the entire length of the axon until it reaches the axon terminus.

Note that the rapid depolarization of the axonal membrane eventually leads to

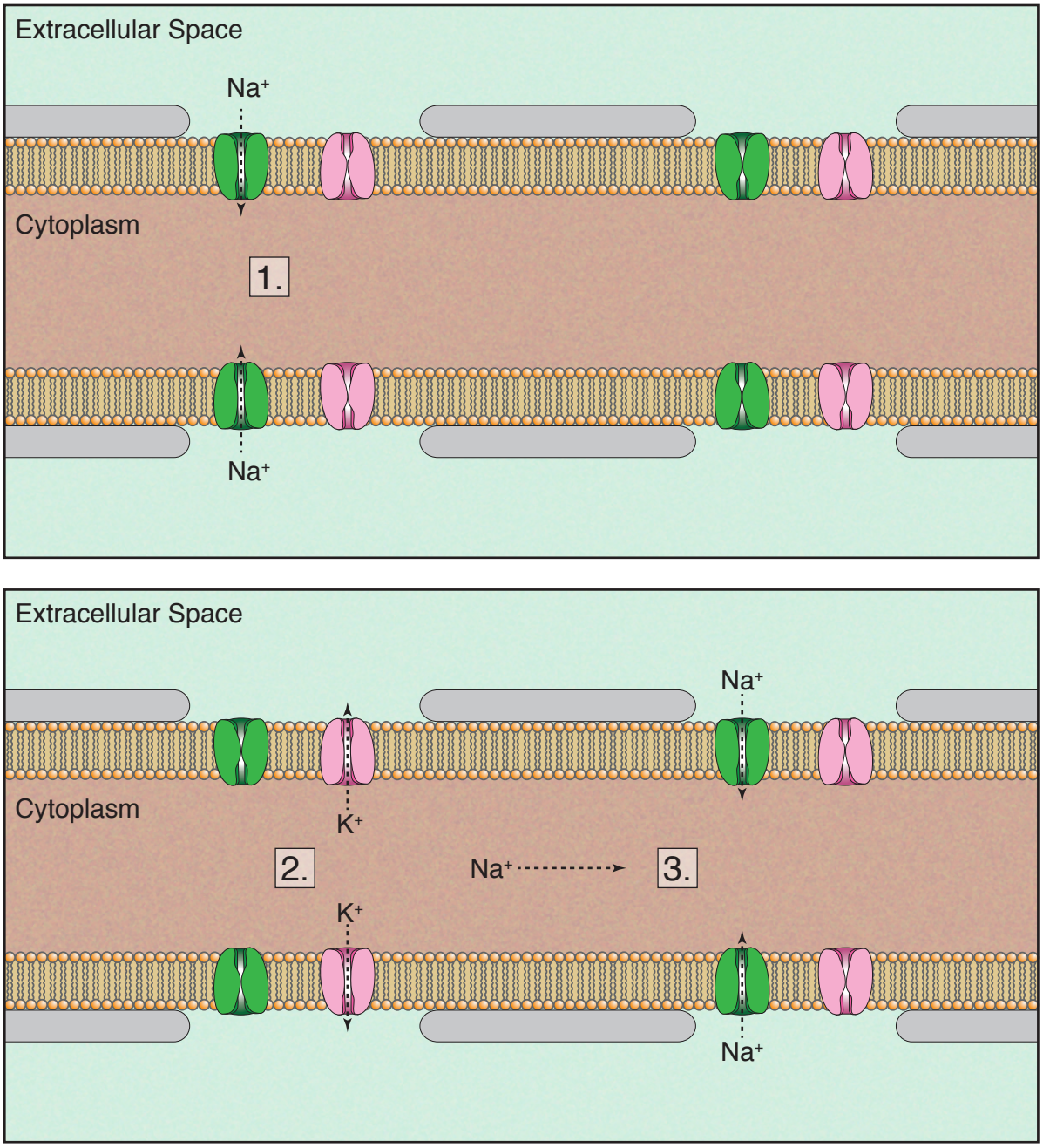


**Figure 1.2: The Action Potential.** A schematic diagram illustrates the propagation of an action potential. The simplified events of an action potential begin once the membrane is sufficiently depolarized causing (1.) the opening of voltage-sensitive sodium channels. The sudden influx of sodium into the axon causes a large membrane depolarization, which then leads to (2.) the closure of the sodium channels and triggers the activation of the voltage sensitive potassium channel causing the efflux of potassium to drive the membrane potential back towards the resting membrane potential. (3.) Sodium travels down its concentration gradient resulting in the activation of neighboring voltage-gated sodium channels.

the closure of the voltage sensitive sodium channels and triggers the activation of voltage sensitive potassium channels. Effectively, the efflux of potassium drives the membrane potential back towards the resting membrane potential.

### 1.2.4 The Synapse

The chemical synapse allows for the communication between neurons or at the neuromuscular junction (Figure 1.3). Once an action potential reaches the axon terminal, voltage sensitive calcium channels open resulting in the influx of calcium ions into the cell. The sudden influx of calcium ions into the cell causes vesicles to fuse with the cellular membrane, releasing their contents into the synaptic cleft. Contained within the vesicles are small molecules called neurotransmitters; these neurotransmitters diffuse across the synaptic cleft to bind to specific receptors on the post-synaptic cell. The binding of a neurotransmitter to a receptor often results in the opening of an ion channel allowing for the influx of cations or anions (depending on receptor type) into the post-synaptic cell, which can either depolarize or hyperpolarize the membrane potential, respectively.

There exist different types of receptors that bind neurotransmitters, all of which are transmembrane proteins. Upon the binding of neurotransmitter, ligand activated ion channels open a pore, as described above, across the cellular membrane, which allows for the flux of cations or anions across the membrane. This thesis focuses primarily on a single excitatory ligand-gated ion channel, called the nicotinic acetylcholine receptor (nAChR). There also exist G-protein coupled receptors that activate G proteins upon neurotransmitter binding.

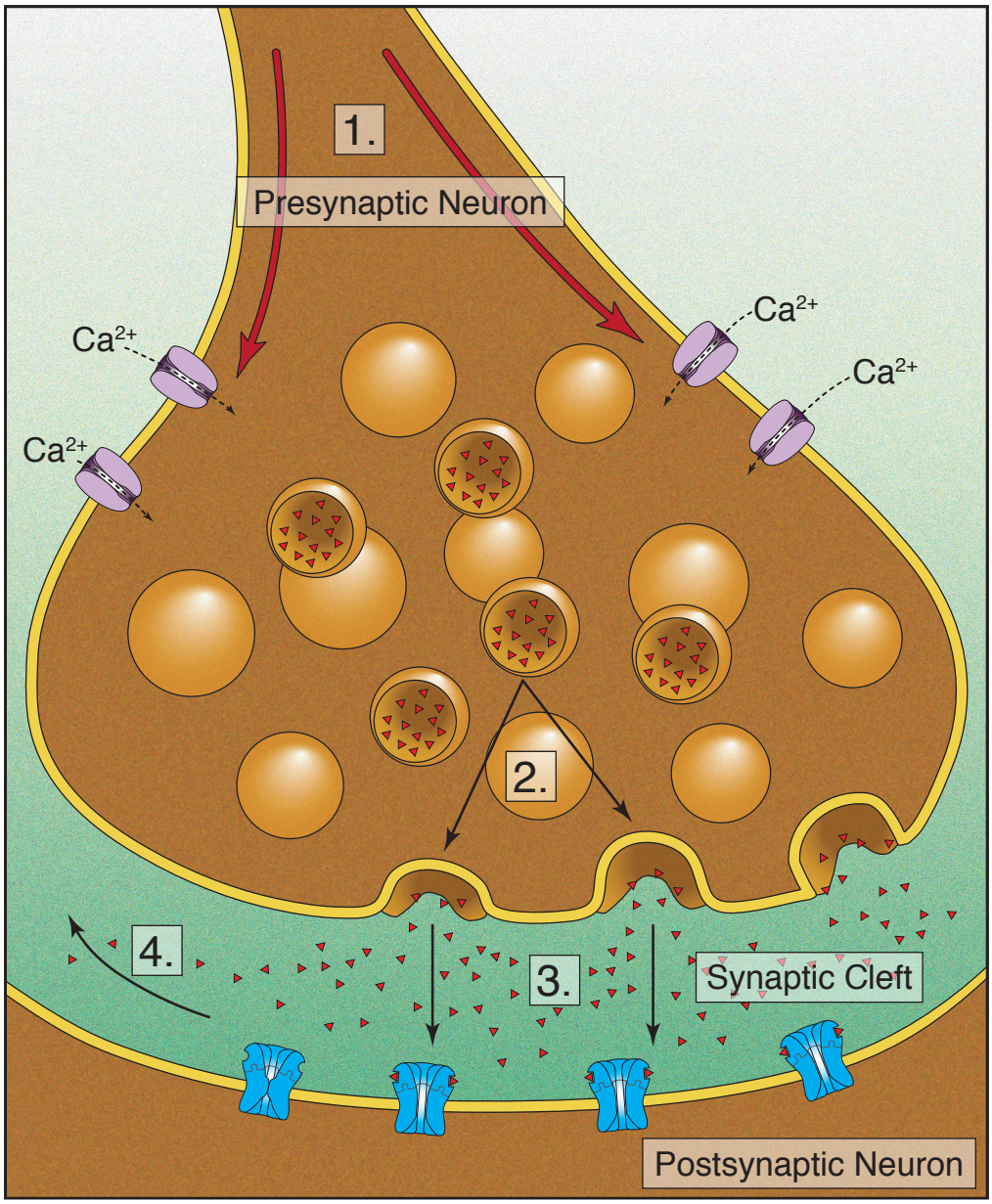


**Figure 1.3: Schematic Diagram of a Chemical Synapse.** The action within the synapse can be simplified into 4 events: (1.) upon receiving an action potential at the axon terminal of the pre-synaptic neuron, voltage sensitive calcium channels open allowing the influx of calcium into the cell. (2.) The sudden influx of calcium causes the release of neurotransmitter containing vesicles into the synaptic cleft. (3.) The neurotransmitters diffuse across the synaptic cleft to bind to specific receptors on the post-synaptic cell. (4.) The neurotransmitter will eventually diffuse out of out of synaptic cleft, be degraded by enzymes, or be reabsorbed into the pre-synaptic cell to be recycled.

## 1.3 Pentameric Ligand-Gated Ion Channel Superfamily

The nAChR is a member of a superfamily of proteins called the pentameric ligand-gated ion channels (pLGICs). Channels in this family fall into two different functional categories based on ion selectivity (Sine and Engel, 2006). In mammals, cation selective excitatory channels depolarize the membrane potential sometimes generating an action potential. The excitatory channels include the nicotinic acetylcholine (nAChR), serotonin ($5HT_3R$), and the zinc-activated (ZAC) receptors. In mammals, anion selective inhibitory channels hyperpolarize the membrane potential making it more difficult to generate an action potential. The inhibitory channels include the γ-aminobutyric acid ($GABA_A$) and glycine (GlyR) receptors. Interestingly, sequence analysis of all of the eukaryotic pLGIC show a pair of conserved cysteine residues separated by thirteen amino acids forming a loop that plays a crucial role in channel activation, which led to the alternate title of "Cys-loop receptors" (Lester et al., 2004). In recent years, prokaryote homologues to the eukaryotic pLGIC super family have been discovered that lack both the Cys-loop and the cytoplasmic domain (CD) (Tasneem et al., 2005).

## 1.4 The Nicotinic Acetylcholine Receptor

### 1.4.1 Overview

The nAChR is the most extensively studied members of the pLGIC family. Much of the success came from our ability to isolate the nAChR from a natural source, the electric ray, *Torpedo* (Changeux et al., 1970). Additionally, the *Torpedo* nAChR shares a high sequence homology to the human nAChRs found within the neuromuscular junction (Hille, 2001). In the wild, the electric rays rely on their electroplaque organ

to generate an electrical current as a means to kill and/or stun their prey. This organ is composed of specialized electrocyte cells, which express the nAChR (Hille, 2001). The nAChR isolated from the electroplaque organ can yield 100-fold greater protein yield in comparison to other natural sources (O'Brien et al., 1972). Isolated *Torpedo* nAChR is composed of 4 non-identical subunits with sizes ranging from 40 kDa to 64 kDa (Weill et al., 1974). Due to their SDS-PAGE migration patterns, subunits were named $\alpha$, $\beta$, $\delta$, and $\gamma$ (smallest to largest) (Weill et al., 1974).

Functional studies of the nAChR show that the receptor can adopt several states (Figure 1.4). The binding of an agonist to the resting state results in a conformational change to the open state, allowing the flow of cations across the cellular membrane. The prolonged exposure to agonist induces a conformational change to the desensitized state, which results in the closure of the pore preventing the flow of cations. While the desensitized and resting states are both closed, there is a marked difference in their affinity for ligand; the nAChR has roughly a 200-fold higher affinity for ligand in the desensitized conformation ($K_d$ = 3-5 nM) as opposed to the resting state ($K_d$ = 800 nM) (Boyd and Cohen, 1980). An uncoupled state has been discovered in recent years. The uncoupled nAChR bind agonist with resting state-like affinity, but does not undergo conformational transitions to the open or desensitized states (see below) (daCosta and Baenziger, 2009).

The current structural model of the nAChR was solved using cryo-electron microscopy (cryo-EM) refined to a resolution of 4 Å taking into account the extensive biochemical data that had been obtained up to this point (Figure 1.5) (Unwin, 2005). The structure shows 5 *Torpedo* subunits (molar ratio of 2:1:1:1, $\alpha$:$\beta$:$\gamma$:$\delta$) arranged pseudo-symmetrically around a central pore. The nAChR is divided into three functional domains: The agonist-binding domain (ABD), the trans-membrane domain (TMD), and the cytoplasmic domain (CD). The ABD serves as the attachment point

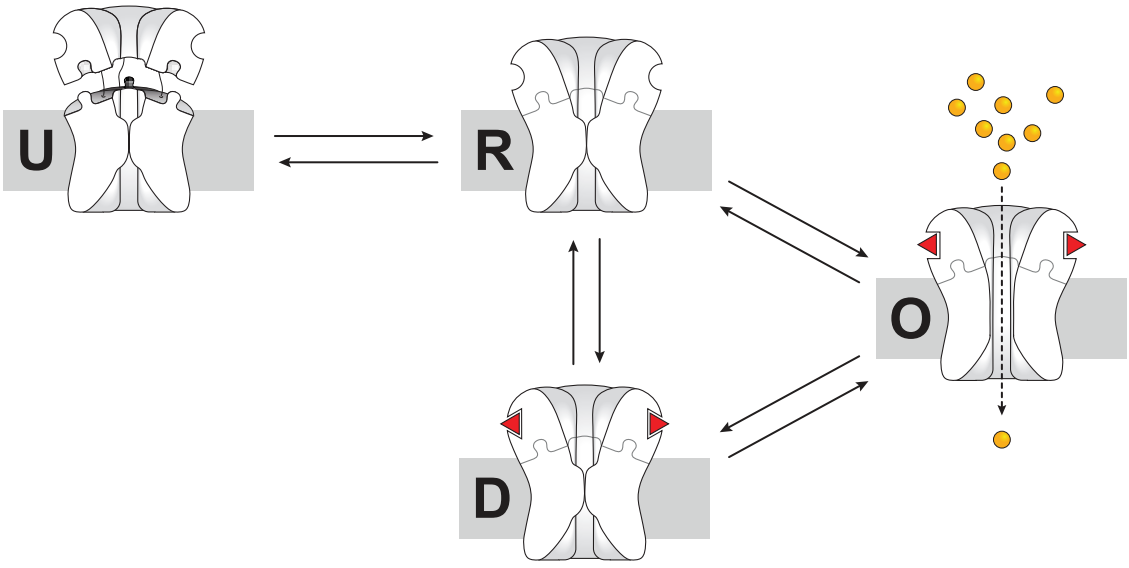


**Figure 1.4: Transition States of the nAChR.** In an agonist-unbound state, the receptor is primarily in the resting state (R). The binding of agonist induces a conformations transition to the open state (O). Prolonged exposed to agonist causes a second conformational change to the desensitized state (D) where agonist remains bound; however the channel gate is closed. The uncoupled (U) conformation is a lipid-dependent conformation that has recently been identified, where agonist binding does not lead to channel gating. Figure adapted from daCosta and Baenziger, 2009.

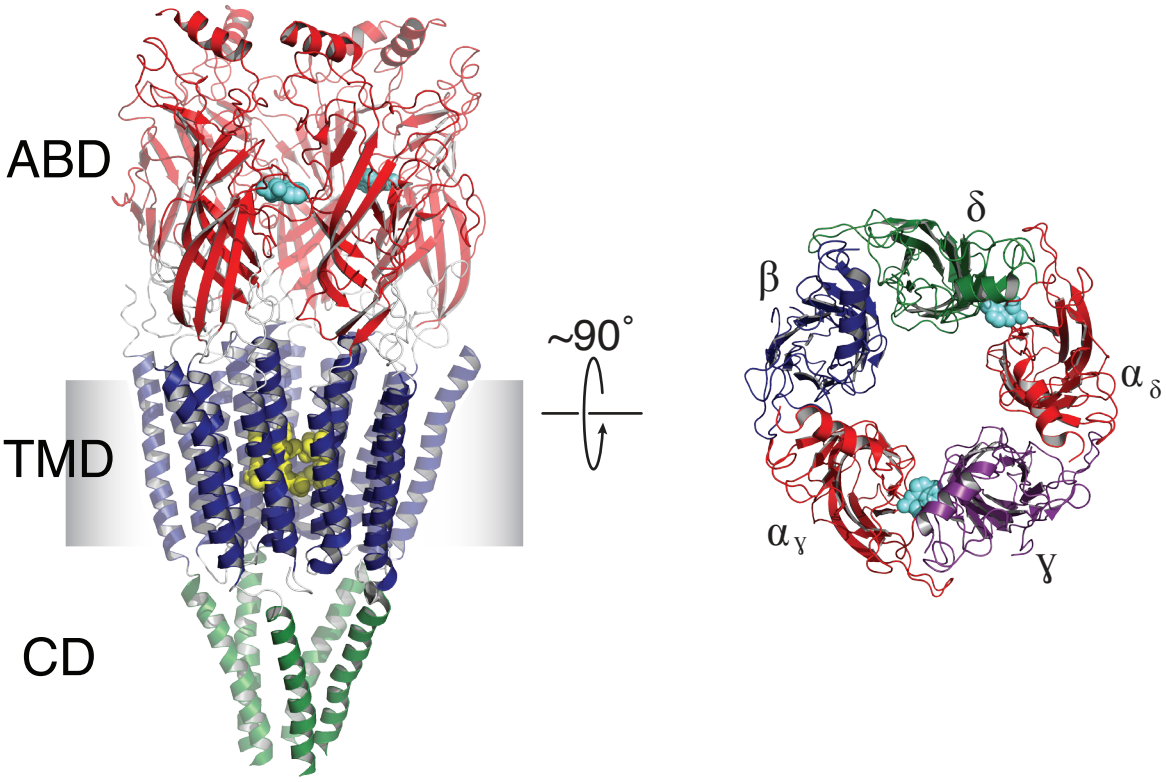


**Figure 1.5: The nAChR Structure.** The 4 Å cryo-EM structure of the *Torpedo* nAChR (PDB ID: 2BG9). The side view of the nAChR (left) shows the 3 domains, the agonist-binding domain (ABD, red), the transmembrane domain (TMD, blue), and the cytoplasmic domain (CD, green). Side chains forming part of the agonist-binding site (αW149) and channel gate (αL251 and αV255, including analogous residues on the other subunits) are shown as cyan and yellow spheres, respectively. Top down views show the ABD with colour coding differentiates the different subunits (α, red; β, blue; γ, purple; δ, green).

in the extracellular space for free agonist. The binding of an agonist causes a conformational change in the ABD that is translated to the TMD, which responds by opening a pore through the membrane allowing the passage of ions. The role of the CD is still under debate, however it is known to interact with the receptor-associated protein of the synapse (rapsyn), which functions as an anchoring protein (Froehner, 1993).

Advances in molecular biology have identified a number of homologous nAChR subunits across a variety of species. Human muscle type nAChRs are made up from 5 types of subunits, which include the $\alpha 1$, $\beta 1$, $\gamma$, $\delta$, and $\varepsilon$ subunits. The human muscle type nAChR has two possible heteropentameric subunit combinations, either the fetal ($(\alpha 1)_2\beta 1\delta\gamma$) or adult ($(\alpha 1)_2\beta 1\delta\varepsilon$) combination. The change from the $\gamma$-subunit in fetal tissue to $\varepsilon$-subunit in adult tissue occurs during synaptic maturation; favoring the adult form once the synapse is formed (Mishina et al., 1986; Sakmann and Brenner, 1978). There also exist neuronal type nAChRs, which are composed of $\alpha$ and $\beta$ subunits. In humans, these include the $\alpha 1$-$\alpha 7$, $\alpha 9$-$\alpha 10$, and $\beta 2$-$\beta 4$ subunits. Neuronal nAChRs are either homopentameric or heteropentameric. Heteropentameric receptors have the capacity to have a number of stoichiometric combinations containing between 2 and 3 $\alpha$-subunits. This large diversity in the nAChR family allow for receptors with unique functional and pharmacological profiles.

### 1.4.2 The Agonist-Binding Domain

There remains the need for high-resolution structural models of the nAChR in order to understand detailed mechanisms of channel function. The discovery and crystallization of a nAChR ABD homologue, the acetylcholine binding protein (AChBP), has given an insight into some of the molecular mechanisms of ligand binding. The AChBP is a soluble protein found in snails that is secreted into the

synapse, which can modulate the transmission of neuronal signals by binding free acetylcholine (ACh), effectively reducing the ACh-response evoked on the post-synaptic neuron (Smit et al., 2001; Smit et al., 2003). Like the nAChR, the AChBP is capable of binding to known agonists, which include acetylcholine (ACh), nicotine, and epibatidine. In addition, the AChBP can bind antagonists, such as the snake venom α-bungarotoxin (α-Btx) (Smit et al., 2001; Smit et al., 2003). The AChBP is a homopentamer composed of 5 subunits that most-closely resembles the α7-subunit of the nAChR. Each subunit is made up from a short N-terminal α-helix followed by a β-sandwich composed of 10 β-strands (β1-β10) (Figure 1.6) (Smit et al., 2001).

Crystal structures of the AChBP in complex with and without ligand have revealed a structural basis for ACh binding. The ACh binding sites are formed by a series of 6 loops (loops A-F) between two subunits, designated as the principal or complementary subunits. The principal subunit (+) contributes residues that make up loops A, B, and C, while the complementary subunit (-) contributes loops D, E, and F. Given the positively charged ammonium group of ACh, the binding pocket has a number of aromatic residues (Hansen et al., 2005). Thus interactions between ACh and the AChBP are coordinated through cation-π interactions. In an unbound state, loop C extends away from the protein, allowing ACh to enter the binding pocket. Binding of ACh triggers the movement of Loop C towards the protein, essentially capturing the ligand in the bound state (Celie et al., 2004; Hansen et al., 2005).

### 1.4.3 The Transmembrane Domain

The structure of the *Torpedo* nAChR shows that the TMD of the nAChR is made up of 4 α-helices per subunit (labeled M1 to M4), which results in a total of 20 membrane-spanning helices (Figure 1.7) (Unwin, 2005). The α-helices are organized

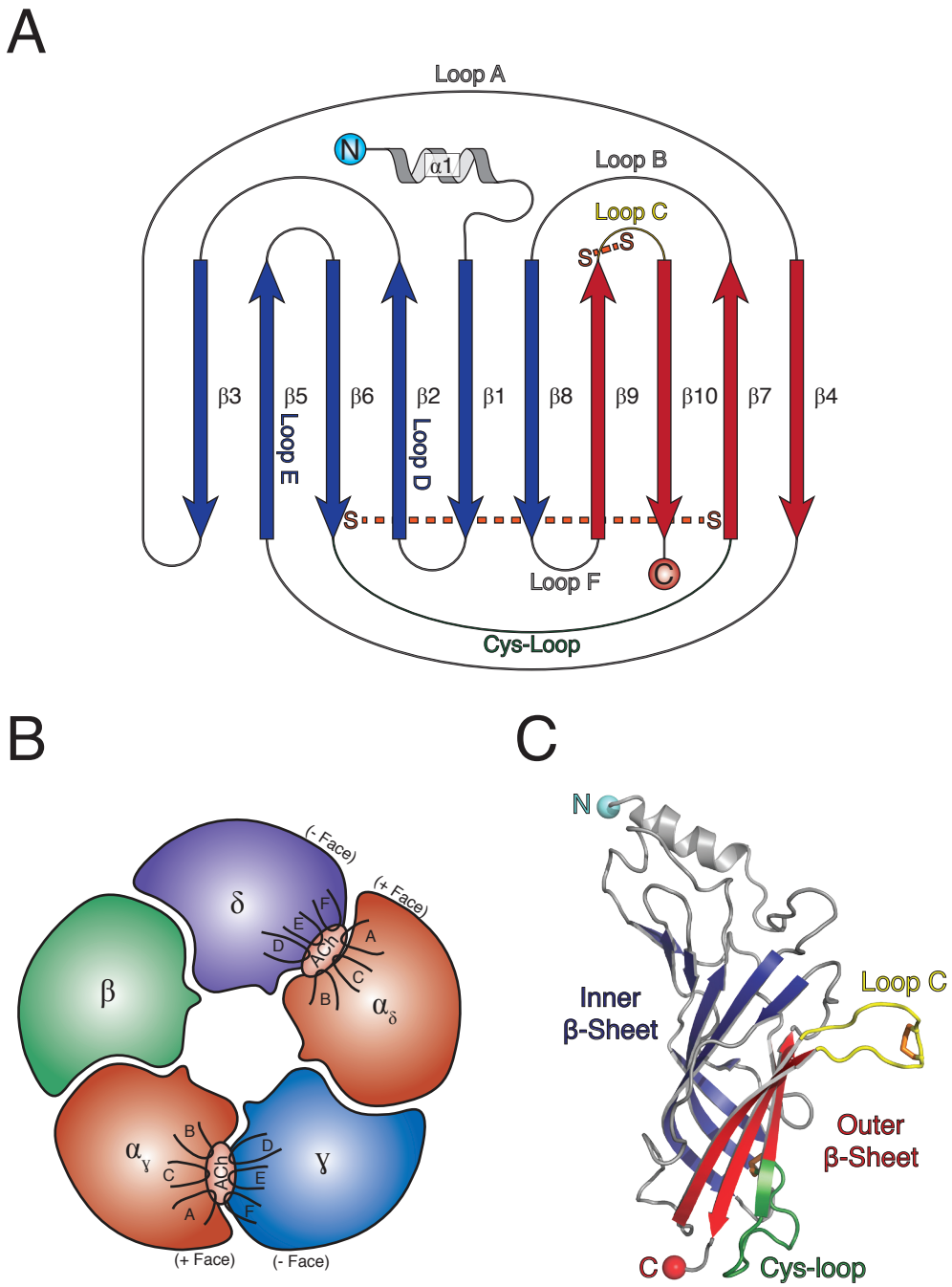


**Figure 1.6: The Agonist Binding Domain Of The nAChR.** (A) Topology map of the nAChR's ABD showing the secondary fold of the ABD. β-strands comprising the inner and outer β-sheets are shown in blue and red, respectively. Disulphide bonds are shown are an orange dashed line. Loops that contribute the agonist-binding site and Cys-loop are labeled. (B) Figure showing the binding sites between two subunits, the principal face (+) and complementary face (-), and the subunit loop contributions to the agonist binding site. Acetylcholine is represented as a red sphere within the binding site. (C) Tertiary fold of a single nAChR subunit (PDB: 2BG9), colours match the same structures as A.

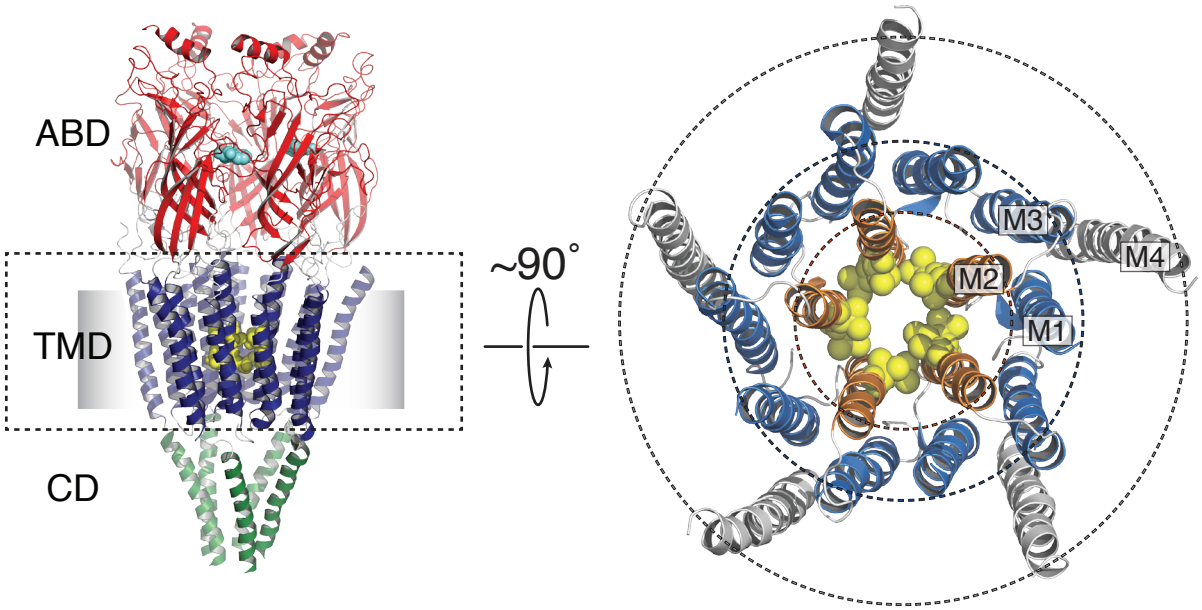


**Figure 1.7: The Transmembrane Domain Of The nAChR.** 4 Å cryo-EM structure of the *Torpedo* nAChR (PDB ID: 2BG9). The side view of the nAChR (left) shows the 3 domains, the agonist-binding domain (ABD, red), the transmembrane domain (TMD, blue), and the cytoplasmic domain (CD, green). Side chains forming part of the agonist- binding site (αW149) and channel gate (αL251 and αV255, including analogous residues on the other subunits) are shown as cyan and yellow spheres, respectively. The TMD show the 3 concentric loops of α-helices that make up the TMD (orange, M2; blue, M1 and M3; white, M4).

into 3 concentric rings arranged pseudosymmetrically around a central pore. The innermost ring is formed by the M2 α-helices, which line the channel pore and form the gate. The 2nd ring is formed from the M1 and M3 α-helices and acts as a barrier shielding M2 from the lipid membrane. The M4 α-helices make up the outermost ring and are the most lipid-exposed of the TMD α-helices.

Unlike sodium or potassium channels, the nAChR's selectivity for ions is less stringent. The opening of the pore allows the passage of most cations, which include, sodium, potassium, and calcium ions. Bulky, hydrophobic residues are found at the thinnest region of the pore, which is estimated to have diameter equal to roughly 6 Å (Huang et al., 1978). While sodium and potassium cations are roughly 2.5 Å in diameter, their hydration shell increases their diameter to roughly 8 Å. Therefore, in the closed state, hydrated cations cannot simply traverse the pore, as there is a steep energetic barrier to removing the hydration shell. Thus, when transitioning to an open conformation, it is anticipated that the pore expands sufficiently to accommodate cations in their hydrated state.

### 1.4.4 Coupling Agonist-Binding to Channel Gating

With a 4 Å structural model of the nAChR, we can begin to develop hypothesis on how agonist binding can induce channel gating. The AChBP has revealed some of the conformational changes in the ABD upon ligand binding; however, the exact mechanisms of channel gating are still under debate. Molecular complementarity between the ABD and TMD is essential for translating agonist binding to channel gating, as demonstrated by pLGIC chimeras formed by linking the ABD of one pLGIC to the TMD of another (Bouzat et al., 2004; Duret et al., 2011). Site directed mutagenesis has also identified key residues at the interface between these 2 domains (Lee and Sine, 2005).

Residues located between the β10 structure of the ABD and the M1 α-helix of the TMD covalently link the ABD and TMD domains of each subunit. A number of non-covalent interactions are mediated by the loops at this interface, which include the Cys-loop (the β6-β7 loop) and the β1-β2 loop on the ABD, and the M2-M3 linker and the C-terminus of M4 within the TMD (Figure 1.8). Residues on the β1-β2 loop and part of the Cys-loop form "V" like structures clamping and securing the M2-M3 linker (daCosta and Baenziger, 2013). The Cys-loop also extends out to interact with the M4 α-helix. It is thought that upon agonist binding, structural changes in both the Cys-loop and β1-β2 loops are translated into movements of the M2-M3 linker, thus leading to the movement of the pore lining M2 α-helix to open the channel gate (Sine and Engel, 2006).

### 1.4.5 Lipid Sensitivity of the nAChR

Early studies on the *Torpedo* nAChR were carried out on receptor rich membranes isolated directly from the native environment. However, given the number of accessory proteins within the native membrane, there remained a question as to what constituted the binding and gating functions. To address this question, a reproducible protocol for reconstituting the nAChR into lipid membranes was required. Early purification attempts presented a large hurdle, as the nAChR is highly sensitive to the conditions used. Using detergents to strip the nAChR from its native lipid membrane led to reconstituted nAChRs that bind agonist, but do not flux cations (Sobel et al., 1977). However, purifying the nAChR in the presence of lipids allowed for the reconstitution of nAChRs that retain both their agonist-binding and cation flux properties (Epstein and Racker, 1978). These first experiments demonstrated that the *Torpedo* nAChR is sensitive to its surrounding membrane environment.

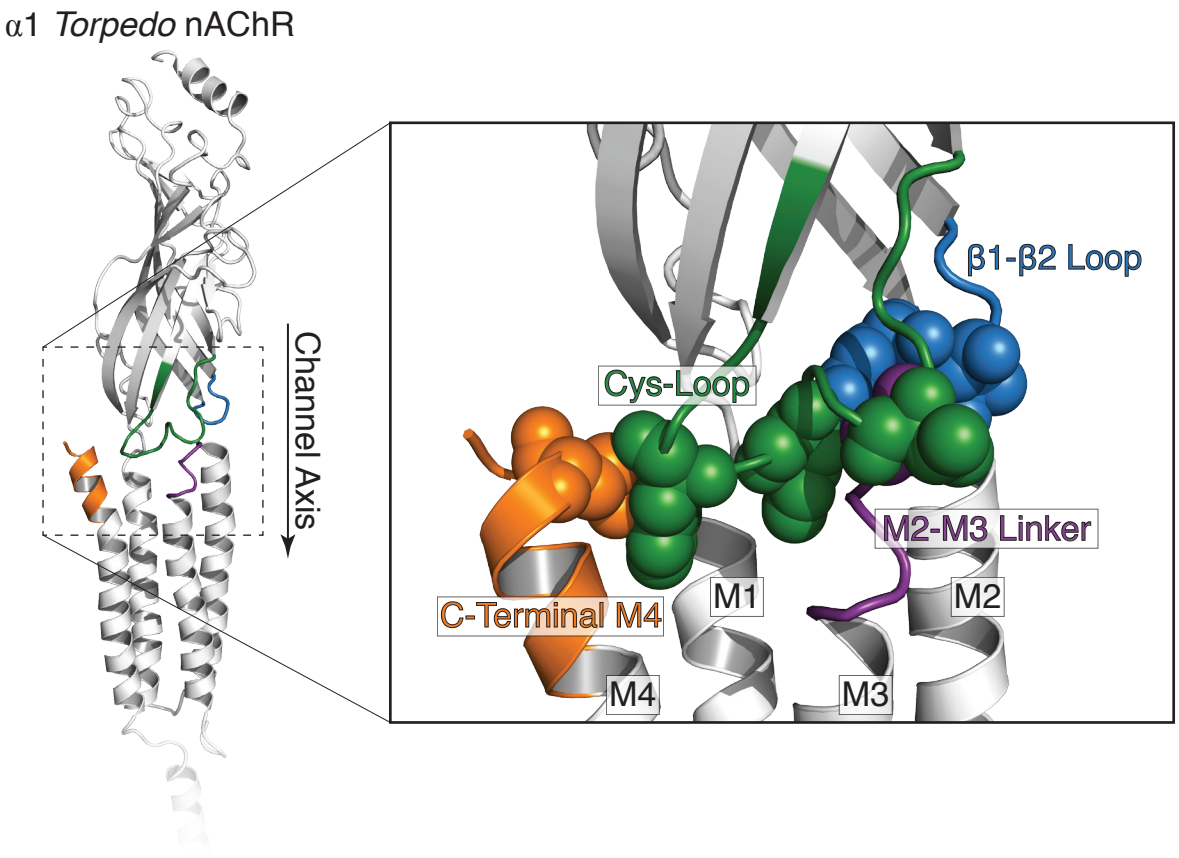


**Figure 1.8: Coupling Agonist Binding to Channel Gating.** A single subunit of the *Torpedo* nAChR (α1) is shown. The coupling interface between the ABD and TMD are coloured (Cys-loop, Green; β1-β2 loop, blue; M2-M3 linker, purple; C-terminal M4, orange). Interactions at the ABD/TMD interface is mediated by residues (shown as spheres) in the ABD forming V like structures around the M2-M3 linker, as well as forming interactions with the C-terminal M4.

Subsequent studies also showed that an appropriate membrane lipid composition is required to support a nAChR function. Early studies of the nAChR reconstituted in different lipid mixtures pointed towards anionic lipids (lipids with a negatively charged head group) and cholesterol (Chol) as being vital for nAChR function (Ochoa et al., 1983; Sunshine and McNamee, 1992). These results were not surprising given the lipid composition of the native *Torpedo* membrane. Chol is one of the major components of the *Torpedo* lipid membrane, making up between 20 to 30 mol percent of the total lipid (Gonzalez-Ros et al., 1982; Schiebler and Hucho, 1978). Anionic lipids make up roughly 15 mol percent of the total lipids, with phosphatidylserine (PS) being the dominant anionic lipid making up roughly 10 mol percent, and other anionic lipids, such as phosphatidic acid (PA) and cardiolipin, making up lesser amounts (Gonzalez-Ros et al., 1982; Schiebler and Hucho, 1978). Therefore, the *Torpedo* nAChR lipid requirements reflect its native lipid membrane environment.

As more sensitive assays were developed, it was shown that the lipid requirement of the nAChR is more complicated. Many of the early assays simply probed if the inclusion of particular lipids in a phosphatidylcholine (PC; a polar lipid with a neutral head group that stabilizes the nAChR in a non-activatable conformation) membrane could stabilize measurable pools of nAChRs that could flux cations. Ultimately, the early experiments failed to take into account that lipids can stabilize different proportions of activatable and non-activatable conformations. Increasing levels of either cholesterol or PA alone in a PC membrane stabilize increasing proportions of agonist-activatable nAChRs (Baenziger et al., 2000). This demonstrates that neither PA nor Chol are absolutely essential for the nAChR to undergo agonist-induced conformational transitions.

The lack of an absolute Chol requirement is further supported with the

observation that Chol analogues and other neutral lipids can essentially replace Chol to support channel function (Sunshine and McNamee, 1992). Also, while a variety of anionic lipids are effective at promoting channel function in the presence of Chol, distinct efficacies emerge in the absence of Chol. Of the anionic lipids, PA is the most effective at stabilizing agonist-responsive nAChRs (daCosta et al., 2009). Other anionic lipids, such as PS or phosphatidylinositol (PI), when placed within a PC membrane lacking Chol, predominantly stabilize non-activatable conformations (daCosta et al., 2009). The distinct efficacies of anionic lipids in supporting nAChR function demonstrate that the net negative charge is insufficient (daCosta et al., 2004). The negative head group of the anionic lipids may promote electrostatic interactions within the nAChR, but only when anionic lipids are immersed in the appropriate physical environment (Xiu et al., 2005). The addition of cholesterol to a lipid membrane dramatically alters the physical properties of the lipid membrane by promoting an ordering effect. In the absence of Chol, certain anionic lipids, such as PA, could mimic the physical properties of a lipid membrane containing Chol as their negative head groups is capable of mediating interactions with other lipids and cations leading to an ordering effect (daCosta et al., 2002; Kwolek et al., 2015).

Many of the mechanisms by which the physical properties of the lipid membrane influence the nAChR are still poorly understood. Understanding the complex relationship between a lipid bilayer's physical properties, such as hydrophobic thickness and bilayer ordering, and nAChR function are difficult because changes in these properties are often brought about by changes in the lipid chemistry (Sunshine and McNamee, 1994). Chapter 2 of this thesis focuses on changing the hydrophobic thickness of the lipid membrane without changing the lipid head group. Increasing hydrophobic thickness could favor an alignment of the outermost M4 $\alpha$-helix normal to the bilayers, thus promoting interactions between the TMD and ABD (daCosta et al., 2013). Ultimately, as it will be discussed in more detail

in chapter 2, the bulk physical properties of the membrane has the capacity to allow agonist-induced conformations transitions in the absence of both anionic lipids and Chol (daCosta et al., 2013).

Research has also hinted at the possible existence of lipid binding sites within the nAChR, however definitive evidence remains to be elucidated. The crystal structure of the homologous glutamate-gated chloride channel (GluCl) has revealed a putative lipid binding site, between the M1 and M3 $\alpha$-helices of adjacent subunits, which influence channel activity (Althoff et al., 2014). Additionally, experimental evidence and molecular dynamic simulation studies propose the existence of non-specific Chol binding sites between transmembrane $\alpha$-helices in the nAChR, which may stabilize the TMD structure facilitating interactions with the ECD (Antollini and Barrantes, 1998; Brannigan et al., 2008; Jones and McNamee, 1988).

The structure of the nAChR gives an insight into the mechanisms of lipid sensitivity. The M4 $\alpha$-helix is ideally situated to interact with the lipid membrane and thus may play a role in lipid sensitivity. Lipid binding sites between M4 and the adjacent $\alpha$-helices M1 and M3 are observed in the prokaryotic pLGIC crystal structures of GLIC (Bocquet et al., 2009). Additionally, mutations of nAChR lipid facing-residues on M4 alter channel function, including mutations that lead to diseases in humans (Bouzat et al., 1998; Li et al., 1992; Tamamizu et al., 2000). Thus, M4 likely plays a role in lipid-sensitivity of the nAChR, and more broadly all members of the pLGIC family.

### 1.4.6 The Uncoupled nAChR

In PC membranes lacking Chol and anionic lipids, the nAChR adopts a non-activatable conformation distinct from the desensitized conformation, called the uncoupled conformation. The uncoupled conformation is characterized by its

resting-state like affinity for agonist, yet its inability to undergo conformational transitions to the open or desensitized states. Structural models have emerged to provide an insight into the mechanisms by which lipids influence the coupling of binding to gating (Figure 1.9). The M4 lipid-sensor model proposes that the M4 $\alpha$-helix in the TMD acts as the lipid sensitive moiety of the nAChR (daCosta and Baenziger, 2009). As previously noted, M4 is highly lipid exposed and thus is ideally situated to interact with the surrounding lipid bilayer, while also interacting with the Cys-loop of the ABD and the adjacent $\alpha$-helices, M1 and M3.

It was suggested that in the uncoupled conformation, the ABD pulls away from the TMD, ultimately leading to a physical separation of these two domains. The separation between the two domains could lead to the more extensive peptide N-$^{1}$H for N-$^{2}$H exchange observed in the uncoupled state (daCosta and Baenziger, 2009). The greater exchange suggests that regions of the protein that are buried from solvent in the coupled conformations become solved exposed in the uncoupled conformation, however the regions of the nAChR that become solvent-exposed have not yet been defined.

While speculative, the uncoupled conformation may exist in biological systems as pools of electrically silent receptors. Receptors in an uncoupled conformation may transition to agonist-activatable conformations through association with lipid rafts, creating pools of electrically silent receptors until they are needed. Some anecdotal evidence supports this notion. Electrically silent receptors are observed when neuronal nAChRs are expressed in heterologous systems (Li and Steinbach, 2010). Also, chronic nicotine exposure appears to, in part, shift a pool of agonist-unresponsive receptors into an agonist-activatable conformation (Govind et al., 2012; Vallejo et al., 2005).

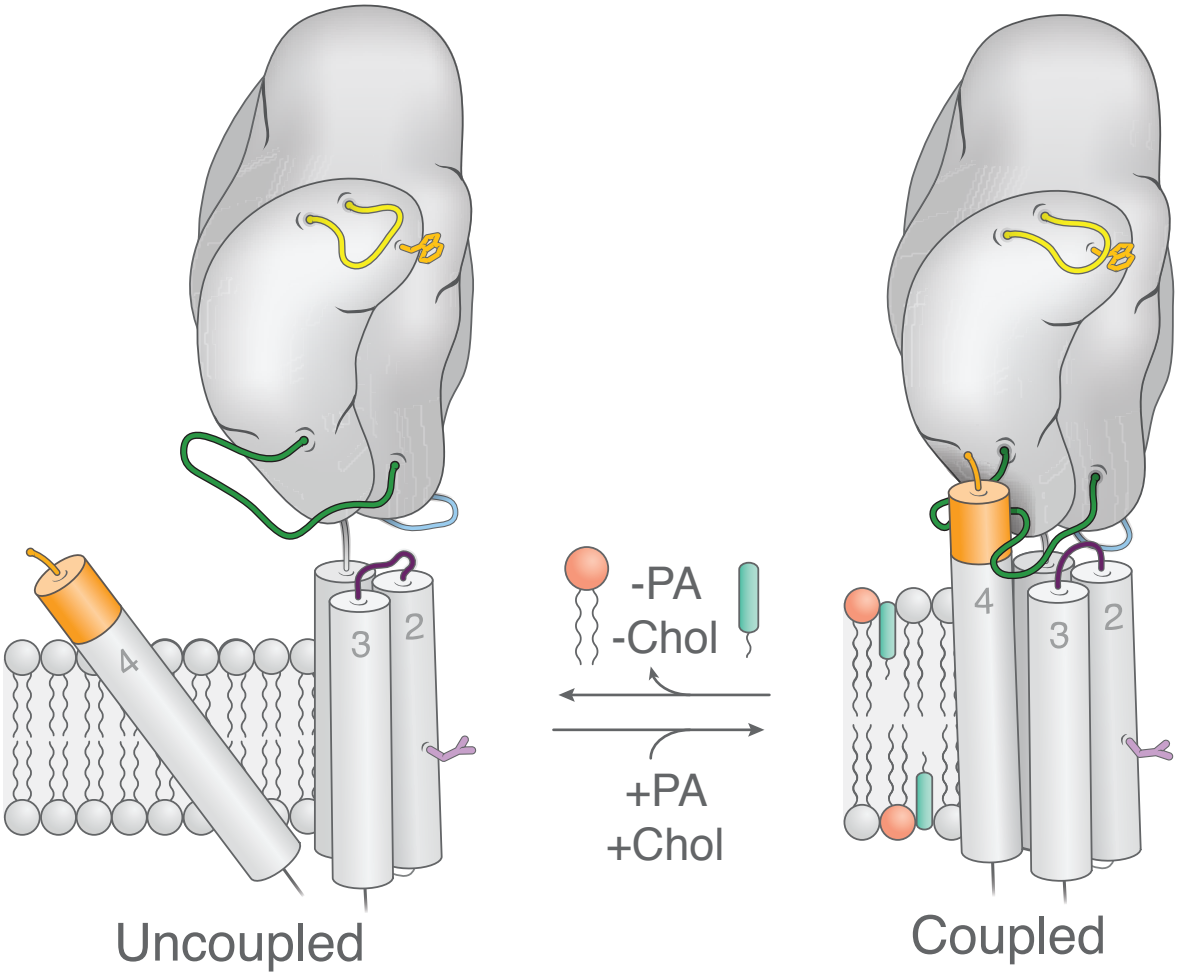


**Figure 1.9: The M4 Lipid Sensor Model of the Uncoupled nAChR.** Schematic diagram showing the lipid-dependent uncoupling model, illustrated as a single subunit. The surrounding lipid environment M4 may act as the lipid sensitive moiety of the nAChR. In unfavorable lipid environments, the M4 may alter its local structure resulting in weakened interactions between the ABD (β1-β2, light blue; Cys-loop, green) and the TMD (M2-M3 linker, purple; C-terminal M4, orange). Figure adapted from daCosta and Baenziger, 2009.

## 1.5 Prokaryotic Homologues of the pLGICs

### 1.5.1 Overview

The discovery of prokaryotic homologues of the nAChR has given researchers additional tools to further understand the relationship between the structure and function of the pLGICs. Their discovery was first made in 2004, where sequence alignment across a number of prokaryotic species identified potential homologues of the eukaryotic pLGICs (Tasneem et al., 2005). Research has primarily focused on two cation-selective prokaryotic homologues, the *Gloeobacter* Ligand-gated Ion Channel (GLIC) and the *Erwinia* Ligand-gated Ion Channel (ELIC). GLIC originates from the cyanobacterium *Gloeobacter violaceus*; ELIC comes from the plant pathogen *Erwinia chrysanthemi* (now renamed to *Dickeya dadantii* due to recent taxonomic revisions). However, to date no definitive role for either of these proteins in their native species has been elucidated. GLIC is a proton-activated channel, which opens in response to a drop in pH (or an increase in the proton concentration), while ELIC opens in response to most primary amines.

Unlike their eukaryotic counterparts, GLIC and ELIC can be expressed in sufficient quantities for biophysical studies using a bacterial system. This makes them attractive models for biophysical studies aimed at probing the mechanisms of channel function. Furthermore, high-resolution crystal structures of both proteins have been solved. Both structures reveal a structural homology with the 4 Å cryo-EM *Torpedo* nAChR structure, although both are homopentameric channels that lack a CD and the two-cysteine residues found in the β6-β7 loop (the Cys-loop in eukaryotic pLGICs) (Figure 1.10) (Bocquet et al., 2009; Hilf and Dutzler, 2008; Hilf and Dutzler, 2009).

Note that while the overall crystal structures of both GLIC and ELIC are similar,

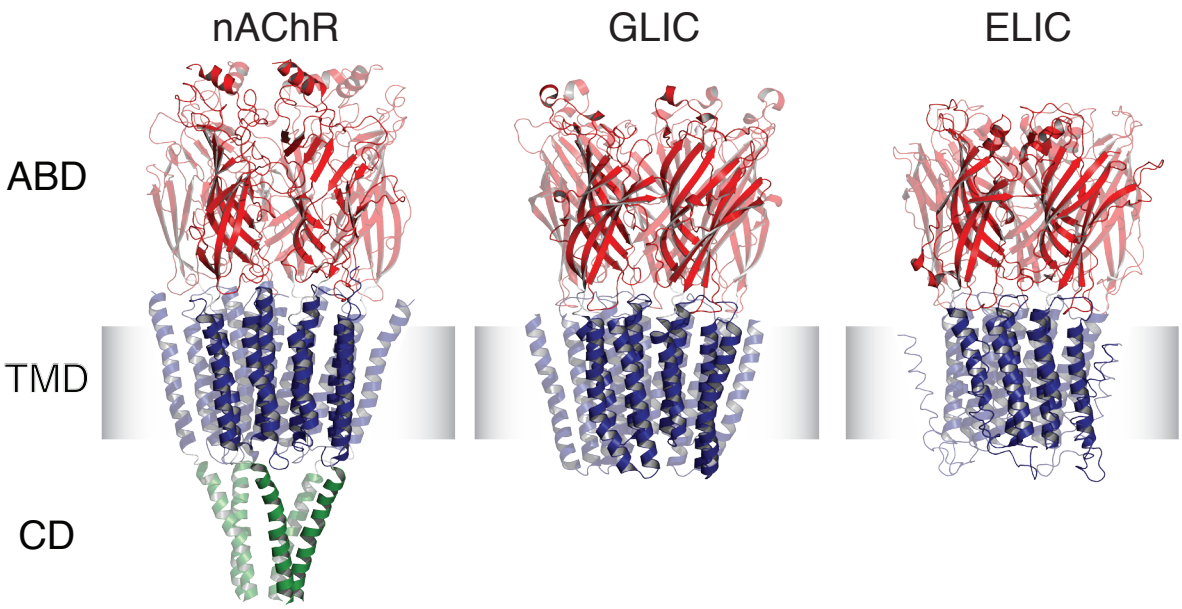


**Figure 1.10: The Prokaryotic Homologues of The nAChR.** Structures of the nAChR (PDB: 2BG9), GLIC (PDB: 4HFI), and ELIC (PDB: 2VL0). Cartoon representations of the cryo-EM *Torpedo* nAChR at a 4.0 Å resolution, and the GLIC and ELIC crystal structures solved to a 2.4 Å and 3.3 Å resolution, respectively. The side view of all proteins shows the agonist-binding domain (ABD, red), the transmembrane domain (TMD, blue), and the cytoplasmic domain (CD, green; both GLIC and ELIC lack a CD).

there are intriguing differences between the conformations of their M4 α-helices (Figure 1.11). The M4 α-helix in GLIC forms extensive interactions along its entire length with the adjacent α-helices, M1 and M3, as well as with the β6-β7 loop of the ABD. In contrast, the C-terminal half of M4 in ELIC tilts away from M1 and M3, with the last 5 residues unresolved; it appears that there are no interactions between M4 and the β6-β7 loop of the ABD. Additionally, the β1-β2 and β6-β7 loops form weak interactions with the M2-M3 linker in ELIC, effectively increasing the distance between the ABD and TMD. Significantly, crystalized ELIC fails to adopt an open conformation in the presence of agonist, even with mutations that stabilize the open state (Gonzalez-Gutierrez et al., 2012). The altered structure of the M4 α-helix and increased physical separation between the ABD and TMD in ELIC's crystal structure are strikingly similar to the structural changes proposed for the uncoupled conformation of the nAChR (daCosta and Baenziger, 2013; Zimmermann and Dutzler, 2011).

Previous studies have shown that aromatic interactions at the interface between M4 and M1/M3 play a key role driving M4 binding to M1/M3 during folding of the homologous Glycine receptor (Haeger et al., 2010). Aromatic residues are capable of forming non-covalent interactions with other aromatic residues, or with polar and charged residues. These interactions are due to the negative dipole created by the cloud of electrons found on either side of the aromatic ring, subsequently creating a positive dipole around the aromatic ring's hydrogens. GLIC exhibits an abundance of aromatic interactions along the entire interface between M4 and M1/M3, while ELIC exhibits fewer interactions located primarily near the N-terminus of M4 (Figure 1.12). It has been suggested that the lower number of aromatic interactions at the M1/M3/M4 interface renders ELIC more susceptible to the perturbing effects of detergent solubilization during crystallization, thus locking ELIC in an uncoupled-like conformation. On the other hand, GLIC appears to

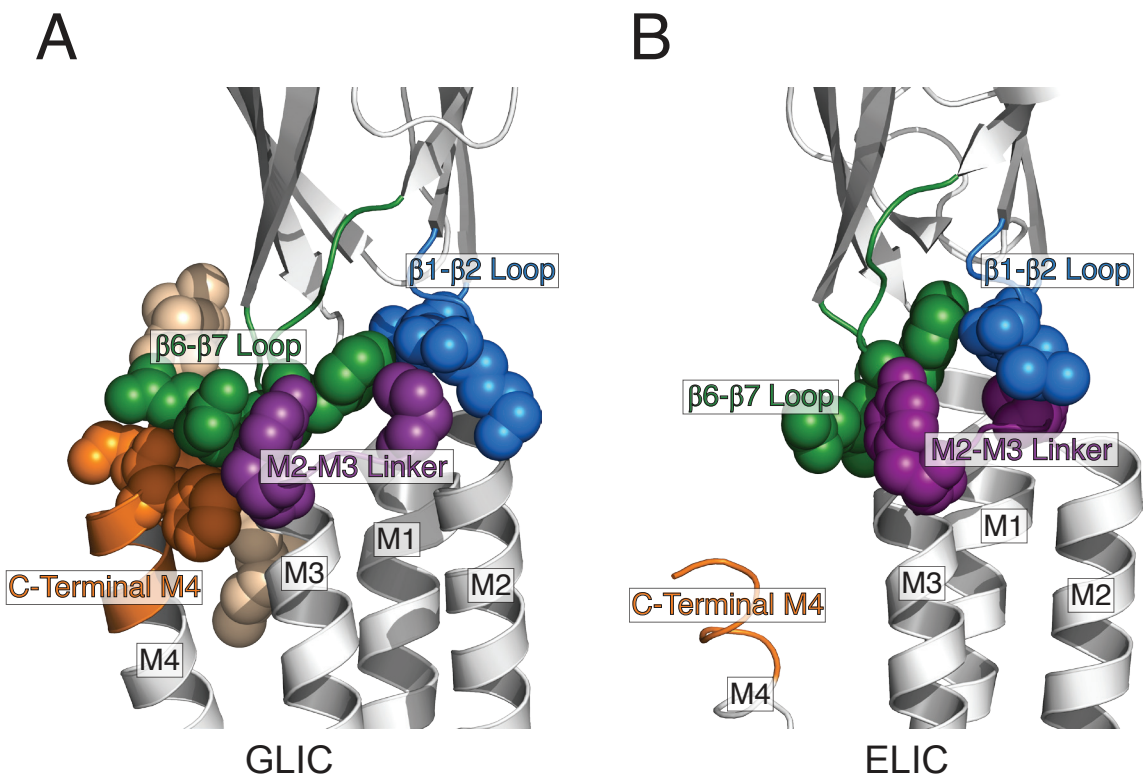


**Figure 1.11: The Interface Between the ABD and TMD of the Prokaryotic pLGICs.** The structures of (A) GLIC (PDB: 3EAM) and (B) ELIC (PDB: 2VL0) highlighting the different structures found at the ABD and TMD interface. In each case the β1-β2 loop, β6-β7 loop, M2-M3 linker, and C-terminal M4 are highlighted in blue, green, purple, and orange, respectively. Residues that likely interact are shown as spheres. A lipid molecule found in the crystal structure is shown as tan spheres in GLIC.

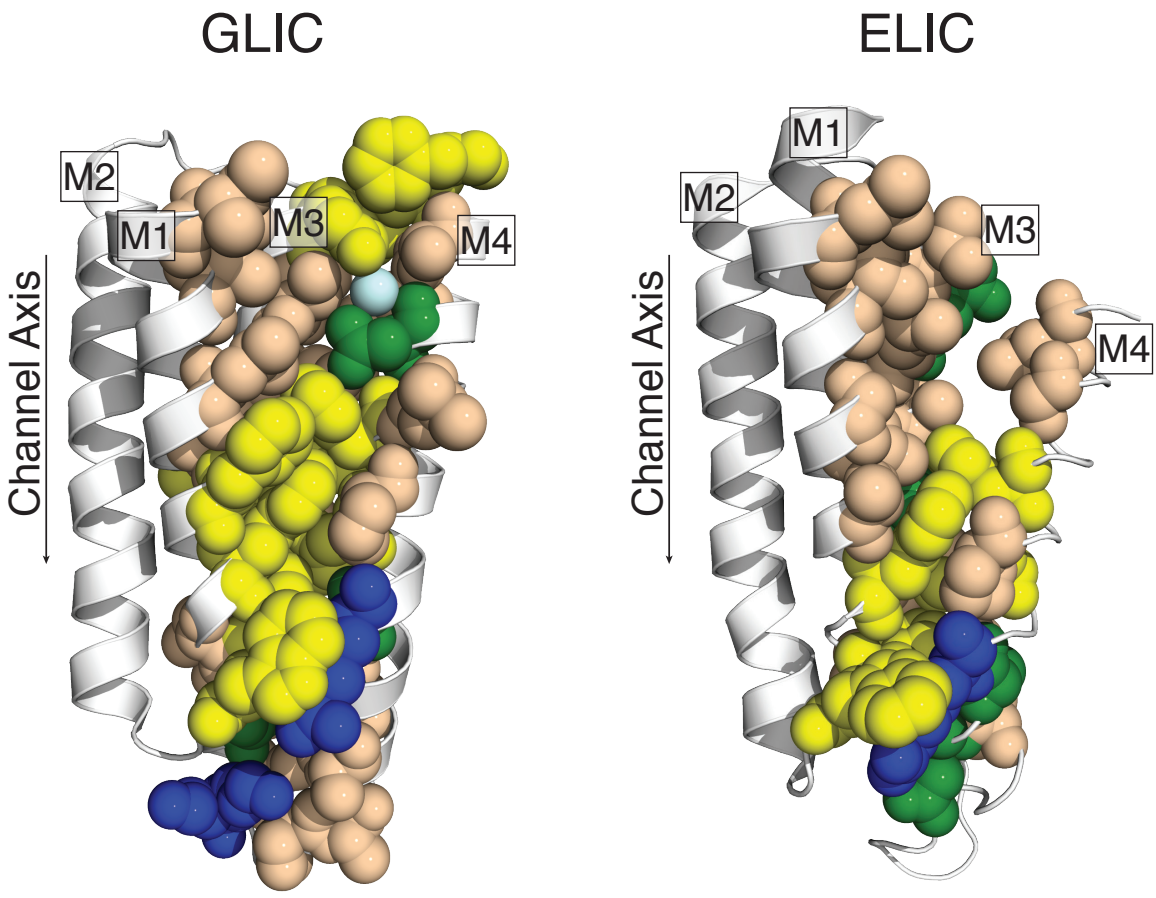


**Figure 1.12: GLIC and ELIC's M4 and M1/M3 Interface.** A single subunit showing the variable chemical interactions found between the M4 and M1/M3 α-helices of GLIC (PDB: 4HFI) and ELIC (PDB: 2VL0). Residues within this interface are shown as spheres, with aliphatic residues colored tan, aromatic residues yellow, negative residues red, positive residues blue, polar/H-bonding residues green, and water molecules cyan.

maintain extensive M4-M1/M3 interactions even after detergent solubilization. Thus, the differing strengths of M4-M1/M3 interactions may lead to the contrasting conformations of M4 in the GLIC and ELIC structures (daCosta and Baenziger, 2013).

### 1.5.2 Probing the Role of M4 in pLGIC Function

GLIC and ELIC have served as excellent models to probe the role of the M4 $\alpha$-helix in pLGIC function. Surprisingly, an alanine-scan of M4 revealed distinct roles for M4 in GLIC and ELIC (Henault et al., 2015). In GLIC, the mutation of residues at the M4-M1/M3 interface to Ala typically leads to detrimental effects on channel function, with the greatest impairment in function occurring at the C-terminus. An interacting network of residues located at the C-terminal M4, M3, and the $\beta$6-$\beta$7 loop was also shown to play an essential role in both folding and function. The results suggested that interactions between M4, M1/M3, and the $\beta$6-$\beta$7 loop are optimized for channel function in GLIC, and that the M4 C-terminus is essential. These findings are consistent with and thus support the M4 lipid sensor model.

In contrast, Ala mutations of residues at the same interface in ELIC typically had the opposite effect, leading to a gain of function. These findings suggest that M4-M1/M3 interactions are not optimized for channel function in ELIC. In addition, no analogous network of interacting residues involving the C-terminus of M4 was identified. In fact, deletion of up to the two C-terminal turns of M4 (7 residues) had no detrimental effect on ELIC's activity, suggesting that the M4 C-terminus is not essential for channel activity (Henault et al., 2015). These data show that although the C-terminus M4 may play an essential role in some pLGICs, it is not important in others.

GLIC and ELIC have also been used to test a basic principle of the M4 lipid

sensor model; that enhanced interactions between M4 and M1/M3 promote channel function. As noted, aromatic residues are thought to be the key energetic determinants of M4-M1/M3 interactions. Aromatic residues at the M4-M1/M3 interface were removed to weaken M4-M1/M3 interactions in GLIC, while aromatic residues were added to this interface to enhance M4-M1/M3 interactions in ELIC (Carswell et al., 2015b). In all cases, weakened M4-M1/M3 interactions in GLIC led to reduced coupling between the agonist site and channel gate, while enhanced interactions in ELIC led to enhanced coupling.

Furthermore, aromatic residues, and thus the intrinsic strengths of M4-M1/M3 interactions, were shown to influence the sensitivities of GLIC and ELIC to allosteric modulators that act on M4. The abundant aromatic interactions leading to intrinsically strong M4-M1/M3 association render GLIC relatively insensitive to its lipid environment, as it retains the ability to gate open in membranes that lead to an uncoupled nAChR (Labriola et al., 2013). When ELIC is placed into a PC membrane, it does not gate open in response to agonist (Carswell et al., 2015a). Aromatic additions to enhance M4-M1/M3 interactions, however, restore ELIC's ability to gate open in PC membranes.

The intrinsic strengths of M4-M1/M3 interactions also dictate the sensitivities of each pLGIC to the potentiating effects of an M4 lipid-facing mutation, that in the muscle type nAChR leads to a congenital myasthenic syndrome (CMS) (Shen et al., 2006). The addition of the CMS causing mutation in GLIC lead to no potentiating effect, while in ELIC lead to a gain of function. The aromatic additions in ELIC abolished the CMS' potentiating effect. The latter suggests that the CMS mutation potentiates channel function by enhancing M4-M1/M3 interactions.

### 1.5.3 The M4 Lipid-Sensor Model in the Context of Prokaryotic pLGIC Function

The finding that aromatic residues at the M4-M1/M3 contribute to the intrinsic strengths of M4-M1/M3 interactions and govern the sensitivities of GLIC and ELIC to allosteric modulation by lipids or mutations acting on M4 is intriguing given the variable abundance of such residues at this interface in eukaryotic pLGICs. For example, the human and *Torpedo* muscle type nAChR subunits have few aromatic interactions at the M4-M1/M3 interface, which may lead to relatively weak intrinsic M4-M1/M3 interactions (Labriola et al., 2013). Such weak interactions could, in part, underlie the sensitivity of the *Torpedo* nAChR to lipids and its propensity to adopt an uncoupled conformation in PC membranes. Few aromatic interactions at the M4-M1/M3 interface are also observed in neuronal nAChR $\alpha$-subunits, in contrast to the $\beta$-subunits, suggesting that the function of these receptors may also prove to be exquisitely sensitive to their surrounding membrane environment given their subunit composition. In contrast, the crystal structures of the glutamate activated chloride channel (GluCl) from *Caenorhabditis elegans*, and $GABA_A$ receptors demonstrate a plethora of aromatic interactions at the M4-M1/M3 interface – suggesting that these pLGICs should be relatively insensitive to the composition of their surrounding lipid environments (Hassaine et al., 2014; Hibbs and Gouaux, 2011; Miller and Aricescu, 2014).

Note, however, that while previous studies have focused on interactions between aromatic residues at the M4-M1/M3 interface, other types of non-covalent interactions have been shown to play an important role in transmembrane helix-helix interactions, and may thus also contribute to the intrinsic strengths of M4-M1/M3 interactions (Daeffler et al., 2012; Fink et al., 2012; Joh et al., 2008; Wootten et al., 2013). A major goal of this research was to explore how other non-covalent interactions at the M4-M1/M3 interfaces of GLIC and ELIC contribute to channel

function.

## 1.6 Thesis Objectives

The general goal of my research is to probe the role of the outermost M4 transmembrane domain α-helix in pLGIC function. My thesis research was divided into two projects:

Chapter 2 describes the work that I performed during the first 6 months of my Master's, which contributed to a publication titled "A distinct mechanism for activating uncoupled nicotinic acetylcholine receptors" in Nature Chemical Biology. In this manuscript, we proposed that increased hydrophobic thickness would favour alignment of the outermost M4 α-helix normal to the bilayer, thus promoting M4-M1/M3 interactions to stabilize coupled (resting, open, desensitized) versus uncoupled conformations. Using biophysical techniques, we showed that although the nAChR is stabilized in an uncoupled state in PC membranes of variable thickness, thicker PC membranes promote very slow conformational transitions from uncoupled to coupled conformations, while thin PC membranes do not. We showed for the first time that the nAChR can function in the absence of both cholesterol and anionic lipids, and that lipids can influence function via a kinetic mechanism – i.e. they can modulate function by altering the activation energies between conformational states.

Chapter 3 presents the main body of work that I accomplished during my Master's degree. In this research I focused on the prokaryotic pLGICs, GLIC and ELIC. Using single site directed mutagenesis, mutant cycle analyses, and two-electrode voltage clamp electrophysiology; I examined how the chemistry at the M4-M1/M3 interfaces influences channel function. My data showed that the capacity

by which M4 modulates channel activity depends on the intrinsic strength of interactions with adjacent helices M1 and M3, determined by the strength, location, and number of non-covalent interactions found at this interface. The chemical variability at the M4-M1/M3 interface could be one of the important factors that lead to distinct pLGIC channel properties.

The majority of alanine substitutions throughout the M4 and M1/M3 interface in GLIC lead to disruptive channel function. However, most analogous mutations performed in ELIC lead to either no change or an increase in channel function. The data suggests that GLIC and ELIC may reflect two different archetypes found in the pLGIC family. One archetype, exemplified by GLIC, maintains that an extensive network of contacts between M4 and M1/M3 is needed for proper channel folding, trafficking, and/or function. The other archetype, exemplified by ELIC, demonstrates that few specific interactions are needed between M4 and M1/M3 to maintain proper channel function. These two archetypes may shape the structure and function of receptors, but may also have a broader role in influencing how these channels respond to a variety of TMD allosteric modulators.

# Chapter 2

## A Distinct Mechanism for Activating Uncoupled Nicotinic Acetylcholine Receptors

## 2.1 Introduction

Increasing levels of anionic and/or neutral lipids in a reconstituted PC membrane stabilize an increasing proportion of *Torpedo* nAChRs in coupled (resting, open, and desensitized) versus uncoupled conformations (daCosta et al., 2009). In the absence of anionic and neutral lipids, the nAChR is stabilized predominantly in an uncoupled conformation, which is characterized by a resting state-like agonist binding affinity, yet an inability to undergo agonist-induced conformational transitions (daCosta and Baenziger, 2009). When my thesis research was initiated, our working model suggested that the lipid-exposed M4 $\alpha$-helix acts as a lipid sensor, with lipids influencing interactions between M4 and the adjacent $\alpha$-helix, M1 and M3. The C-terminus of M4 extends beyond the lipid bilayer to interact directly with the Cys-loop, a structure at the ABD/TMD interface that plays a key role in coupling agonist binding into channel gating (daCosta and Baenziger, 2009). The M4 lipid sensor model proposes that M4 “tilt” away from M1 and M3 in PC membranes lacking activating lipids, ultimately altering M4 - Cys-loop interactions to eliminate coupling between the ABD and TMD.

The hydrophobic thickness of a lipid bilayer influences the activities of numerous membrane proteins by altering helix-helix interactions and/or the tilt angle of transmembrane helices in the lipid bilayer (Baenziger and daCosta 2013; Holt and Killian, 2010; Jensen and Mouritsen, 2004; Lee, 2004). In thinner lipid membranes, $\alpha$-helices favour a tilt toward the membrane plane to minimize exposure of hydrophobic side chains to the aqueous environment, while thicker membranes favour an alignment normal to the lipid bilayer. The tilt angle of the M4 helix in a reconstituted bilayer is altered by hydrophobic thickness (de Almeida et al., 2006). In the intact nAChR, increasing hydrophobic thickness could favour alignment of M4 normal to the lipid bilayer thereby promoting interactions between M1/M3.

The initial goal of this work was to examine whether membrane hydrophobic thickness influences the relative proportions of uncoupled versus coupled conformations stabilized in PC membranes lacking activating lipids. Although we found that the nAChR in different PC membranes with varying hydrophobic thickness is predominantly stabilized in an uncoupled conformation, relatively thick PC membranes promote very slow (minutes to hours) transitions from uncoupled to coupled states. In contrast to the conformational selection mechanism used by anionic lipids to stabilize different proportions of uncoupled versus coupled conformations, thick PC membranes promote function via a kinetic mechanism, i.e. they lower the activation energy between uncoupled and coupled states. Our results also raise the possibility that thick membranes, such as those found as the nAChR traffics from internal membranes to the plasma membrane or upon lipid raft association, promote awakening of uncoupled nAChRs in biological membranes.

My involvement with this project extended through the first $\sim$6 months of my Master's. I performed a number of affinity purifications/reconstitutions, and functionally characterized newly prepared nAChR proteoliposomes. In some cases, the goal was simply to obtain additional replicates. In other cases, I obtained completely new data or analyzed previously obtained data in more detail. In this chapter, I present my contributions – although the contributions of others are presented when their findings are essential to the biological conclusions. The contributions of others are acknowledged throughout the results section. This work has now been published in Nature Chemical Biology (daCosta et al., 2013).

## 2.2 Experimental Procedures

### 2.2.1 Materials

*Torpedo californica* electroplax tissue was obtained from Aquatic Research Consultants (San Pedro, CA). All synthetic lipids were from Avanti Polar Lipids, Inc. (Alabaster, AL). Soybean asolectin, carbamylcholine chloride (Carb), dibucaine and ethidium bromide were from Sigma (St. Louis, MO). High-purity Burdick and Jackson $CHCl_3$ and $CH_3OH$ were obtained from Honeywell (Morristown, NJ).

### 2.2.2 Preparation of nAChR Proteoliposomes

The nAChR was affinity purified on a bromoacetylcholine affinity column. Crude *T. californica* membranes from electroplax tissue were solubilized for 1 hour at 4°C in dialysis buffer (100 mM NaCl, 10 mM Tris-HCl, 0.1 mM EDTA, 0.02% (w/v) $NaN_3$, pH 7.8) containing 1% cholate. The solubilized membranes were centrifuged for 30 min at 87,000*g* to pellet insoluble material, and the supernatants were applied to an affinity column. The affinity column-bound nAChR was washed with three column volumes each of dialysis buffer supplemented with 1% cholate and 1.3 mM, 3.2 mM and then 1.05 mM lipid. The nAChR was eluted in 250 mM NaCl, 0.1 mM EDTA, 0.02% $NaN_3$ and 10 mM Tris-HCl, pH 7.8, supplemented with 1.05 mM lipid, 1.0% cholate and 10 mM Carb. Fractions with $A_{280} > 0.05$ were pooled and diluted with extra dialysis buffer (with cholate and lipid) to make the final $A_{280}$ = 1.0, resulting in a final lipid/protein ratio of roughly 500:1 (mol/mol).

The pooled eluates were dialyzed against 2 L x 5 of fresh dialysis buffer. The dialyzed proteoliposomes were pelleted and layered onto a step sucrose gradient before centrifugation at 41,000 r.p.m. for 20 hours in a SW41 swinging bucket rotor

(Beckmann). Aliquots (0.4 mL) were sequentially removed and assayed for both protein (BCA assay, Pierce) and lipid (Phospholipid C/Choline assay, Wako Chemicals USA Inc.). The reconstituted proteoliposomes were collected and dialyzed to remove sucrose. Samples were stored at -80°C in 2 mM phosphate buffer, pH 7.0.

The lipid composition of each reconstituted membrane was assessed using TLC on silica gel 60 $WF_{253}8$ plates (EMScience). The plates were developed with $CHCl_3$:$CH_3COH$:HCOOH:$H_2O$ 50:37.5:3.5:2 (v/v/v/v) and were stained with Coomassie Blue in a 30% $CH_3OH$ aqueous solution containing 0.1 M NaCl.

### 2.2.3 Fourier Transform Infrared Spectroscopy

FTIR spectra were recorded at 22.5°C on either a Digilab (now Agilent Technologies) FTS40 or FTS 7000 spectrometer. To record the spectrum in $^1H_2O$, 250 μg of the nAChR was deposited on a $CaF_2$ window, and the bulk solvent was evaporated with a gentle stream of $N_2$ gas. For both the protein amide I band analysis and the thermal denaturation studies, 250 μg of the nAChR was first incubated at 4°C in $^2H_2O$ phosphate buffer for precisely 72 hours to exchange peptide N-$^1$H for N-$^2$H. The samples were stored at -80°C until use. Samples were individually thawed, deposited between two $CaF_2$ windows with a gentle stream of $N_2$ gas, and rehydrated with 8 μL of *Torpedo* Ringer buffer in $^2H_2O$ (5 mM Tris, 250 mM NaCl, 5 mM KCl, 2 mM $MgCl_2$ and 3 mM $CaCl_2$, pD 7.0).

For analysis of the protein amide I band shape, spectra were recorded at 2 $cm^{-1}$ resolution, averaging 4,000 scans. Spectra were deconvolved between 1,900 $cm^{-1}$ and 1,300 $cm^{-1}$ using GRAMS/AI v.7.01 software (Thermo Scientific), with = 7.0 and 70% smoothing. Presented spectra are averages of spectra recorded from six samples (at least two separate affinity purifications and reconstitutions).

To assess thermal stability, 128 scan spectra were recorded at 1°C intervals as the sample was heated using a circulating water bath. The fraction denatured was assessed from the intensity changes in the secondary structure-sensitive amide I band at 1,681 $cm^{-1}$. The thermal denaturation temperature ($T_d$) was calculated by fitting with a Boltzmann sigmoidal, where the fraction denatured ($F_d$) at temperature $x$ is defined as $F_d\,(x) = y_{initial} + [(y_{final} - y_{initial})/\,(1 + exp((T_d - x)/m_b))]$, where $m_b$ corresponds to the Boltzmann slope.

### 2.2.4 Carb-Difference Spectra

Carb-difference spectra were recorded at 22.5°C using the attenuated total reflectance technique. Spectra of sample deposited on a germanium internal reflection element were recorded while flowing *Torpedo* Ringer buffer past the membrane film. Two spectra were recorded in the absence of agonist. The buffer was then switched to an identical buffer containing 50 μM Carb, and a spectrum of the Carb-bound state was recorded. Control-difference spectra (the difference between two spectra recorded in the absence of Carb) and Carb-difference (spectrum with Carb minus the second spectrum without Carb) were calculated. The Carb was then washed from the membrane film, and the process was repeated many times. Presented difference spectra are averages of $>$100 individual difference measurements recorded from several different samples.

### 2.2.5 Fluorescence Spectroscopy

Fluorescence spectra were acquired at 22.5°C on a Cary Eclipse fluorescence spectrometer (Agilent Technologies). *Torpedo* Ringer buffer (1.8 mL) was premixed with ethidium bromide to a final concentration of 0.3 μM in a fluorescence cuvette (10-mm light path, quartz glass; Hellma (Canada)), with the temperature equilibrated

at 22.5°C. Fluorescence intensity was recorded as a function of time with excitation and emission wave-length set to 500 nm and 590 nm, respectively, and the excitation and emission slits were set to 5 nm and 20 nm, respectively. 200 μL of a 0.75 mg/ml solution of the nAChR in *Torpedo* Ringer solution were added to give a final concentration of roughly 500 nM acetylcholine binding sites. This was followed by 10 μL of 100 mM Carb and then 10 μL of 100 mM dibucaine. Final Carb and dibucaine concentrations were roughly 500 μM.

## 2.3 Results

### 2.3.1 Effect of Membrane Hydrophobic Thickness on the Structure of the nAChR

To assess how membrane hydrophobic thickness influences the activity of the *Torpedo* nAChR, we first affinity purified and reconstituted the nAChR into lipid bilayers composed of soybean asolectin (Aso-nAChR), POPC (POPC-nAChR), di14:1PC (di14:1PC-nAChR), di18:1PC (di18:1PC-nAChR) and di22:1PC (di22:1PC-nAChR). Aso-nAChR and POPC-nAChR served as positive and negative controls, stabilizing predominantly activatable resting and non-activatable uncoupled nAChRs, respectively (daCosta and Baenziger, 2009). The di14:1PC-nAChR, di18:1PC-nAChR and di22:1PC-nAChR membranes allow us to vary the hydrophobic thicknesses of the bilayers from roughly 24 to 35 Å (Kucerka et al., 2005; Ramadurai et al., 2010; Rawicz et al., 2000). Note that each reconstitution was further subjected to sucrose density gradient centrifugation to separate protein aggregates and free liposomes from the desired nAChR proteoliposomes. The nAChR incorporates well into Aso, POPC, di18:1PC, and di22:1PC (Figure 2.1A) membranes, but not into di14:1PC (daCosta et al., 2013). Lipid extractions also showed that each of the nAChR reconstitutions contained the desired PC lipid, with no contaminating lipids

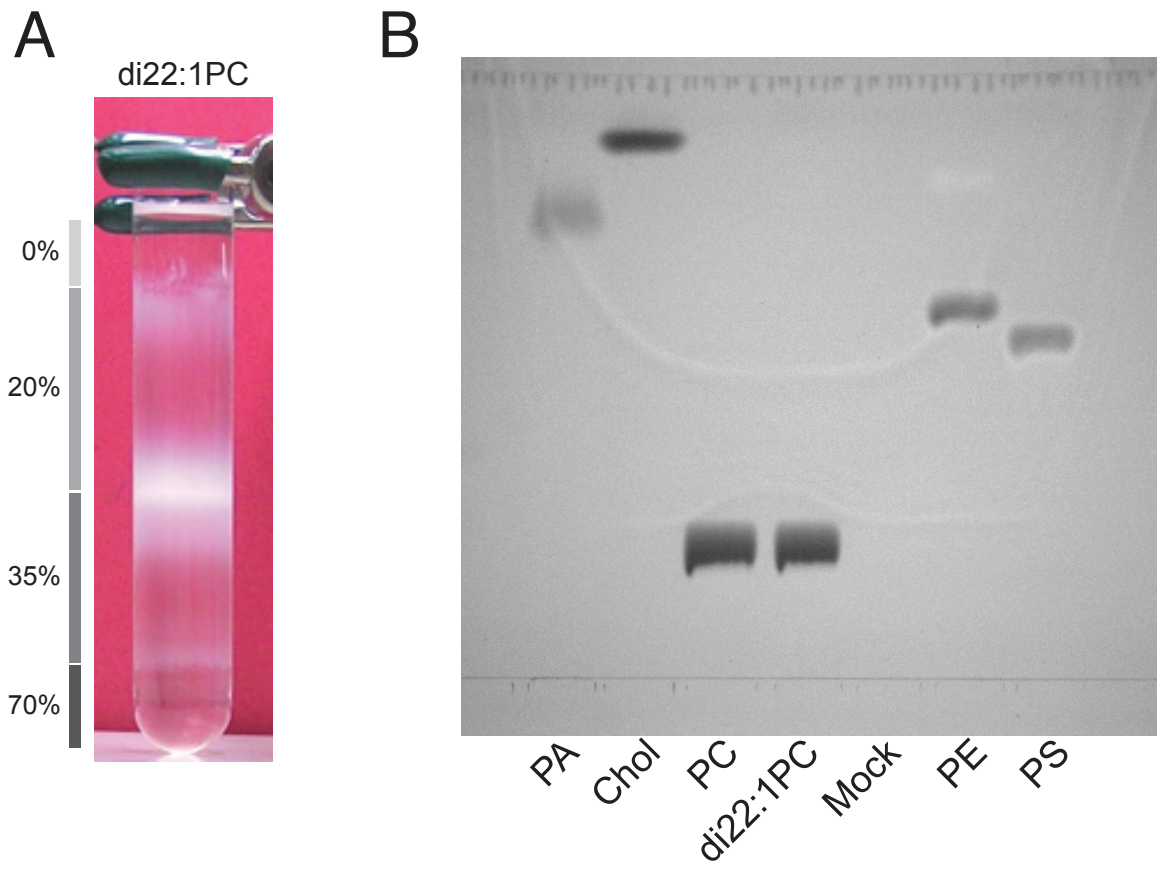


**Figure 2.1. Incorporation of the nAChR Into a di22:1PC Bilayer.** (A) Representative sucrose gradient of the di22:1PC-nAChR reconstitution. Proper incorporation of the nAChR is determined by the formation of proteoliposomes found at the 20%/35% interface. Liposomes and protein aggregate are found at interface between 0%/20% and 35%/75%, respectively. (B) Thin Layer Chromatography (TLC) of Lipids Extracted from the di22:1PC-nAChR Reconstitution. The TLC includes lipid standards diacylglycerol (DAG), cholesterol (Chol), phosphatidylcholine (PC), phosphatidylethanolamine (PE), and phosphatidylserine (PS). The Mock lane refers to a mock lipid extraction performed in the absence of any reconstituted nAChR membranes.

(Figure 2.1B). Note that I performed affinity purifications and reconstitutions into all of the membranes, except di14:1PC. My data was included as replicates for the analysis presented below.

Both as a quality control for our purifications/reconstitutions and to gain insight into the conformations stabilized in the various membranes, we next examined the various biophysical properties of the nAChR using infrared (IR) spectroscopy. The secondary structure sensitive amide I bands in IR spectra of the nAChR in each of the five membranes are similar with relatively intense component bands due to $\alpha$-helix and $\beta$-sheet (located near 1650-1655 $cm^{-1}$ and 1625-1640 $cm^{-1}$, respectively), indicating that each reconstituted nAChR exhibits the expected mixed $\alpha$-helix/$\beta$-sheet secondary structure. Note, however, that relative to Aso-nAChR, the amide I band of POPC-nAChR shows a slightly reduced intensity of the $\alpha$-helix component band near 1655 $cm^{-1}$. While this could reflect a slight decrease in the helical content in the uncoupled state, previous studies have shown that this subtle spectral difference reflects enhanced peptide N-$^1$H for N-$^2$H exchange (for technical reasons, spectra are recorded in $^2H_2O$ buffer), which leads to a shift in the frequency of the $\alpha$-helical component band from 1655 $cm^{-1}$ down to near 1645 $cm^{-1}$ (daCosta and Baenziger, 2009; Methot et al., 1995). Enhanced peptide N-$^1$H for N-$^2$H exchange is further demonstrated by a reduction in the residual intensity of the amide II band centered near 1547 $cm^{-1}$ in spectra of POPC-nAChR versus Aso-nAChR. The amide II band shifts in frequency from 1547 $cm^{-1}$ down to 1450 $cm^{-1}$ upon peptide N-$^1$H for N-$^2$H exchange (Baenziger and Methot, 1995; Methot et al., 1995). As noted in the introduction, this enhanced peptide N-$^1$H for N-$^2$H exchange may reflect weakened interactions between the ABD and TMD leading to increased solvent exposure of the ABD/TMD interface in the uncoupled state. Significantly, the amide I bands in spectra recorded from the di14:1PC-nAChR, di18:1PC-nAChR and di22:1PC-nAChR are essentially identical to those observed for the uncoupled POPC-nAChR in that each

exhibits a slightly reduced intensity near 1655 $cm^{-1}$ (Figure 2.2A). Additionally, di14:1PC-nAChR, di18:1PC-nAChR and di22:1PC-nAChR each exhibits enhanced peptide N-$^{1}$H for N-$^{2}$H exchange. The spectral data suggest that membrane hydrophobic thickness does not influence the global secondary structure of the nAChR. The data also suggest that in each of the PC membranes, the nAChR is stabilized in an uncoupled state, regardless of membrane hydrophobic thickness.

Note that as an additional quality control of our purifications and reconstitutions, others (I performed di22:1PC-nAChR replicates) examined the thermal stability of the nAChR in the various reconstituted membranes (Figure 2.2B). Each exhibited a thermal denaturation temperature near 52°C, further suggesting that membrane hydrophobic thickness has no impact on the global structure. The nAChR in coupled conformations, however, exhibits a slightly higher thermal denaturation temperature (around 56°C) with greater cooperativity in unfolding than the uncoupled nAChR (daCosta et al., 2013). Both the lower thermal denaturation temperature and reduced cooperativity of unfolding observed for di14:1PC-nAChR, di18:1PC-nAChR and di22:1PC-nAChR further suggest they are stabilized in an uncoupled state.

### 2.3.2 The Effect of Membrane Hydrophobic Thickness on Agonist-Induced Conformational Transitions

We next examined whether membrane hydrophobic thickness influences the ability of the nAChR to undergo agonist-induced conformational transitions. Note that given the above data suggesting that di14:1PC-nAChR, di18:1PC and di22:1PC is stabilized in the uncoupled conformation, we expected that none of these samples would respond to agonist binding. We first examined function using IR difference spectroscopy, a technique that detects subtle agonist-induced shifts in molecular

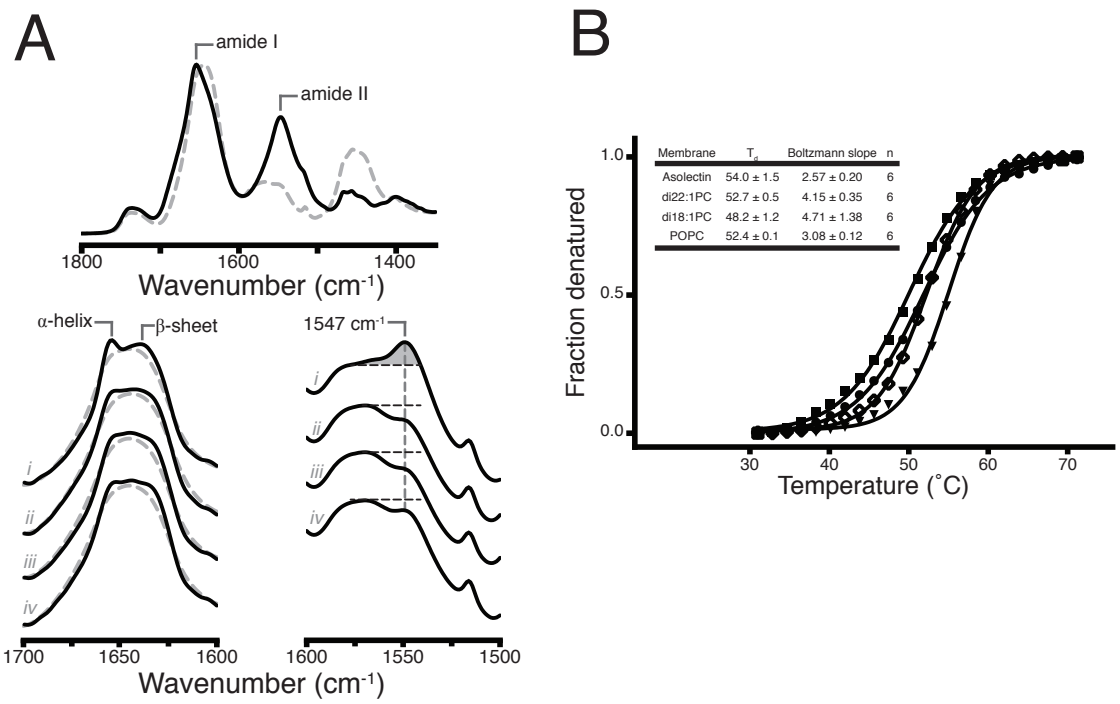


**Figure 2.2. The Effect of Hydrophobic Thickness on the nAChR Secondary Structure and Thermal Stability.** (A) The IR spectra recorded in either $^{1}H_2O$ (solid black line) or $^{2}H_2O$ (dashed grey line), highlighting the amide I (1700-1600 $cm^{-1}$) and amide II (1580-1500 $cm^{-1}$) polypeptide backbone vibrations. The lower left panel shows the amide I spectra and the lower right panel shows the amide II spectra recorded from (i) Aso-nAChR, (ii) di22:1PC-nAChR, (iii) di18:1PC-nAChR, and (iv) POPC-nAChR. In each case the amide I band was deconvolved (solid black line) to highlight the α-helix (~1655 $cm^{-1}$) and β-sheet (~1630 $cm^{-1}$) component. The amide II bands are centered around 1547 $cm^{-1}$. The horizontal dashed lines and shading provide visual reference for the amount of peptide N-$^{1}H$/N-$^{2}H$ exchange. (B) Thermal denaturation of (▼) Aso-nAChR, (●) di22:1PC-nAChR, (■) di18:1PC-nAChR, and (◇) POPC-nAChR. Values are presented ± the standard deviation, and the increasing slope reflects a decrease in the cooperativity. Data collected for (A) is a combination of my data with the previous students data, while the di22:1PC-nAChR data in (B) is a combination of my data with the previous students data.

vibrations. In this case we used the agonist carbamylcholine chloride (Carb), thus referring to the difference spectra as Carb difference spectra (Baenziger and Methot, 1995; Ryan et al., 2002). Here, we focus on a small region of the difference spectra between 1500 and 1800 $cm^{-1}$ (Figure 2.3A).

One band in this region reflects nAChR-bound Carb (a positive intensity centered at 1724 $cm^{-1}$), demonstrating that Carb is capable of binding to the resting Aso-nAChR and the uncoupled POPC-nAChR (daCosta et al., 2011; Ryan et al., 2002). Bands at 1515 and 1620 $cm^{-1}$ reflect the physical interactions between the quaternary amine of Carb and binding site aromatics (Ryan et al., 1996). The relative intensities of the peaks at 1515 and 1620 $cm^{-1}$ are lower in difference spectra recorded from POPC-nAChR, likely due to the altered ABD binding pocket of the uncoupled state (daCosta and Baenziger, 2009). Finally, the two relatively intense amide I and II vibrations observed near 1655 and 1547 $cm^{-1}$, respectively, reflect structural changes in the polypeptide backbone associated with the conformational transition from resting to desensitized states (Baenziger et al., 1993; Ryan and Baenziger, 1999). The strong positive intensity at these two frequencies in difference spectra recorded from Aso-nAChR suggests that it is predominantly in the resting state, and undergoes Carb-induced transitions to the desensitized state. These vibrations are much weaker or absent in difference spectra recorded from POPC-nAChR, consistent with POPC-nAChR being stabilized in an uncoupled conformation that does not undergo agonist-induced conformational transitions (Baenziger et al., 1993; Ryan and Baenziger, 1999).

Difference spectra recorded for di18:1PC-nAChR and di22:1PC-nAChR show a positive peak at 1724 $cm^{-1}$, indicative of Carb binding. In addition, di18:1PC-nAChR and di22:1PC-nAChR show similar intensities to POPC-nAChR in regards to the two peaks that correspond to Carb's interactions with the binding pocket aromatics (at

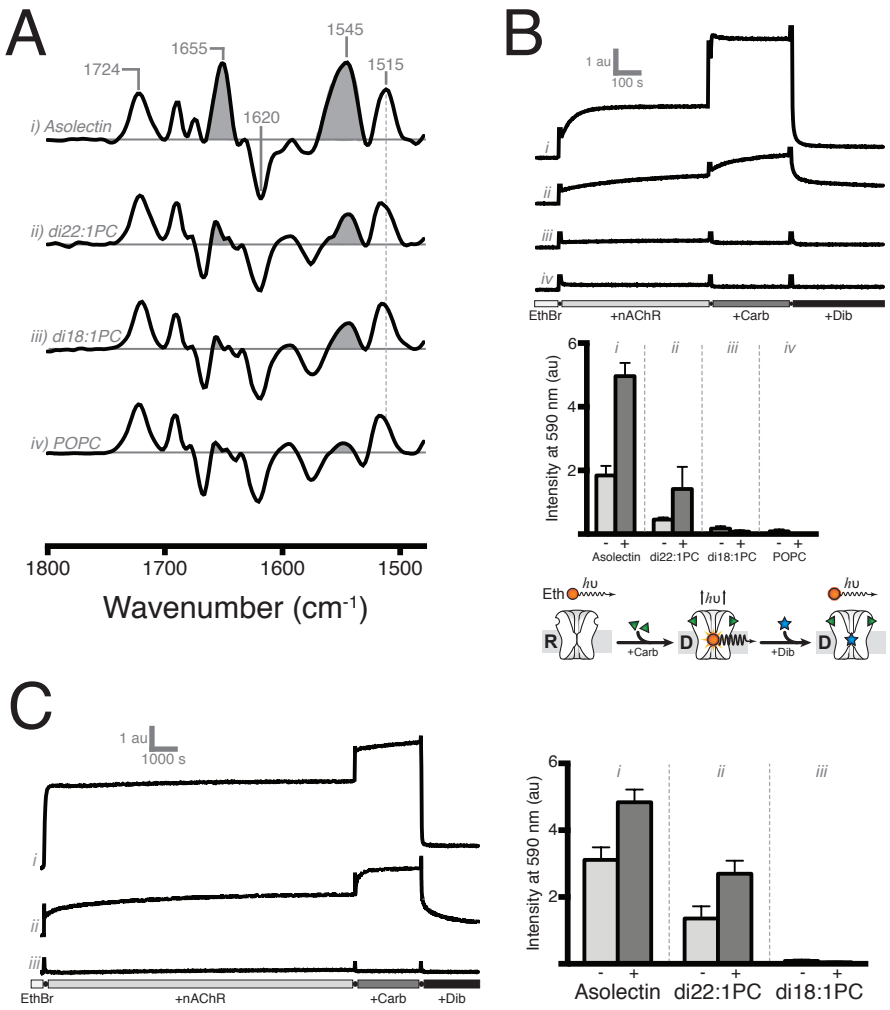


**Figure 2.3. The Effect of Hydrophobic Thickness on the nAChR's Conformational Transitions.** (A) Carb-difference spectra recorded from the nAChR reconstituted into the noted membranes. Vibrations due to the nAChR-bound Carb (1724 $cm^{-1}$), physical interactions between the quaternary amine of Carb and binding site aromatic residues (1620 $cm^{-1}$ and 1515 $cm^{-1}$) and structural changes associated with the resting to desensitized transitions (1655 $cm^{-1}$ and 1545 $cm^{-1}$) are highlighted. (B) EthBr fluorescence emission intensity (shown as arbitrary units (au)) plotted as a function of time after addition of the same reconstituted nAChR membrane studied in A. At the indicated time points, nAChR membranes, 500 μM Carb, 500 μM dibucaine (Dib) were added. Traces are the average of six individual experiments recorded from at least two separate affinity purifications and reconstitutions. The bottom schematic represents the changes in fluorescence that occurs upon the addition of the nAChR, Carb, and Dib. (C) Extended EthBr kinetic experiments performed with (i) Aso-nAChR, (ii) di22:1PC-nAChR, and (iii) di18:1PC-nAChR. Traces are the average of four separate measurements from at least two affinity purifications and reconstitutions. In B and C, the Dib-displaceable fluorescence intensity changes are summarized as a bar graph, shown with the s.d. Data shown in panels (A) and (B) are a combination of my data with the previous students data.

1515 and 1620 $cm^{-1}$). Consistent with the POPC-nAChR, the di18:1PC-nAChR show similar peak intensities at 1655 and 1547 $cm^{-1}$. However, the di22:1PC-nAChR displays a slight increase in intensity at 1655 and 1547 $cm^{-1}$, which hints at a small population of receptors that transition to the desensitized state on the timescale of the difference spectra measurements ($\sim$7 min after Carb addition).

I further characterized (on a longer time scale) the effect of hydrophobic thickness on nAChR function using the conformationally selective fluorescent probe, ethidium bromide (EthBr) (Figure 2.3B and Figure 2.3C). EthBr exhibits an $\sim$1000-fold higher affinity for the desensitized state (Kd $\approx$ 0.3 μM) versus the resting state (Kd $\approx$ 1 mM) (Herz et al., 1987). The fluorescence emission intensity also increases 13-fold upon nAChR pore binding. In a kinetic binding assay, the addition of Aso-nAChR to a 0.3 μM EthBr solution leads to a small increase in fluorescence emission intensity as EthBr binds to nAChRs that pre-exist in the desensitized state, although some of the apparent increase in fluorescence intensity reflects scattering from the proteoliposomes (Herz et al., 1987). Addition of Carb results in a rapid increase in fluorescence as resting state nAChRs transition to the high EthBr binding affinity open and then desensitized conformation (see below). This increase in fluorescence is displaced by the addition of a competitive binding channel pore blocker, dibucaine. In contrast, no dibucaine-displaceable EthBr binding to POPC-nAChR is observed both before and after Carb addition. The absence of EthBr binding is consistent with POPC-nAChR being predominantly stabilized in a low affinity uncoupled conformation that does not transition to the desensitized state (daCosta and Baenziger, 2009).

Similar kinetic ethidium binding experiments were also performed with di14:1PC-nAChR, di18:1-PC-nAChR, and di22:1PC-nAChR. No detectable EthBr binding was observed for either di14:1PC-nAchR or di18:1PC-nAChR in the

presence or absence of Carb, consistent with both samples adopting an uncoupled conformation. To our great surprise, however, di22:1PC-nAChR exhibited slow EthBr binding over time, which is further sped up by the addition of Carb. In comparison to the Aso-nAChR samples, EthBr binding to di22:1Pc-nAChR is significantly slower as it occurs over the minutes to hours time scale (in Aso-nAChR these transitions occur on the seconds to minutes timescale). Thus, the thicker di22:1PC membrane is capable of stabilizing a nAChR that can undergo conformational transitions to the desensitized state.

### 2.3.3 Thicker PC Membranes Facilitate Transitions from the Uncoupled to the Coupled State

To better elucidate the events that lead EthBr binding to the di22:1PC-nAChR, I further analyzed the kinetics of EthBr binding to the nAChR (Figure 2.4). Despite being initially stabilized in an uncoupled conformation, it is intriguing that the di22:1PC-nAChR is capable of binding EthBr, albeit very slowly. Previous studies in our lab had established that EthBr binds essentially instantaneously and with a high affinity to the open state after the addition of Carb (daCosta et al., 2009). However, before the addition of Carb to Aso-nAChR, we observe EthBr binding to receptors that are already stabilized in a desensitized conformation. The rate of binding to these desensitized conformations could be governed by access to the desensitized pore. Alternatively, the rate of binding could reflect the rates of transient excursions of desensitized nAChRs into the highly accessible open state. Transient excursions from the desensitized to the open conformations are also thought to control the displacement of EthBr by noncompetitive channel blockers, such as dibucaine (Herz et al., 1991). To test whether the rate of binding is governed by access to the desensitized pore, I compared the rate of binding to Aso-nAChR in the absence of

A

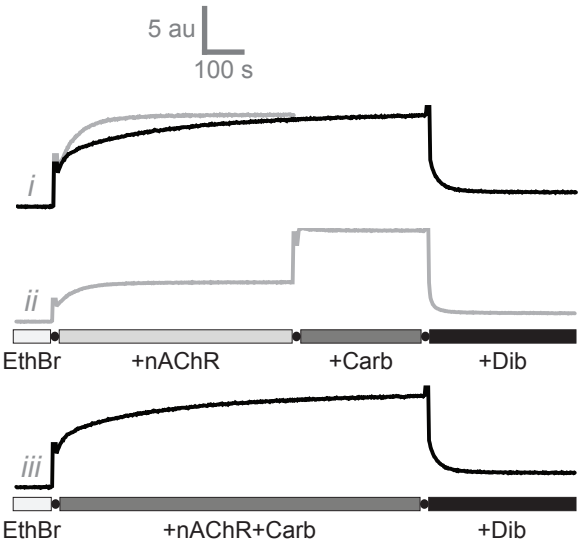


B

Best Fit Parameters for Ethidium Binding

| Membrane (curve fit phase) | no Carb $T_{\frac{1}{2}}$ (s)[a] | % | with Carb $T_{\frac{1}{2}}$ (s)[a] | % | Dibucaine Displacement $T_{\frac{1}{2}}$ (s)[a] | % |
|---|---|---|---|---|---|---|
| Asolectin | | | | | | |
| (1) | 38 | 100 | —[b] | —[b] | 1 | 78 |
| (2) | | | | | 13 | 22 |
| Asolectin Desensitized | | | | | | |
| (1) | — | — | 14 | 32 | — | — |
| (2) | | | 217 | 68 | | |
| di22:1PC | | | | | | |
| (1) | 176 | 35 | 36 | 61 | 20 | 43 |
| (2) | 3126 | 65 | 282 | 39 | 503 | 57 |
| PCPA | | | | | | |
| (1) | 96 | 100 | —[b] | —[b] | 1 | 96 |
| (2) | | | | | 18 | 4 |
| PCPG | | | | | | |
| (1) | 138 | 100 | —[b] | —[b] | 3 | 89 |
| (2) | | | | | 23 | 11 |
| PCPS | | | | | | |
| (1) | 140 | 100 | —[b] | —[b] | 4 | 72 |
| (2) | | | | | 24 | 28 |
| PCChol | | | | | | |
| (1) | —[c] | —[c] | 4 | 39 | 10 | 34 |
| (2) | | | 44 | 61 | 28 | 66 |

[a]Parameters from fitting with 1 or 2 phase exponential
[b]Binding within mixing time
[c]Insufficient binding observed to measure binding rate

**Figure 2.4. The Kinetics of EthBr Binding to the nAChR.** (A) The fluorescence emission intensity of EthBr recorded as a function of time after the addition of Aso-nAChR ii) without (grey line) or iii) with (black line) 30 min prior incubation with Carb. Traces are superimposed in i) highlighting the difference rates of EthBr binding under the two different conditions. (B) Results from the curve fitting of the EthBr binding data. The data (except for Aso-nAChR and di22:1PC-nAChR) was obtained from a previous publication, I performed the curve fits.

Carb, and after preincubation with Carb for 30 min to promote desensitization. If binding is governed by access to the desensitized pore, then I expected these rates of binding in both conditions to be the same. In contrast, the binding of EthBr to desensitized Aso-nAChR in the absence of Carb is faster than to Carb-induced desensitized Aso-nAChR, suggesting that binding is governed by transient excursions to the open state. Note that while individual nAChRs undergo rapid openings, the rates of EthBr binding report on the stochastic behaviour of the total nAChR population, which are governed by the activation energies leading to the open state (Herz et al., 1991).

The rate of EthBr binding to the thick di22:1PC-nAChR both in the presence and absence of Carb is remarkably slower than what is observed in Aso-nAChR and other reconstitutions that include anionic lipids, suggesting that the excursions to the open state occur much less frequently after Carb addition to di22:1PC-nAChR. Given that di22:1PC-nAChR is stabilized in an uncoupled conformation prior to ligand addition, the very slow component of EthBr binding in the absence of Carb is likely the result of an EthBr induced transition from the uncoupled to coupled conformations. These very slow transitions suggest that the transition between uncoupled and coupled conformations act as a rate-limiting step. The activation energy between uncoupled and coupled conformations is likely much higher than the activation energy barriers between the resting, open, and desensitized conformations. Note that the activation energy between uncoupled and coupled conformations in thinner PC membranes lacking activating lipids is likely much higher, acting as an insurmountable barrier to prevent any detectable conformational transitions from occurring on the time scale of our experiments. In contrast, the thicker di22:1PC membranes are capable of sufficiently lowering the activation energy of the nAChR to promote transitions between the uncoupled and coupled conformations – i.e. the thicker membranes promote activation by a kinetic

mechanism (see below).

### 2.3.4 Functional Effects of Cholesterol on the nAChR

Chol's effect on the nAChR is still poorly understood. Chol is a neutral lipid that increases the ordering of the lipid bilayer, which in turn increases membrane hydrophobic thickness (Andersen and Koeppe, 2007; Lundbaek et al., 2003). It has also been suggested to influence nAChR function through direct interactions with the TMD, however definitive binding sites remain to be elucidated (Brannigan et al., 2008; Jones and McNamee, 1988). To better develop a sense of how Chol might influence the nAChR, I reconstituted and characterized the nAChR in a POPC/Chol (3:2, mol/mol) membrane (POPC/Chol-nAChR). Using EthBr, I found that the POPC/Chol membranes stabilize a small proportion of desensitized nAChRs, consistent with its proposed role as a conformational selection modulator (Figure 2.5). However, there also exists a slow carb-induced component to EthBr binding to POPC/Chol-nAChR, suggesting that the presence of Chol (like di22:1PC) may promote slow transitions between the uncoupled to coupled conformations through changes in bulk membrane physical properties.

### 2.3.5 The Link Between Temperature and nAChR Conformational Transitions

We also considered the possibility that it was not membrane hydrophobic thickness, per se, but in fact the temperature of the membrane relative to its gel to liquid crystal phase transition that governed conformational transitions in our reconstituted membranes. Specifically, POPC and di22:1PC have different gel-to-liquid transitions (POPC $\sim$-1.8$^{o}$C; di22:1PC $\sim$13.2$^{o}$C). The interval between the gel-to-liquid transitions was not consistent during our experiments (22.5$^{o}$C). In order to rule out any temperature effects on POPC-nAChR function, I measured the

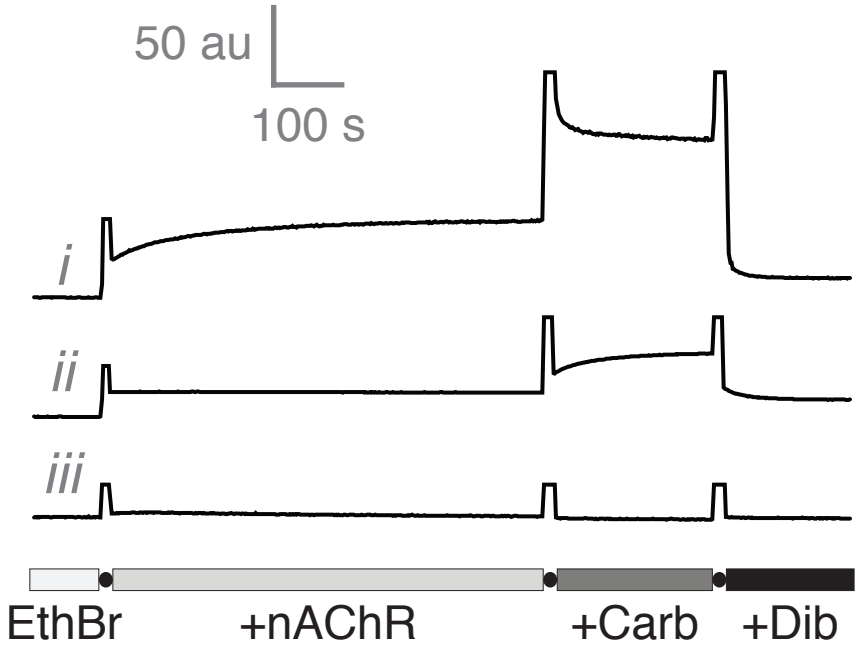


**Figure 2.5. The Effect of Cholesterol on the nAChR's Conformational Transitions.** EthBr fluorescence emission intensity plotted in arbitrary units (au) as a function of time. Spectra are recorded from (i) PC/PA(3:2,mol:mol)-nAChR, (ii) PC/Chol(3:2,mol:mol)-nAChR, and (iii) POPC-nAChR. PC/PA-nAChR data was obtained from previous students, while the POPC/Chol-nAChR data is my own data. The POPC-nAChR traces are a combination of my data with previous data.

effects of temperature, ranging from roughly 5 to 30°C above the gel-to-liquid phase transition temperature, on the ability of POPC-nAChR to undergo conformational transitions (Figure 2.6). Regardless of the temperature, the POPC-nAChR showed no EthBr binding, and thus was locked in an uncoupled conformation. In contrast, nAChR reconstitutions that contain PA are capable of undergoing conformational transitions throughout a variety of temperatures both above and below the gel-to-liquid crystal phase transitions of the reconstituted bilayer (daCosta et al., 2002). The ability of the nAChR to transition between uncoupled and coupled conformations likely has no connection to the temperature interval between the gel-to-liquid crystal phase transition temperature and the temperature of the system.

## 2.4 Discussion

Considerable research over the past 30 years on nAChR-lipid interactions has suggested that neutral and/or anionic lipids are essential to support a nAChR conformation that responds to agonist binding by undergoing conformational transitions. As a result, we expected membrane hydrophobic thickness to simply modulate the functional effects of these activating lipids. However, much to our surprise, the increased hydrophobic thickness of di22:1PC-nAChR promotes conformational transitions in the absence of both neutral and anionic lipids, demonstrating that nAChR activity can be achieved in the absence of activating lipids, as long as there is an appropriate physical environment.

The data in my lab suggest that lipids can influence the nAChRs response to agonist via two distinct thermodynamic mechanisms, a conformational selective and a kinetic mechanism (Figure 2.7) (Andersen and Koeppe, 2007). Different proportions of activatable resting versus non-activatable (uncoupled and desensitized) conformation can be obtained by the presence of different proportions

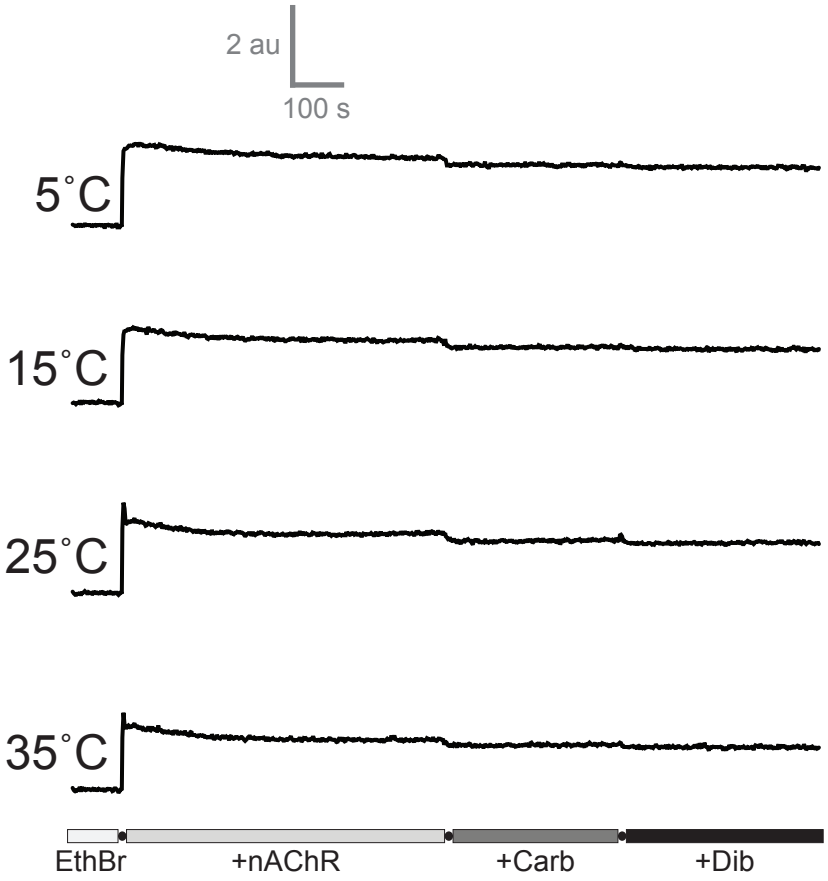


**Figure 2.6. The Effect of Temperature on the Conformational Transitions of POPC-nAChR.** No EthBr binding is detected within the temperature range of the experiment (5-30˚C), showing that the POPC-nAChR is locked in an uncoupled conformation. Thus, the temperatures close to or well above the gel-to-liquid crystal phase transitions of POPC have no impact on conformational transitions in the POPC-nAChR reconstitution. I performed the experiment for this figure.

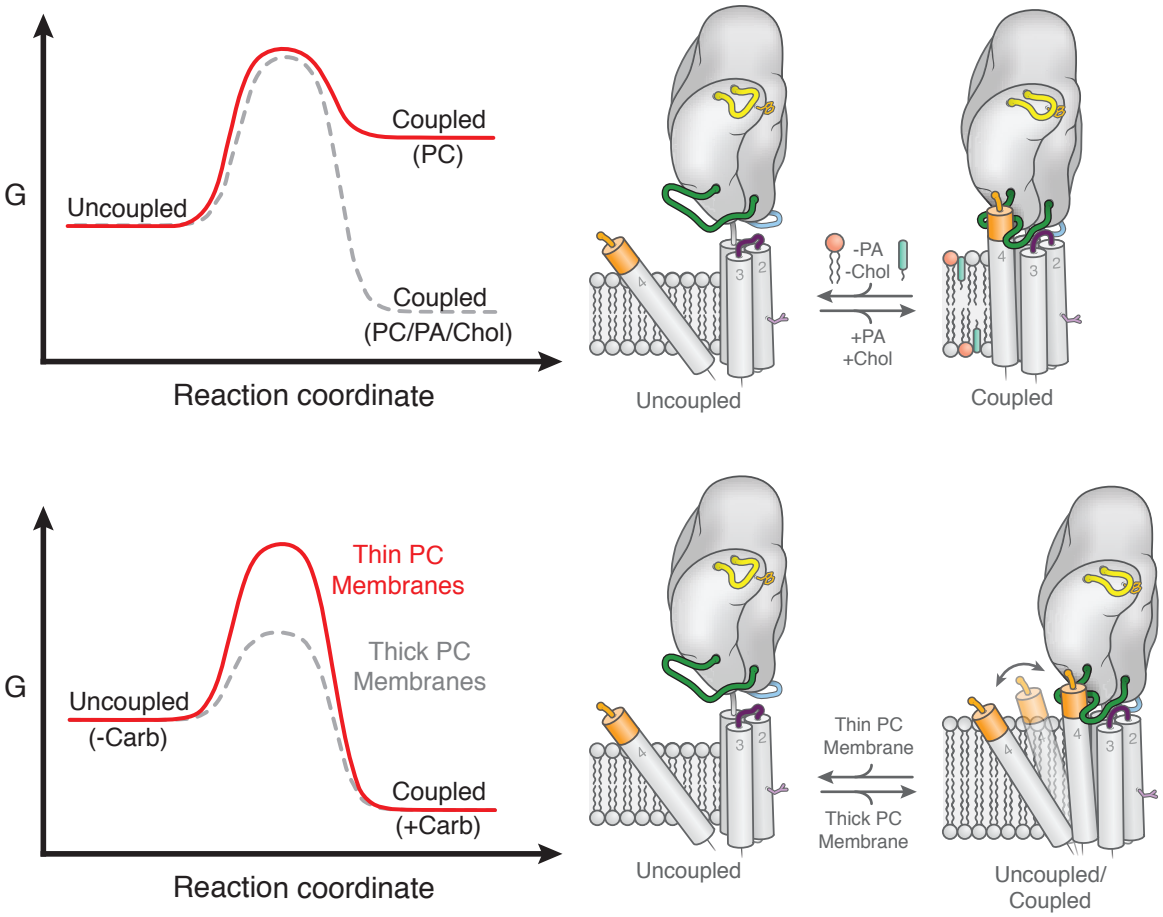


**Figure 2.7. Proposed Models of the Conformational Selection and Kinetic Mechanisms of nAChR-Lipid Interactions.** In each case a single subunit is shown, highlighting key structures: the β1-β2 loop (light blue), the Cys-loop (green), the M2-M3 linker (purple), and the C-terminus of M4 (orange). The conformational selection mechanism is shown in the top panel; the kinetic mechanism is shown in the bottom panel.

of anionic lipids (daCosta, et al., 2009). In those cases, the lipids shape nAChR function through a conformational selective mechanism. In contrast, activity of the nAChR in the thicker di22:1PC membrane occurs through a kinetic mechanism, which allow for dynamic transitions between uncoupled and coupled conformations as a result of the lowered energetic barrier between the conformations. Thinner PC membranes preferentially stabilize an uncoupled nAChR, and the nAChR is incapable of overcoming the high energetic barrier between the uncoupled and coupled conformations. Interestingly, Chol's effect may be a combination of both the conformational selective and kinetic mechanisms, stabilizing a proportion of coupled receptors and promoting transitions from uncoupled to coupled conformations. The former might occur through direct interactions with the TMD, while the latter may occur via an effect on the bulk physical properties of the membrane (Brannigan et al., 2008; Jones and McNamee, 1988; Lundbaek et al., 2003).

The effects of membrane hydrophobic thickness on nAChR function can be rationalized in terms of the current model of lipid-dependent uncoupling. This model suggest that lipids influence how M4 interacts with the adjacent $\alpha$-helices M1 and M3, which allow it to extend beyond the lipid bilayer to interact with the directly with the ABD through the Cys-loop (daCosta and Baenziger, 2009). Upon reconstitution into a model membrane, the interactions between M4, M1/M3 and the Cys-loop could be stabilized through the direct binding of neural and/or anionic lipids. In their absence, M4 may tilt away from M1/M3 to interact more effectively with the lipid bilayer. In thinner PC membranes, there may be an insurmountable energy barrier between M4 tilted away from M1/M3 and M4 bound to M1/M3, thus leading to insurmountable transitions between uncoupled and coupled conformations. The thicker di22:1PC membranes, however, could have a sufficient thick hydrophobic core that allows the M4 to transition between uncoupled and coupled conformations, as a result of the reduced exposure of M4's hydrophobic segments with the aqueous

environment.

This model implies that the interactions between M4 and both M1/M3 and the Cys-loop are dynamic. The M4 of the nAChR contains few anchoring residues (which include tryptophan, lysine, or arginine residues), which have the capacity to interact with the surrounding lipid head groups (de Planque and Killian, 2003). Additionally, the M4 across various nAChR subunits are longer than the adjacent M1 and M3 transmembrane $\alpha$-helices. Thus, the lack of anchoring residues and additional length of M4 could be additional factors that influence the sensitivity of M4 to the hydrophobic thickness of the lipid bilayer.

The sensitivity of the nAChR to hydrophobic thickness may have biological implication. Neuronal nAChRs traffic to the cell surface via lipid rafts, with the disruption of these rafts resulting in altered cell surface expression and nAChR function (Baier et al., 2010; Borroni and Barrantes, 2011). Lipid rafts tend to be rich in cholesterol and sphingolipids, which increase the ordering of the lipid acyl chains, thus increasing membrane hydrophobic thickness. Partitioning the nAChR into these lipid rafts could favour transitions from uncoupled to coupled conformations. Lastly, a more speculative hypothesis suggests that shuttling the nAChR from thinner to thicker membrane environments at the cell surface could influence the number of activatable nAChRs.

# Chapter 3

## Two Distinct Transmembrane Domain Archetypes for Pentameric Ligand-Gated Ion Channels

## 3.1 Introduction

The outermost TMD α-helix, M4, in each of the nAChR's subunits is likely involved in lipid sensing, and thus likely influences channel function (Hénault et al., 2015). One model proposes that lipid-M4 interactions influence function by modulating M4 "binding" to the adjacent transmembrane α-helices, M1 and M3 (daCosta and Baenziger, 2009). Recent studies on GLIC and ELIC support this proposed role of M4 in both channel function and lipid sensing. In the GLIC crystal structure, M4 "binds" tightly to M1/M3 along its entire length, with critical interactions formed between residues on the M4 C-terminus, the M3 N-terminus and the β6-β7 loop (Figure 3.1) (Bocquet et al., 2009; Henault et al., 2015; Hilf and Dutzler, 2009). In ELIC, the final five C-terminal residues are unresolved, suggesting weak M4 C-terminal interactions with both M1/M3 and the ABD β6-β7 loop (Hilf and Dutzler, 2008). Significantly, mutations that weaken M4-M1/M3 interactions in GLIC hinder or eliminate channel folding and/or function, while mutations that enhance M4-M1/M3 interactions in ELIC potentiate channel function (Carswell et al., 2015b; Henault et al., 2015). The intrinsic strengths of M4-M1/M3 interactions also govern the sensitivities of the two pLGICs to both their lipid environments and the potentiating effects of a lipid facing mutation that in the nAChR leads to a congenital myasthenic syndrome (Carswell et al., 2015a; Carswell et al., 2015b; Labriola et al., 2013).

Although a role for aromatic residues in M4-M1/M3 interactions has been established, there is surprising variability in interface chemistry across the pLGIC superfamily (Carswell et al., 2015b; Haeger et al., 2010; Henault et al., 2015). The goal of the research presented in this chapter was to explore the relative functional importance of aromatic, polar and nonpolar interactions at the M4-M1/M3 interfaces of GLIC and ELIC. To assess the relative importance of these residues, I examined the effects of mutations of every M4-facing residue along M1 and M3 on GLIC and

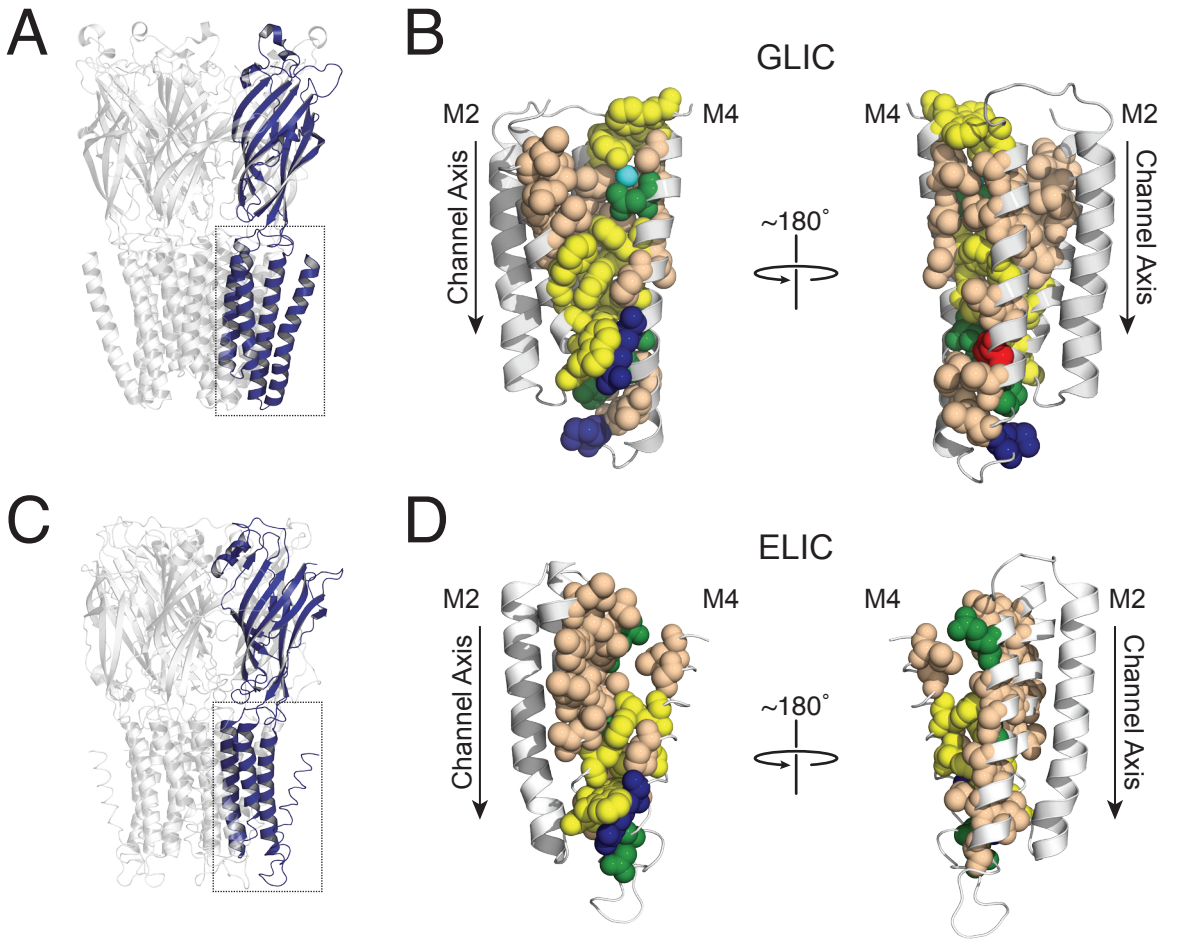


**Figure 3.1. Chemistry of the M4-M1/M3 Interface in GLIC and ELIC.** Full structures of GLIC (A, PDB: 4HFI) and ELIC (C, PDB: 2VL0) are shown as cartoon representations. The grey box highlights the TMD region of interest in a single subunit (shown in blue). The TMD from a single subunit of GLIC (B, PDB: 4HFI) and ELIC (D, PDB: 2VL0) is shown, highlighting the different chemistries found at the M4-M1/M3 interface. Residues are coloured depending on their properties, aliphatic (tan), aromatic (yellow), hydrogen bonding (green), negatively charged (red), and positively charged (blue). A water molecule in GLIC's M4-M1/M3 interface is also shown (cyan).

ELIC function. I also combined my data with that obtained in a recent study, which explored the functional role of M1/M3-facing residues along M4 in GLIC and ELIC function (Henault et al., 2015). A striking finding of the combined data is that Ala-mutations at this interface in GLIC almost invariably lead to detrimental effects on expression and function, while even analogous mutations in ELIC typically have either little effect or even lead to gains in function. Comparisons of the M4-M1/M3 interface chemistries across the pLGIC superfamily suggest that GLIC and ELIC represent two distinct archetypes in the design of a pLGIC TMD. One archetype, exemplified by GLIC and the glycine receptor, has an extensive network of contacts between M4 and M1/M3 that appear to be optimized for tight binding to promote both folding and function (Du et al., 2015). The other archetype, exemplified by ELIC and many of the nicotinic subunits, has few specific contacts leading to a more malleable structure. These two archetypes may reflect a different balance between the need for strong M4 “binding” to M1/M3 to facilitate folding and thus pentamer formation, and the need for weaker interactions that allow for conformational flexibility of the TMD (Haeger et al., 2010).

## 3.2 Experimental Procedures

### 3.2.1 RNA Constructs for Oocyte Expression

The GLIC and ELIC coding sequences, preceded by an α7 nAChR signal sequence and were cloned into plasmids pSP64 and pTLN, respectively. The two plasmids were linearized by EcoRI and MluI, respectively. The linearized plasmids were then used to produce capped cRNA by in vitro transcription using the mMESSAGE mMACHINE® SP6 kit (Ambion). All mutants were created using QuikChange™ Site Directed Mutagenesis kits (Agilent) and were verified by sequencing (Centre de Recherche du CHUL).

### 3.2.2 Electrophysiology

Stage V-VI oocytes were collected as previously described, injected with cRNA, and allowed to incubate one to four days at 16°C in ND96+ buffer (5 mM HEPES, 96 mM NaCl, 2 mM KCl, 1 mM $MgCl_2$, 1 mM $CaCl_2$, and 2 mM Pyruvate) (Laitko et al., 2006). Whole cell currents were recorded using a two-electrode voltage clamp (TEVC) apparatus (OC-725C oocyte clamp; Holliston, MA). For GLIC, whole cell currents were recorded from injected oocytes (3 – 20 ng cRNA) immersed in MES buffer (140 mM NaCl, 2.8 mM KCl, 2 mM $MgCl_2$, and 10 mM MES). Currents through the plasma membrane in response to pH jumps (pH 7.3 down to the indicated pH values) were measured with the transmembrane voltage clamped at voltages between -20 mV and 40 mV depending on the level of expression, typically 20 mV. For ELIC, whole cell currents were recorded from injected oocytes (0.1 – 10 ng cRNA) immersed in HEPES buffer (150 mM NaCl, 0.5 mM $BaCl_2$, and 10 mM HEPES, pH 7.0). In most cases, currents through the plasma membrane in response to cysteamine concentration jumps (from 0 mM up to the indicated values) were measured with the transmembrane voltage clamped at 30 mV.

Dose responses for each mutant were acquired from at least two different batches of oocytes. Each individual dose-response experiment was fit with a variable slope sigmoidal dose-response and the individual $EC_{50}$'s from each experiment averaged to give the values $\pm$ standard deviation.

## 3.3 Results

To explore how the M4-M1/M3 interface chemistry influences pLGIC function, I generated individual Ala-mutations of each residue on M1 and M3 that faces the M4-M1/M3 interface in both GLIC and ELIC. Others in the lab generated similar data

for M1/M3-facing residues on M4 (Henault et al., 2015). The effects of each mutation on agonist-induced channel gating were characterized using TEVC electrophysiology. The injection of either wild type (WT) or mutant cRNAs into *Xenopus laevis* oocytes for both GLIC and ELIC typically led to robust proton-induced (GLIC) or cysteamine-induced (ELIC) currents across the plasma membrane (Figure 3.2 and Annex Figures 5.1 to 5.4). Numerous mutations in GLIC and one in ELIC, however, did not express and/or function.

The Ala-mutations in GLIC and ELIC led to quantitatively similar effects in that all measured $pH_{50}/EC_{50}$ values were within one full log unit (i.e. $\leq$10-fold) of WT values. The lack of dramatic changes in channel function is not surprising given the predominantly modest changes in chemistry; in addition, the mutated side chains are not directly involved in coupling agonist binding to channel gating (Grutter et al., 2005; Lee and Sine, 2005; Lummis et al., 2005). As the sites of the mutations are distant from the canonical agonist-binding site(s), the changes in $pH_{50}/EC_{50}$ are likely due primarily to the effects on the coupling of binding to gating, not changes in agonist affinity. However, this interpretation for GLIC is less definitive as protonatable His residue at position 235 located at the M2-M1/M3 interface contributes to channel gating (Rienzo et al., 2014; Wang et al., 2012). The studied mutations could alter GLIC function by directly influencing the $pK_a$ of H235.

The qualitative effects of the mutations, however, were different. In GLIC, twelve Ala mutations led to alterations in the $pH_{50}$ of 0.5 log units or more, with nine of these leading to loss-of-function phenotypes. An additional five single mutations and most double mutations of interacting residues led to non-functional and/or non-expressed channels. In contrast, eight Ala substitutions led to changes in the $EC_{50}$ of 0.5 log units or more in ELIC, with seven of these resulting in gain-of-function phenotypes. Only one mutation led to a non-functional and/or non-expressed channel, with one

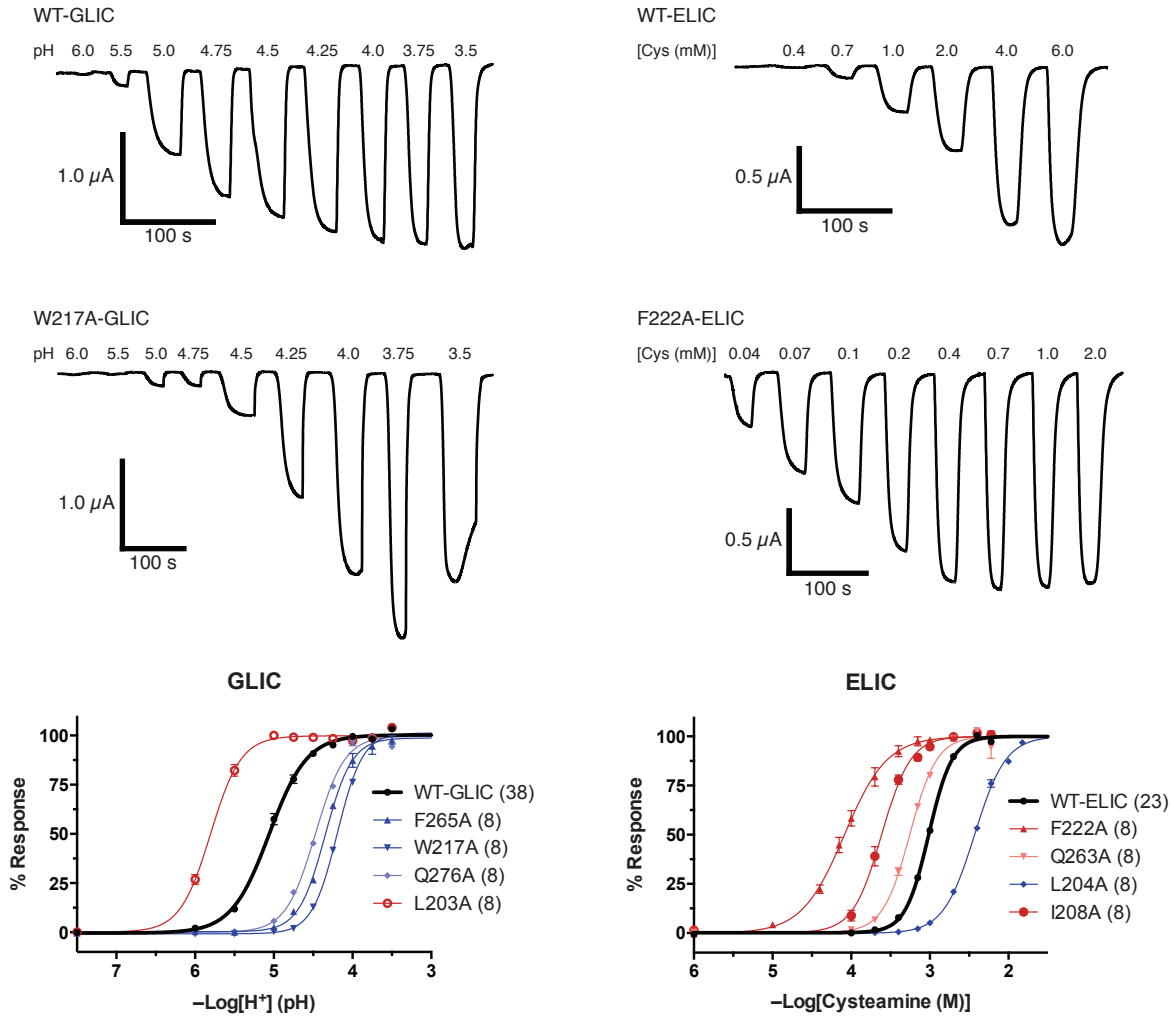


**Figure 3.2. Functional Characterization of the GLIC and ELIC Ala-mutants.** Whole cell electrophysiological traces recorded using two-electrode voltage clamp electrophysiology. Currents were recorded from *Xenopus laevis* oocytes expressing either GLIC (Left panel) or ELIC (Right panel) in response to protons or cysteamine, respectively. The lower panels presents dose response curves (normalized current ($I/I_{max}$) versus ligand concentration) for select Ala mutants, with the number (n) of averaged traces. Error bars represent the standard error.

additional mutant leading to oocyte cell death. Even subtle changes to the M4-M1/M3 interface in GLIC have detrimental effects on channel function, while changes to the M4-M1/M3 interface in ELIC are easily tolerated.

To better understand how the chemistry at the M4-M1/M3 interfaces influences GLIC and ELIC function, the measured $pH_{50}/EC_{50}$ are grouped according to the chemistry of the mutated side chain in Tables 3.1 and 3.2. The functional effects of the mutations are also heat-mapped onto M1, M3 and M4 in Figure 3.3, with a more detailed presentation in Figures 3.4 and 3.5.

### 3.3.1 GLIC aromatic residues

The interface between M4 and M1/M3 in GLIC contains a network of ten interacting aromatic residues, with one additional aromatic, W217 on M1, involved in a cation-π interaction with R296 on M4. These ten aromatic residues interact with each other via canonical π-π stacking or CH-π interactions that fall within the expected aromatic ring center-to-center distances of 4.5 to 7.0 Å (Burley and Petsko, 1985; Waters, 2002). Three interacting aromatic residues located at the M4 C-terminus (F314 and F315) and the M3 N-terminus (Y254) also interact with F121 on the β6-β7 loop to form what I refer to as the “extracellular cluster” (Henault et al., 2015). Another seven interacting residues on M1, M3 and M4 is located primarily in the cytoplasmic leaflet of the bilayer (the “cytoplasmic cluster”) forms the bulk of the contacts between M4 and M1/M3.

Individual Ala-mutations of eight of the ten aromatic residues led to loss-of-function phenotypes, with one of these eight leading to non-expressed or non-functional channels (W213A) and two mutations (between F210A and F299A) having no effect. Of the latter, F210 on M1 interacts only weakly with F303 on M4 (centroid distance of 6.5 Å), while F299 on M4 interacts across the M4-M1/M3

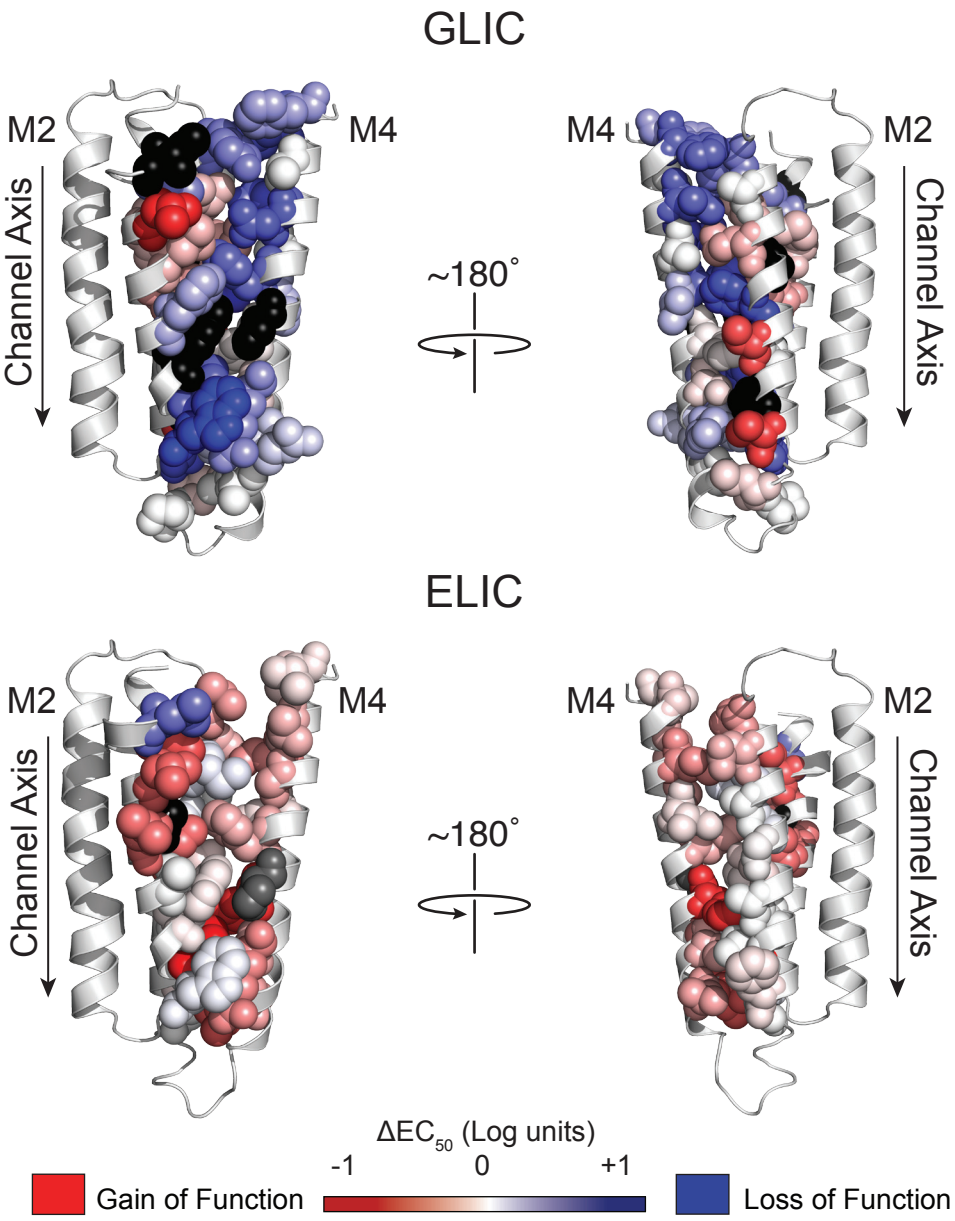


**Figure 3.3. Heat Map of the M4-M1/M3 Interface of GLIC and ELIC.** The top panel heat maps the changes in the $pH_{50}$ values resulting from the Ala-mutation of each individual residue in GLIC (PDB: 4HFI). The magnitude of the shift in $pH_{50}$ is depicted via color intensity, with no change in $pH_{50}$ in white, gain-of-function in red, and loss-of-function in blue. Non-functional mutations are shown in black. The lower panel heat maps (using an ELIC homology model based on the GLIC structure (PDB: 3EHZ)) the changes in the -Log($EC_{50}$) values resulting from the Ala-mutation of each individual residue in ELIC. The magnitude of the shift in -Log($EC_{50}$) is depicted via color intensity, with no change in $EC_{50}$ in white, gain-of-function in red, and loss-of-function in blue. Non-functional mutations are shown in black. The $EC_{50}$ of the corresponding P304A mutant (coloured grey) in ELIC is not presented, due to altered desensitization kinetics.

Table 3.1– The Functional Effects of Alanine Mutations of Residues located at the M4-M1/M3 Interface of GLIC

GLIC[a] (WT $EC_{50}$= 9.33 ± 1.7 μM ($pH_{50}$ = 5.03) n=38)

| Aromatic | | | |
|---|---|---|---|
| TMD α-helix | Mutant | $EC_{50}$ (μM) ($pH_{50}$) | n |
| M1 | F210A | 10.5 ± 1.6 (4.98)[e] | 8 |
| | W213A | NC[b] | 17 |
| | F216A | 35.5 ± 3.1 (4.45)[e] | 8 |
| | W217A | 66.1 ± 3.0 (4.18)[e] | 8 |
| M3 | Y254A | 26.9 ± 1.8 (4.57)[e] | 8 |
| | F265A | 47.9 ± 1.1 (4.32)[e] | 8 |
| M4 | F299A | 9.1 ± 1.7 (5.04)[c] | 6 |
| | F303A | 33.1 ± 6.2 (4.48)[c,e] | 8 |
| | F314A | 33.1 ± 1.5 (4.48)[d,e] | 10 |
| | F315A | 20.4 ± 0.5 (4.69)[d,e] | 8 |
| Charged | | | |
| M3 | E272A | NC[b] | 10 |
| | K280A | 15.1 ± 2.5 (4.82)[e] | 8 |
| M4 | R296A | 22.4 ± 1.5 (4.65)[c,e] | 9 |
| Hydrogen Bonding | | | |
| M3 | Q276A | 36.3 ± 3.2 (4.44)[e] | 8 |
| M4 | T292A | 13.8 ± 1.5 (4.86)[c,e] | 6 |
| | S295A | 7.6 ± 1.6 (5.12)[c] | 6 |
| | N307A | 38.0 ± 0.9 (4.42)[c,e] | 10 |

| Aliphatic | | | |
|---|---|---|---|
| TMD α-helix | Mutant | $EC_{50}$ (μM) ($pH_{50}$) | n |
| M1 | I198A | NC[b] | 10 |
| | I202A | 25.7 ± 3.3 (4.59)[e] | 8 |
| | L203A | 1.6 ± 0.2 (5.79)[e] | 8 |
| | M205A | 6.3 ± 0.4 (5.20) | 8 |
| | L206A | 6.2 ± 0.4 (5.21) | 8 |
| | L209A | 4.9 ± 0.3 (5.31)[g] | 8 |
| M3 | I258A | 6.5 ± 0.8 (5.19) | 8 |
| | M261A | 5.4 ± 0.5 (5.27) | 8 |
| | I262A | NC[b] | 10 |
| | V268A | 2.6 ± 0.2 (5.59)[e] | 8 |
| | V275A | 2.2 ± 0.1 (5.65)[e] | 8 |
| | L279A | 7.2 ± 0.9 (5.14) | 8 |
| M4 | I291A | 16.6 ± 1.8 (4.78)[c,e] | 7 |
| | P300A | NC[c,b] | 8 |
| | V302A | 15.5 ± 1.4 (4.81)[c,f] | 7 |
| | L310A | 33.9 ± 1.5 (4.47)[c,e] | 6 |

[a] Data collected 1-4 day(s) after cRNA injection ($V_{Hold}$ ranging from -20 to -40 mV). Error Values represent the standard deviation.
[b] No current (NC) observed in oocytes after 1-4 day(s) of cRNA injection
[c] Data taken from Henault et al. 2015
[d] Data taken from Carswell et al. 2015b
[e] $p < 0.001$ relative to WT GLIC via one-way ANOVA followed by Dunnet's post hoc test
[f] $p < 0.01$ relative to WT GLIC via one-way ANOVA followed by Dunnet's post hoc test
[g] $p < 0.05$ relative to WT GLIC via one-way ANOVA followed by Dunnet's post hoc test

Table 3.2 – The Functional Effects of Alanine Mutations of Residues located at the M4-M1/M3 Interface of ELIC

ELIC[a] (WT $EC_{50}$ = 0.93 ± 0.13 mM (-Log[$EC_{50}$(M)]) = 3.03) n = 23)

| Aromatic | | | |
|---|---|---|---|
| TMD α-helix | Mutant | $EC_{50}$ (mM) (-Log[$EC_{50}$(M)]) | n |
| M1 | Y219A | 0.91 ± 0.05 (3.04) | 8 |
| | F222A | 0.09 ± 0.03 (4.05)[d] | 8 |
| | W223A | 1.23 ± 0.06 (2.91)[d] | 8 |
| M3 | F281A | 0.88 ± 0.05 (3.06) | 8 |
| M4 | F303A | 0.19 ± 0.07 (3.73)[c,d] | 10 |
| | F307A | 0.57 ± 0.09 (3.24)[c,d] | 8 |

| Charged | | | |
|---|---|---|---|
| M4 | R300A | 0.40 ± 0.05 (3.40)[c,d] | 11 |

| Hydrogen Bonding | | | |
|---|---|---|---|
| M3 | Q263A | 0.58 ± 0.04 (3.24)[d] | 8 |
| | S271A | 0.82 ± 0.05 (3.09) | 8 |
| M4 | C299A | 0.56 ± 0.08 (3.25)[c,d] | 9 |

| Aliphatic | | | |
|---|---|---|---|
| TMD α-helix | Mutant | $EC_{50}$ (mM) (-Log[$EC_{50}$(M)]) | n |
| M1 | L204A | 3.55 ± 0.31 (2.45)[d] | 8 |
| | I208A | 0.25 ± 0.05 (3.60)[d] | 8 |
| | L209A | 0.29 ± 0.05 (3.54)[d] | 8 |
| | G212A | NC[b] | 10 |
| | L213A | 0.32 ± 0.02 (3.49)[d] | 8 |
| | I215A | 0.32 ± 0.04 (3.49)[d] | 8 |
| M3 | V260A | 0.46 ± 0.05 (3.34)[d] | 8 |
| | M264A | 1.29 ± 0.12 (2.89)[d] | 8 |
| | G268A | 1.19 ± 0.14 (2.92)[d] | 8 |
| | G270A | 1.02 ± 0.10 (2.99) | 8 |
| | L278A | 1.07 ± 0.10 (2.97) | 8 |
| M4 | L295A | 0.50 ± 0.10 (3.30)[c,d] | 8 |
| | I296A | 0.27 ± 0.03 (3.57)[c,d] | 10 |
| | P304A | –[c,e] | 10 |
| | I310A | 0.88 ± 0.09 (3.05)[c] | 10 |
| | G311A | 0.51 ± 0.10 (3.29)[c,d] | 11 |
| | L314A | 0.42 ± 0.05 (3.38)[c,d] | 8 |
| | V315A | 0.60 ± 0.08 (3.22)[c,d] | 9 |
| | G318A | 0.76 ± 0.13 (3.12)[c,d] | 10 |
| | I319A | 0.86 ± 0.16 (3.06)[c] | 11 |

[a] Data collected 1-4 day(s) after cRNA injection ($V_{Hold}$ ranging from -20 to -40 mV). Error Values represent the standard deviation.
[b] No current (NC) observed in oocytes after 1-4 day(s) of cRNA injection
[c] Data taken from Henault et al. 2015
[d] $p < 0.001$ relative to WT ELIC via one-way ANOVA followed by Dunnet's post hoc test
[e] Functionally distinct, $EC_{50}$ Values were not obtained.

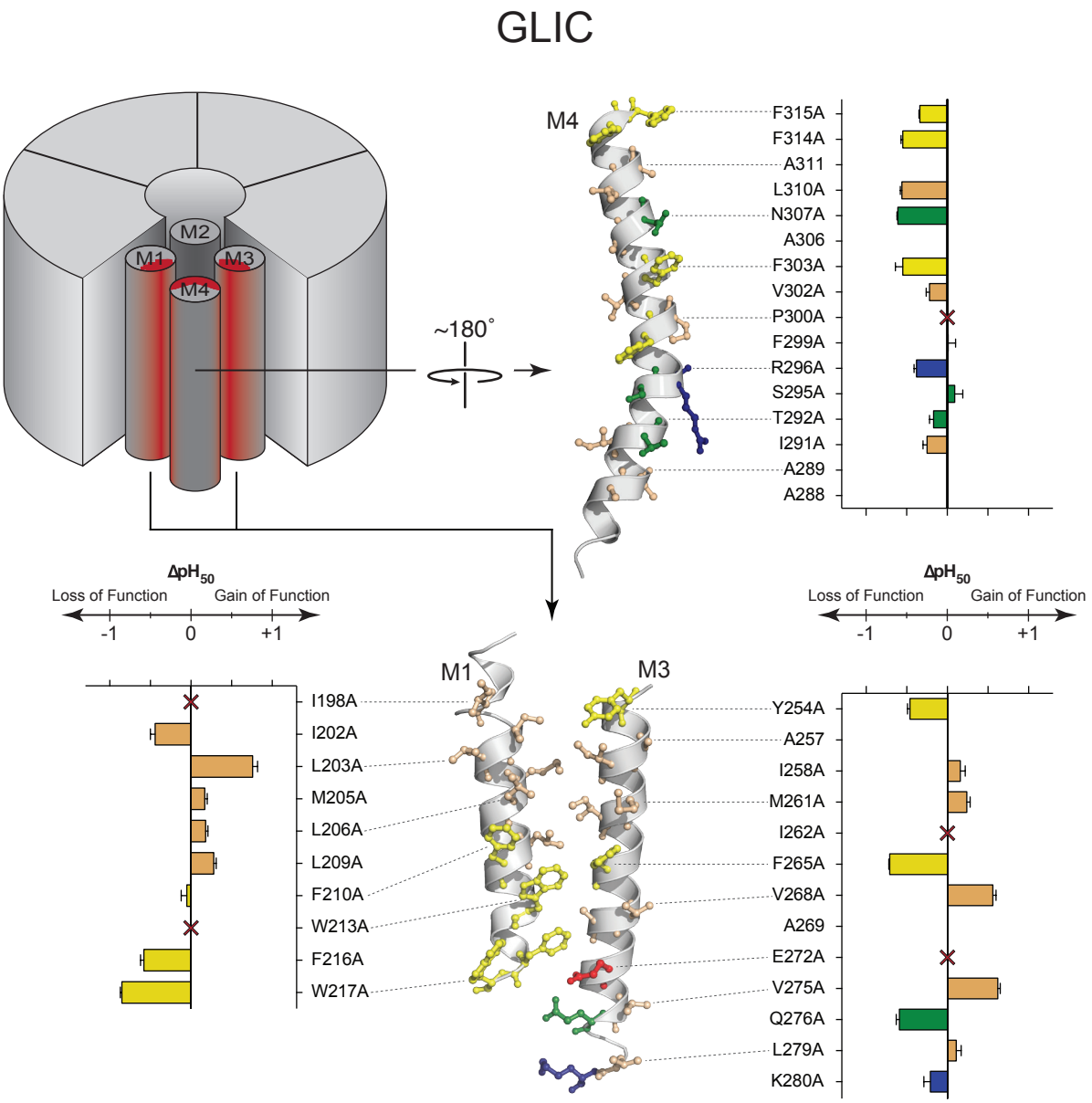


**Figure 3.4. Ala-Scan of the GLIC M4-M1/M3 Interface.** Detailed changes in the $pH_{50}$ of GLIC's M4 (top right panel) and M1/M3 α-helices (bottom panel) (PDB: 4HFI). Residues and bar graph residues follow the same colour scheme as Figure 3.1. The bar graphs represent the magnitude of change ± the standard deviation. Dashed lines are used to show corresponding residues between the graph and structure.

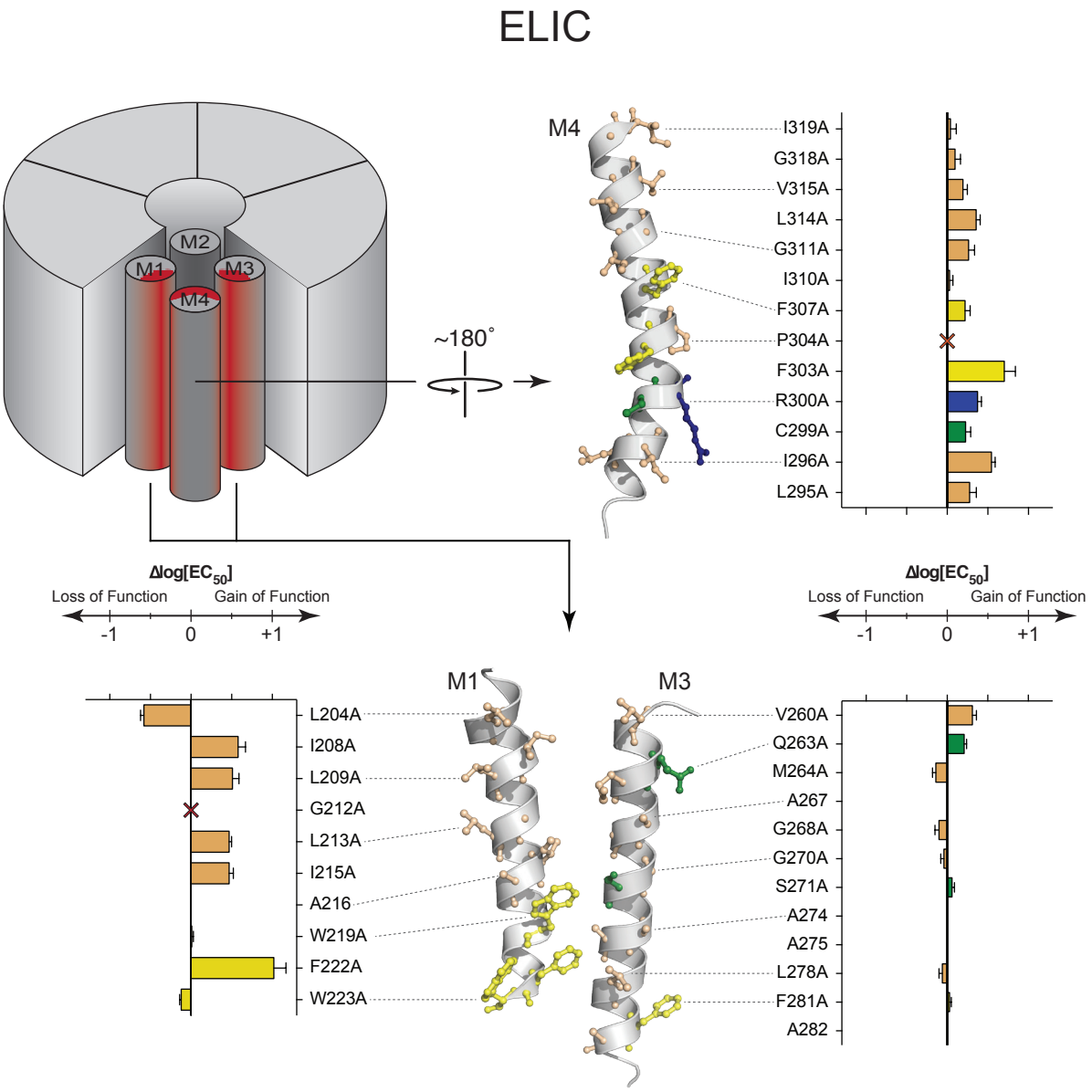


**Figure 3.5. Ala-Scan of the ELIC M4-M1/M3 Interface.** Detailed changes in the -Log($EC_{50}$) of ELIC's M4 (top right panel) and M1/M3 α-helices (bottom panel) (homology model based on the GLIC structure PDB: 3EHZ). Residues and bar graphs residues follow the same colour scheme as Figure 3.1. The bar graphs represent the magnitude of change ± the standard deviation. Dashed lines are used to show corresponding residues between the graph and structure.

interface only weakly with F265 on M3 and W213 on M1 (centroid distances of 6.3 and 6.4 Å, respectively). In the latter case, the cation-$\pi$ interaction between the adjacent R296 on M4 and W217 on M1 may stabilize functionally important M1-M4 interactions despite the F299A mutation. Of all the aromatic-to-Ala substitutions, W217A produced the largest loss-of-function.

While the individual aromatic-to-Ala mutations are suggestive, the critical importance of aromatic interactions at this interface in GLIC is revealed when two interacting aromatic residues are simultaneously mutated to Ala (Table 3.3). Ala mutations of any two of the four aromatic side chains in the extramembranous cluster lead to a complete loss of expression and/or function. The simultaneous Ala substitution of two interacting aromatic residues in the cytoplasmic cluster was also not tolerated in four of five cases. The one double mutant that still functions involve the above noted F210 on M1 and F303 on M4. The double F210A/F303A mutant is only slightly more detrimental to GLIC function than the individual F303A mutation ($pH_{50}$ = 4.26 vs 4.48, respectively), while F210A alone has no effect.

### 3.3.2 GLIC Aliphatic residues

Through van der Waals interactions, aliphatic residues play an important role in transmembrane helix-helix associations (Cymer et al., 2015). In GLIC, Ala mutations of aliphatic residues at the M4-M1/M3 interface show the largest variability in their effects on function. Many of the Ala mutations, however, involve residues that face the M4-M1/M3 interface, but that are not directly involved in M4-M1/M3 interactions. For example, M4-facing residues on the N-terminal half of M1 do not directly contact M4 (Figure 3.1). Two residues on M3, V268 and V275 extend from M3 towards M4, but their contacts with residues on M4 are minimal - they likely interact more extensively with lipids. I262 extends from M3 towards M1 and contacts directly the above noted

Table 3.3 – Double Alanine Mutations Between Pairs of Residues Found Within the M4-M1/M3 Interface

| GLIC[a] | | |
|---|---|---|
| Mutant | $EC_{50}$ (μM) ($pH_{50}$) | n |
| WT-GLIC | 9.33 ± 1.7 (5.03) | 38 |
| Extracellular Cluster | | |
| Y254F | 7.24 ± 0.83 (5.14) | 8 |
| Y254F+N307A | 27.5 ± 6.40 (4.56) | 8 |
| Y254A+N307A | 40.7 ± 9.46 (4.39) | 8 |
| Y254A+F314A | NC[b] | 12 |
| Y254A+F315A | NC[b] | 11 |
| F314A+F315A | NC[b] | 11 |
| Cytoplasmic Cluster | | |
| F210A+F303A | 55.0 ± 11.5 (4.26) | 8 |
| F216A+F299A | NC[b] | 10 |
| W217A+R296A | 40.7 ± 9.46 (4.39) | 8 |
| F265A+F299A | NC[b] | 10 |
| F265A+F303A | NC[b] | 10 |
| Q276A+T292A | 9.55 ± 1.77 (5.02) | 8 |
| F299A+F303A | NC[b] | 10 |
| ELIC[c] | | |
| Mutant | $EC_{50}$ (mM) (-Log[$EC_{50}$(M)]) | n |
| WT-ELIC | 0.93 ± 0.13 (3.03) | 23 |
| Cytoplasmic Cluster | | |
| Y219A+F303A | 0.55 ± 0.12 (3.26) | 8 |
| Y219A+F307A | 0.45 ± 0.07 (3.35) | 8 |
| F222A+C299A | 0.10 ± 0.02 (4.00) | 8 |
| F222A+F303A | -[d] | - |
| W223A+R300A | 0.80 ± 0.11 (3.10) | 8 |
| S271A+F303A | 0.62 ± 0.13 (3.21) | 8 |
| S271A+F307A | 0.77 ± 0.09 (3.11) | 8 |

[a] Data collected 1 day after injection, with a $V_{Hold}$ of -20 mV. Error Values represent the standard deviation.
[b] No current (NC) observed in oocytes after 1-4 day(s)
[c] Data collected 1 day after injection, with a $V_{Hold}$ of -30 mV. Error Values represent the standard deviation.
[d] Injected oocytes gave weak response to cysteamine and died past day 1

H235 on M2, possibly explaining why the I262A mutant leads to a loss of expression and/or function. Many of the changes in function observed with the Ala mutations of aliphatic residues likely occur via mechanisms that do not directly involve the M4-M1/M3 interface.

A few of the aliphatic mutations that alter channel function, however, are notable. L209A, which leads to a modest gain-of-function, is located in a pocket formed by three interacting aromatic residues, F210 and W213 on M1 and F303 on M4 in the intracellular cluster. The smaller Ala side chain may allow greater conformational flexibility to promote more effective aromatic interactions. On the other hand, L310A, which leads to a modest loss of function, is located just below the extracellular cluster of aromatic residues. In this case, the bulky Leu side chain may be advantageous, as it fills a void between M4 and M3 created by the adjacent aromatic residues.

Finally, the Ala-mutation of a proline residue on M4 (P300A) leads to a complete loss of channel expression/function. P300 kinks M4 so that the C-terminus projects towards the N-terminus of M3. P300A will eliminate this kink, and thus should dramatically alter M4-M1/M3 interactions. This mutation highlights the critical importance of M4-M1/M3 interactions in folding, trafficking and/or function. Note that P300 may also interact favourably with the W213 on M1 (Biedermannova et al., 2008).

### 3.3.3 GLIC polar residues

Polar residues are key drivers of helix-helix interactions in the hydrophobic membrane environment (Cymer et al., 2015). Three charged residues are found at the M4-M1/M3 interface in GLIC; E272 and K280 on M3, and R296 on M4. E272 is surrounded by three polar hydrogen bonding residues (Q276, S295, and T292) and forms a weak hydrogen bond with T292 (3.1 Å from proton donor to acceptor). The

E272A mutation did not express and/or function, possibly due to its role solvating these three polar groups. On the other hand, individual mutations of any of these three hydrogen bonding groups had minimal effects on function, with the largest being a modest loss-of-function with the Q276A mutant. Even simultaneous Ala substitutions of the two closest hydrogen bonding residues, Q276A and T292A, had no effect on activity. Interactions with other residues likely satisfy the electrostatic requirements of E272.

As noted above, R296 on M4 forms a cation-$\pi$ interaction with W217 on M1. The R296A mutation leads to a modest loss-of-function ($pH_{50}$ = 4.65), while the W217A mutation leads to the largest quantifiable loss-of-function ($\sim$10-fold) observed in this study. The double R296A/W217A mutation has a similar effect ($pH_{50}$ = 4.39), suggesting that these two residues are energetically coupled and can modestly promote GLIC function.

K280, which is found near the C-terminus of M3, has no potential interacting polar residues on M4 and likely projects into the bilayer to interact with the polar headgroups of lipids. The K280A mutant had no effect on channel function.

Finally, Y254 at the N-terminus of M3 not only interacts with adjacent aromatic residues, but also forms a hydrogen bond with N307 on M4 through an intervening water molecule in four out of the five subunits (Sauguet et al., 2013). Y254 was mutated to both Phe and Ala, and N307 to Ala. Both Ala mutations had modest detrimental effects on channel function. The Y254F/N307A has $EC_{50}$ values close to the $EC_{50}$ value for N307A, suggesting that the H-bonding interactions between Tyr and Asn are not energetically coupled. However, the Y254A/N307A double mutants had $EC_{50}$ values similar to the $EC_{50}$ values of the single mutants. The aromatic group of Y254 and the side chain of N307 are energetically coupled, with the interaction having a positive effect on channel function.

### 3.3.4 ELIC aromatic residues

ELIC contains only six of the ten interacting aromatic residues found at the M4-M1/M3 interface in GLIC, including a Trp residue (W223) on M1 involved in an analogous cation-$\pi$ interaction with R300 on M4. Notably absent are the three aromatic residues that form the extracellular cluster in GLIC. Surprisingly, while the aromatic residues in ELIC share homologous positions with those found in GLIC, Ala substitutions have either little effect or actually lead to gain of function phenotypes. In fact, the F222A mutation leads to a 10-fold gain-of-function, while the same mutation in GLIC (F216A) leads to a loss-of-function. Even more surprising, double Ala mutations of interacting aromatic residues had no detrimental effect on expression and/or function. Even the W223A mutation, which eliminates the cation-$\pi$ interaction with R300, has close to WT activity. In contrast to GLIC, aromatic residues at the M4-M1/M3 interface in ELIC have a negative impact on channel function.

### 3.3.5 ELIC Aliphatic residues

Ala mutations of aliphatic residues at the M4-M1/M3 interface in ELIC lead to $\geq$0.5 log unit changes in $EC_{50}$ in only six of eighteen cases, with only one of these leading to a modest loss-of-function. Ala mutations leading to gain-of-function phenotypes could enhance inter-helix packing to enhance channel function. Alternatively, the smaller side chains may create space that allows greater conformational flexibility to promote conformational change.

Notably, the loss of function Ala mutation, L204A, is located on M1, but does not interact directly with M4. L204 is found at the same position as I198 in GLIC. I198A leads to a complete loss of expression and/or function. G212A, which did not express and/or function, is located in the N-terminal half of M1. Flexibility at this site

appears to be essential for expression and/or function. Finally, P304A on M4 leads to channels with substantially altered desensitization kinetics, which made it impossible to accurately predict the effective $EC_{50}$. The analogous P300A mutation in GLIC is not functional.

### 3.3.6 ELIC polar residues

ELIC has only one charged residue, R300 on M4, which forms a cation-π interaction with W223 on M1. As noted, the W223A mutant had little effect on channel function. Both R300A and the W223A/R300A double mutant led to slight gain-of-function phenotypes, suggesting that unlike in GLIC, this cation-π interaction does not promote channel gating.

ELIC has three hydrogen bonding side chains at the M4-M1/M3 interface, with Q263 and S271 located on M3, and C299 located on M4. None of these residues form strong hydrogen bonds with other polar residues, although S271 and C299 are both close to adjacent aromatic side chains. Mutation of any of these residues alone or in combination with potential interacting partners either led to no change or a decrease in $EC_{50}$, indicating no or gain-of-function phenotypes, respectively.

## 3.4 Discussion

Although Ala mutations of residues at the M4-M1/M3 interface of both GLIC and ELIC typically have modest functional effects (i.e. less than 10-fold), several mutations lead to a loss of expression and/or function and thus highlight the importance of M4-M1/M3 interactions in pLGIC folding and function. The functional consequences also reveal intriguing trends that shed light on both the relative importance of different side chain chemistry at this interface and the potential role(s) played by this chemistry in

pLGIC function.

The data show that aromatic interactions play a defining role at the M4-M1/M3 interface. Aromatic residues form the dominant contacts between M4 and M1/M3 in GLIC and to a lesser degree in ELIC. In GLIC, the aromatic to Ala mutations almost invariably reduce agonist sensitivity or lead to a complete loss of expression and/or function, suggesting that aromatic interactions are essential to both folding and gating. In ELIC, however, the aromatic interactions appear to be detrimental to channel function, with their mutation to Ala often leading to gains in function. The distinct effects of the Ala mutations in GLIC and ELIC will be discussed in more detail below.

In contrast to the effects of the aromatic residue substitutions, both polar and aliphatic residues at the M4-M1/M3 interface seem to have little effect on folding and/or function. A few exceptions to these trends are worth noting:

First, the E276A mutation in GLIC leads to a complete loss of expression and/or function. E276 is located on M3 and projects towards the core of the interface between M4 and M1/M3. The E276A mutation shows that charged residues can play an essential role pLGIC expression and/or function, particularly if they are located at the core of interacting TMD $\alpha$-helices.

Second, two Leu to Ala mutations at the interface between M4-M1/M3 have opposite effects. L209A leads to a modest gain-in-function; L209 is located in a pocket formed by three interacting aromatic residues at the M4-M1/M3 interface. The smaller Ala side chain may allow greater conformational flexibility of adjacent aromatic side chains to promote more effect aromatic interactions. In contrast, L310A leads to a modest loss of function. L310 is located just below the extracellular cluster of aromatic residues. In this case, the bulky Leu side chain may be required to fill a void between M4 and M3 created by the adjacent bulky aromatic side chains.

Third, mutation of a Pro residue midway through the M4 α-helix dramatically influences function in both GLIC and ELIC. The Pro residue kinks the M4 α-helix, thus having a dramatic effect on how the M4 α-helix is positioned relative to M1/M3. The dramatic effects that result from removal of this kink further highlights the importance of M4-M1/M3 interactions in folding and function.

The data also show that the role played by aromatic, polar, and non-polar residues is context dependent. For example, three individual charged residues at the M4-M1/M3 interface in GLIC were each mutated to Ala, with two having only a modest effect on function and the third leading to a complete loss of expression and/or activity. While the context dependence is not surprising, the opposite effects that arise when residues involved in even analogous interactions in GLIC and ELIC is surprising. For example, residues involved in a cation-π interaction between M1 and M4 in GLIC contribute positively to gating, while residues involved in the same cation-π interaction in ELIC are detrimental. As noted, mutations of aromatic residues in GLIC overwhelmingly lead to a loss of function, while many of the same mutations in ELIC lead to gains-in-function. In fact, the general trend is that the Ala mutation of any residues directly involved in M4-M1/M3 contacts in GLIC leads a loss in function, while similar mutations in ELIC are easily tolerated and often beneficial.

As noted, the M4-M1/M3 interface in GLIC is packed with aromatic residues that form a complex network of interacting side chains. Each aromatic residue forms at least two π-π and/or CH-π interactions with other aromatic side chains in the network (Figure 3.6 and Table 3.4). There are far fewer aromatic interactions between M4 and M1/M3 in ELIC. The data suggest that the interface in GLIC has evolved to maximize interactions that promote folding and function, and almost any substitution at this interface is detrimental. In contrast, specific contacts at this interface in ELIC seem unimportant for folding and/or function. In fact, the ability to

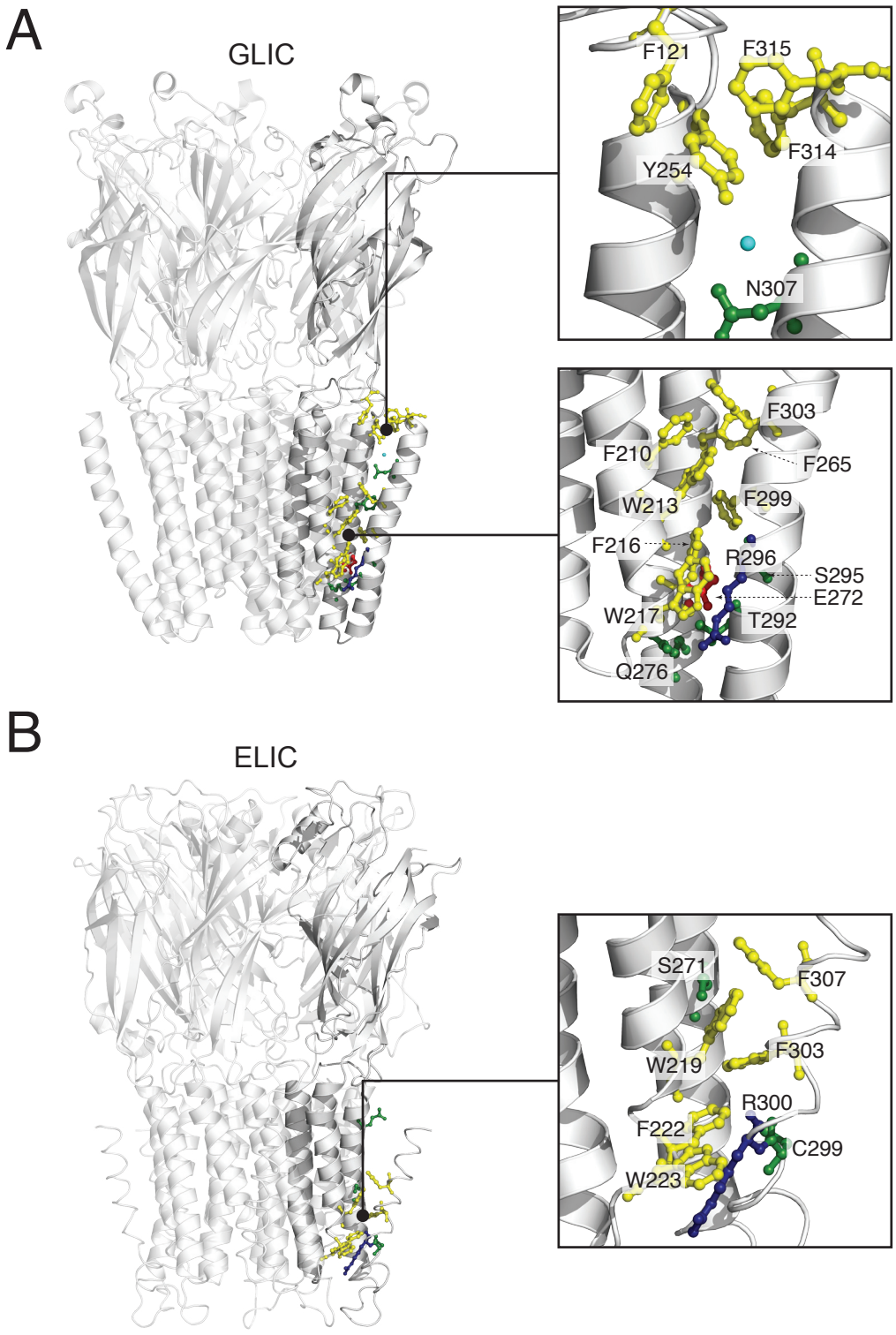


**Figure 3.6. Detailed View of the M4-M1/M3 Interface of GLIC and ELIC.** Structures of GLIC (A, PDB: 4HFI) and ELIC (B, PDB: 2VL0) showing on the left the full structure. The boxes on the right show the highlighted regions of GLIC and ELIC with the residue labels. Residues follow the same colour scheme as Figure 3.1. Note that aliphatic residues are not shown for clarity.

Table 3.4 – Interacting Pairs of Aromatic Residues in GLIC and ELIC

| GLIC | | |
|---|---|---|
| Aromatic Residue | Interacting Partner | Centroid Distance (Å) |
| Extracellular Cluster | | |
| Y254 (M3) | F314 (M4) | 4.8 |
| | F315 (M4) | 5.7 |
| | F121 (β6-β7) | 6.1 |
| F314 (M4) | Y254 (M3) | 4.8 |
| | F315 (M4) | 6.9 |
| | F121 (β6-β7) | 6.2 |
| F315 (M4) | Y254 (M3) | 5.7 |
| | F314 (M4) | 6.9 |
| F121 (β6-β7) | Y254 (M3) | 6.1 |
| | F314 (M4) | 6.2 |
| Cytoplasmic Cluster | | |
| F210 (M1) | W213 (M1) | 5.3 |
| | F303 (M4) | 6.5 |
| W213 (M1) | F210 (M1) | 5.3 |
| | F216 (M1) | 7.2 |
| | F265 (M3) | 6.4 |
| | F299 (M4) | 6.4 |
| | F303 (M4) | 5.7 |
| F216 (M1) | W213 (M1) | 7.2 |
| | F299 (M4) | 4.5 |
| F265 (M3) | W213 (M1) | 6.4 |
| | F299 (M4) | 6.3 |
| | F303 (M4) | 5.3 |
| F299 (M4) | W213 (M1) | 6.4 |
| | F216 (M1) | 4.5 |
| | F265 (M3) | 6.3 |
| F303 (M4) | F210 (M1) | 6.5 |
| | W213 (M1) | 5.7 |
| | F265 (M3) | 5.3 |
| ELIC | | |
| Aromatic Residue | Interacting Partner | Centroid Distance (Å) |
| Cytoplasmic Cluster | | |
| W219 (M1) | F303 (M4) | 6.9 |
| | F307 (M4) | 5.6 |
| F222 (M1) | F303 (M4) | 5.0 |
| F303 (M4) | W219 (M1) | 6.9 |
| | F222 (M1) | 5.0 |
| | F307 (M4) | 7.5 |
| F307 (M4) | W219 (M1) | 5.6 |
| | F303 (M4) | 7.5 |

accommodate mutations at this interface suggest that the helix-helix interactions are weaker and thus perhaps more malleable. Even the mutations of residues involved in similar interactions in GLIC and ELIC have opposite effects on function, as noted extensively above.

In this context, it is interesting to note that many neuronal pLGICs have chemistry at the M4-M1/M3 interfaces similar to GLIC, while others are more similar to ELIC (Figure 3.7 and Figure 3.8). For example, the $GABA_A$, GlyR and GluCl channels each has an extensive network of interacting aromatic residues at the M4-M1/M3 interface, as well as a Pro residue in M4 that kinks the helix to maximize aromatic contacts between the C-terminal half of M4 and the N-terminal half of M3 (Althoff et al., 2014; Huang et al., 2015; Miller and Aricescu, 2014). These pLGICs also have the same cation-$\pi$ interaction linking M1 to M4. Significantly, Ala mutations of residues at the M4-M1/M3 interface in the GlyR typically lead to a similar pattern of phenotypes as in GLIC – predominantly losses of function phenotypes with many mutations leading to a complete loss of expression and/or function (Haeger et al., 2010).

In contrast, other pLGIC subunits, such as the various $\alpha$-subunits of the nAChR and the $5HT3_A$ receptor, have relatively few interacting aromatic residues across the M4-M1/M3 interface (Hassaine et al., 2014; Unwin, 2005). Both the nicotinic subunits and the $5HT3_A$ receptor lack a Pro residue in M4, which alters how M4 interacts with both with M1 and M3, as well as the Arg-Trp cation-$\pi$ interaction between M1 and M4.

Based on the data, I predict that the absence of an extensive aromatic network in the nAChR subunits creates a relatively non-specific M4-M1/M3 interface with weaker contacts, thus rendering helix-helix interactions relatively malleable. This prediction is consistent with the observation that functional nAChRs are still observed when the hydrophobic transmembrane portion of M4 in the $\alpha$-subunit of the *Torpedo*

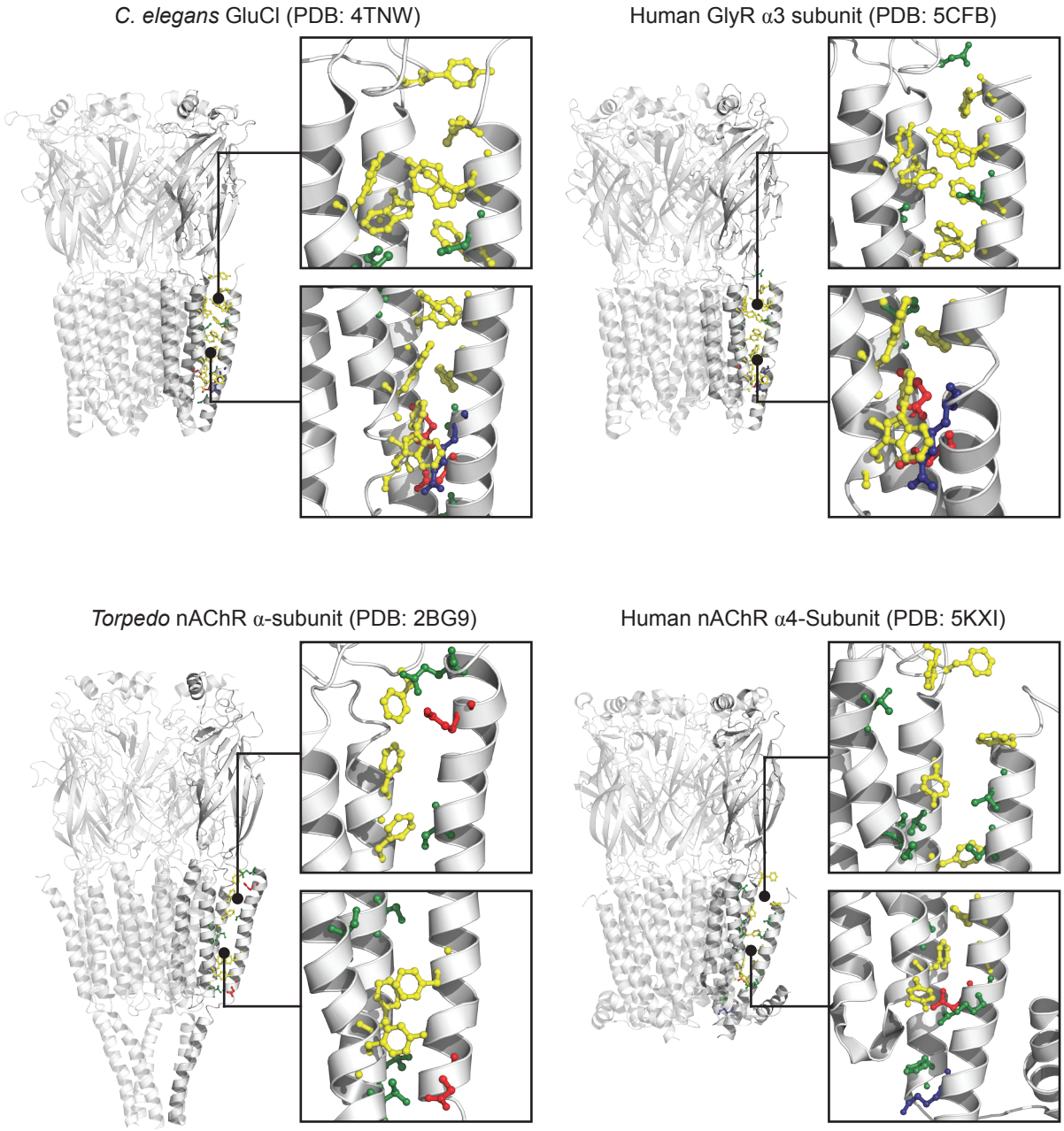


**Figure 3.7: The M4-M1/M3 Interface of Eukaryotic pLGICs.** Structures of GluCl (top left, PDB: 4TNW), GlyR (top right, PDB: 5CFB), nAChR (bottom left, PDB: 2BG9), and α4β2 (bottom right, PDB: 5KXI). Each structure shows a zoomed in region of a single subunit of the M4-M1/M3 interface, focusing on either the extracellular cluster (top box) or cytoplasmic cluster (bottom box). Residues follow the same colour scheme as Figure 3.1.

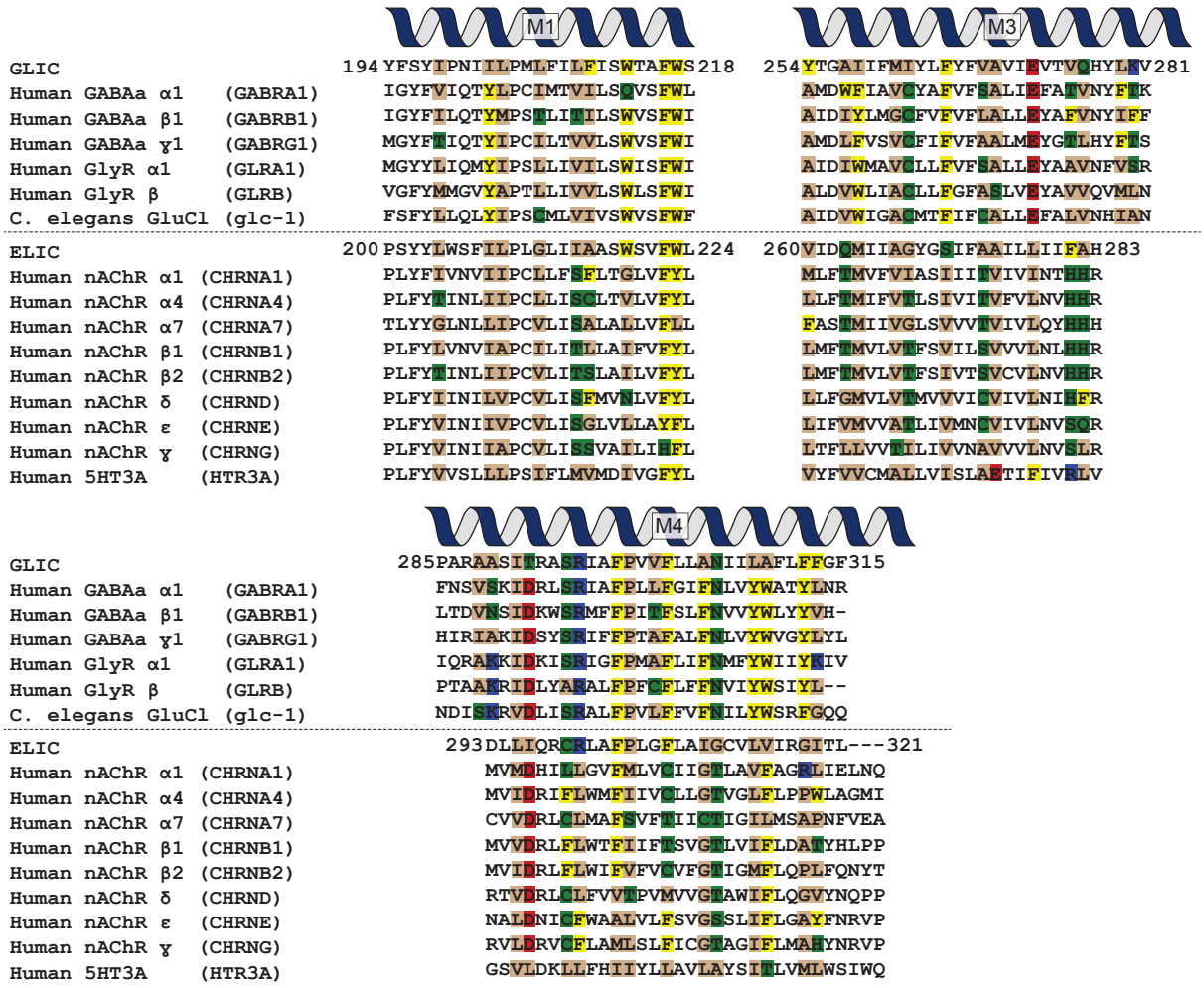


**Figure 3.8: pLGIC M4-M1/M3 sequence alignments.** Sequence alignments of different eukaryotic pLGICs grouped into the two archetypes. Highlighted residues represent those that are most likely to be found in the M4/M1-M3 interface, and follow the same colour scheme as Figure 3.1.

nAChR is replaced by the hydrophobic transmembrane segments of either the vesicular stomatitis virus glycoprotein or of the human interleukin-2 receptor (Tobimatsu et al., 1987). Preliminary studies in my lab show that aromatic to Ala substitutions at this interface in the human muscle-type α-subunit lead to gains of function.

An intriguing question that arises from these two observations is how these distinct chemistries ultimately impact on both folding and function. In the glycine receptor, extensive aromatic contacts between M4 and M1/M3 are required to drive M4 binding to M1/M3 during folding, ultimately leading to pentamer formation (Haeger et al., 2010). Tight interactions between M4 and M1/M3, however, could hinder conformational movements of the helices during both gating and desensitization. On the other hand, although weaker interactions between M4 and M1/M3 could facilitate helix conformational change, they could weaken M4 "binding" to M1/M3 during folding thus hindering pLGIC assembly. In the end, these two archetypal TMDs may strike different balances between high fidelity folding and conformational flexibility in the folded state.

Across a large number of membrane proteins and transmembrane peptides, van der Waals and polar interactions play a major role driving α-helical packing. In transmembrane peptides, van der Waals interactions are often mediated by a leucine-zipper like motif ("small-xxx-small", where small refers to Ala, Gly or Ser), which facilitates tight interactions between adjacent helices, although hydrogen bonding and ion pairs are often essential (Curran and Engelman, 2003; Kleiger et al., 2002). Such motifs are absent in the TMDs of pLGIC. In complex polytopic membrane proteins, the tight packing of α-helices is not as prevalent given the increased number of α-helices and the necessity to allow for the conformational flexibility required to execute function. Hydrogen bonding interactions in polytopic

membrane proteins are also weaker than expected for a hydrophobic transmembrane environment (Choma et al., 2000; Joh et al., 2008; Zhou et al., 2000). This data add to an increasing literature showing that aromatic residues play a dominant role governing helix-helix interactions in both transmembrane peptides and polytopic membrane proteins (Carswell et al., 2015b; Haeger et al., 2010; Henault et al., 2015; Johnson et al., 2007). An intriguing question to address is how these interactions contribute to the strengths of helix-helix associations, while still allowing the conformational flexibility required for pLGIC function.

# Chapter 4

## General Discussion

In this thesis, I focus on the relationship between the structure and function of pLGICs, more specifically on the outermost TMD $\alpha$-helix, M4. Many mechanisms of pLGIC channel folding and function remain to be elucidated, and research maintains that M4 is involved in these processes (daCosta and Baenziger, 2013). Further, M4 may serve a broader function, as it may modulate channel activity (daCosta and Baenziger, 2009). Thus, understanding the role M4 plays in channel structure and function is of interest due to its capacity to support and influence pLGIC function.

The second chapter has remodeled over 30 years of research on nAChR-lipid interactions. A large body of research has suggested that anionic and/or neutral lipids are essential to support a nAChR conformation that responds to agonist binding. I was able to show that in the absence of both anionic and neutral lipids, but in an appropriate physical environment, nAChR function can be achieved. The underlying mechanisms of nAChR-lipid interactions are still a subject of debate, given the lack of detailed structural and functional information. While speculative, the M4-lipid sensor model proposes how lipids could influence channel function (daCosta and Baenziger, 2009). However, there remains a lot of work to be done to further elucidate the mechanisms underlying nAChR-lipid interactions. Single channel electrophysiology is one avenue for potential future work, as giant unilamellar vesicles can be generated from reconstituted nAChR that are suitable for single channel electrophysiology (Kreir, M., et al., 2008). Single channel electrophysiology can give detailed functional information to further assess how the presence of specific lipids influences nAChR function both in the presence and absence of agonist. Another potential future direction includes how the presence of anionic and/or neutral lipids influences nAChR activity in the thicker PC membranes, as it would be interesting to see how a more complex membrane can influence nAChR activity (either via a conformational selective mechanism, kinetic mechanism, or a combination of the two).

The discovery of the prokaryotic pLGICs, GLIC and ELIC, has opened the door to research that is currently not possible with most eukaryotic pLGICs. Chapter 3 focuses on how the chemical interactions found between M4 and M1/M3 influence channel function using GLIC and ELIC as models, as they display different levels of chemical interactions found between M4 and M1/M3. An alanine scan of residues within the M4 and M1/M3 interface demonstrate that GLIC and ELIC have contrasting activities when similar residues are mutated. Most Ala-mutations in GLIC lead to a loss of function, while in ELIC many analogous mutations produce a gain of function. These results suggest that two different archetypes may exist within the pLGIC family. Future directions would include more detailed studies to further demonstrate the differences and similarities of the two archetypes across a variety of different channels. Further, the two archetypes may have differences in how they respond to a variety of TMD allosteric modulators, which include lipids, as weakening or strengthening the interactions between M4 and M1/M3 could impact how TMD allosteric modulators act on the pLGIC. Lastly, the role of lipids remains to be explored in more detail, as the crystal structure of GLIC contains a tightly bound lipid molecule found at the interface between the C-terminal M4 and the ABD. While GLIC and ELIC have been shown in some capacity to have different lipid sensitivities, detrimental mutations in GLIC remain to be explored (Carswell et al., 2015a; Carswell et al., 2015b; Labriola et al., 2013). Loss of function Ala-mutations in GLIC may result in an increased sensitivity to the lipid environment.

In conclusion, the ability of M4 to influence channel function may be a combination of internal (i.e. interactions between M1 and M3) and external (i.e. TMD allosteric modulators, such as lipids) factors. As research moves forward, the role of the pLGIC's M4 $\alpha$-helix serves in structure and function are sure to be elucidated in greater detail.

# Chapter 5

## Annex

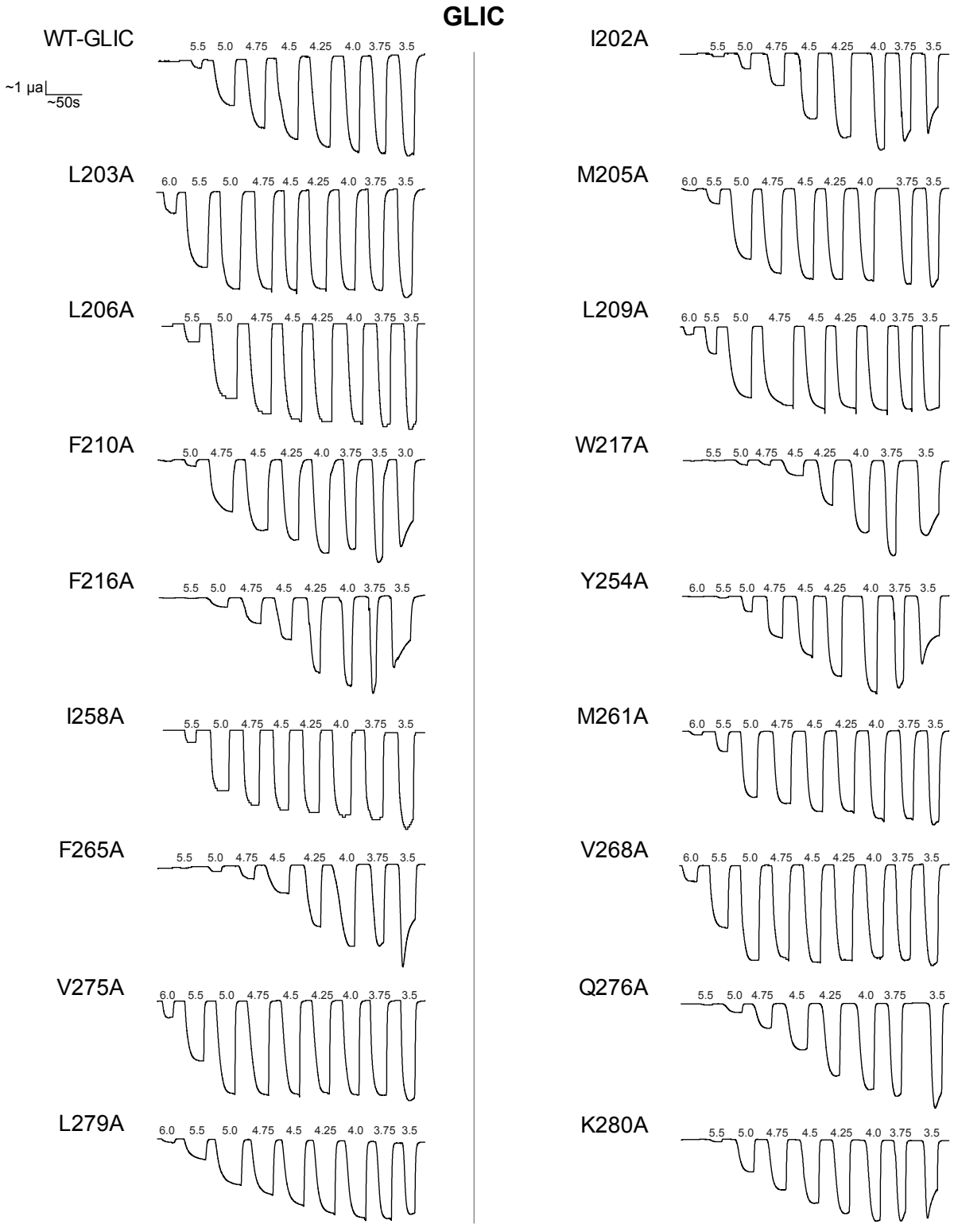


**Figure 5.1. Dose Response Traces for the Single GLIC Ala-Substitutions.** Whole cell electrophysiological traces recorded using two-electrode voltage clamp electrophysiology. Currents were recorded from *Xenopus laevis* oocytes expressing either GLIC response to an increase in proton concentration.

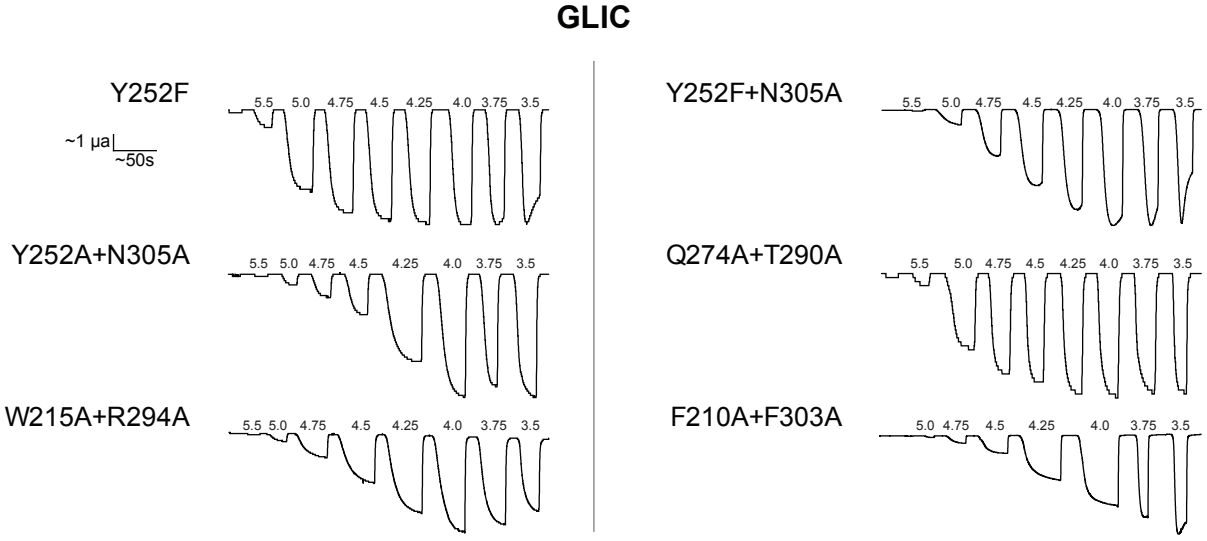


**Figure 5.2. Dose Response Traces for the Double GLIC Ala-Substitutions.** Whole cell electrophysiological traces recorded using two-electrode voltage clamp electrophysiology. Currents were recorded from *Xenopus laevis* oocytes expressing either GLIC response to an increase in proton concentration.

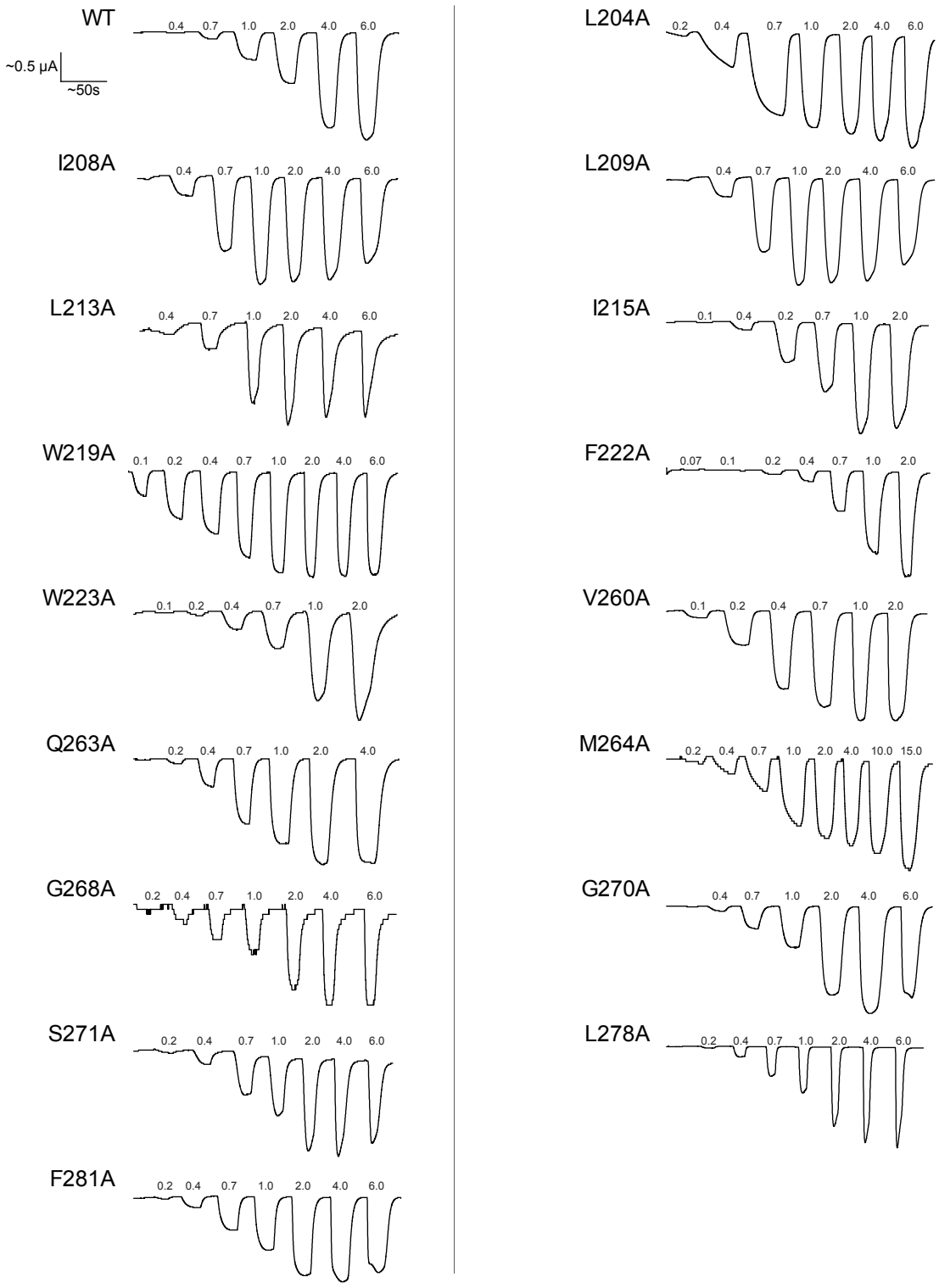


**Figure 5.3. Dose Response Traces for the Single ELIC Ala-Substitutions.** Whole cell electrophysiological traces recorded using two-electrode voltage clamp electrophysiology. Currents were recorded from *Xenopus laevis* oocytes expressing either ELIC response to an increase in cysteamine concentration.

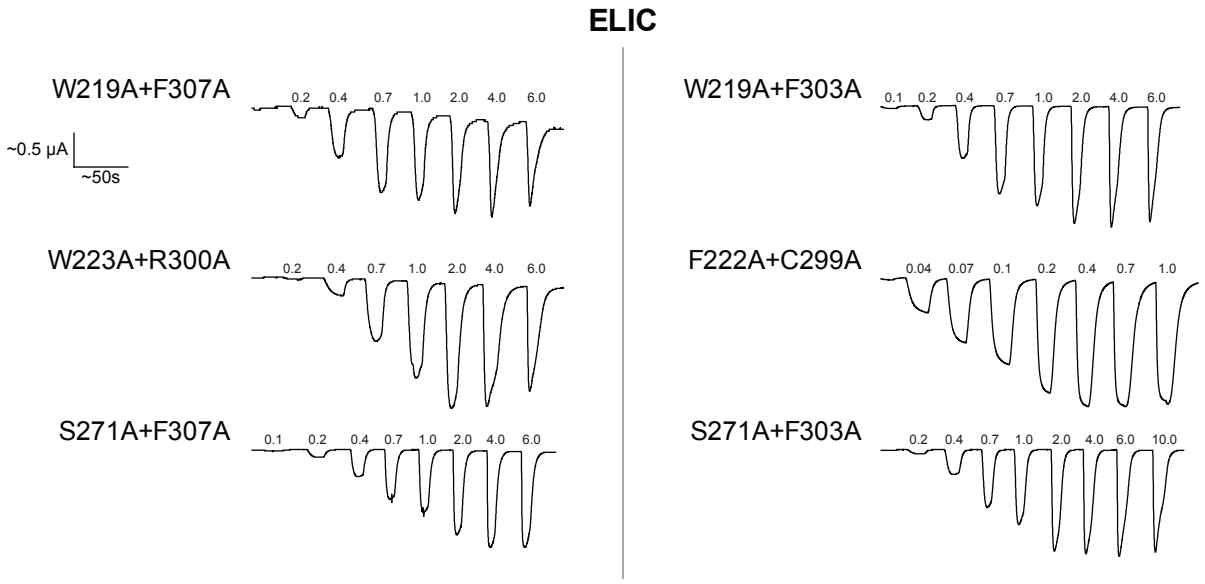


**Figure 5.4. Dose Response Traces for the Double ELIC Ala-Substitutions.** Whole cell electrophysiological traces recorded using two-electrode voltage clamp electrophysiology. Currents were recorded from *Xenopus laevis* oocytes expressing either ELIC response to an increase in cysteamine concentration.

# Chapter 6

## References

Althoff, T., Hibbs, R.E., Banerjee, S., and Gouaux, E. (2014). X-ray structures of GluCl in apo states reveal a gating mechanism of Cys-loop receptors. Nature. 512, 333-337.

Andersen, O.S., and Koeppe, R.E.,2nd. (2007). Bilayer thickness and membrane protein function: an energetic perspective.Annu Rev Biophys Biomol Struct. 36, 107-130.

Antollini, S.S., and Barrantes, F.J. (1998). Disclosure of discrete sites for phospholipid and sterols at the protein-lipid interface in native acetylcholine receptor-rich membrane. Biochemistry. 37, 16653-16662.

Baenziger, J.E., and Methot, N. (1995). Fourier transform infrared and hydrogen/deuterium exchange reveal an exchange-resistant core of alpha-helical peptide hydrogens in the nicotinic acetylcholine receptor. J Biol Chem. 270, 29129-29137.

Baenziger, J.E., Miller, K.W., and Rothschild, K.J. (1993). Fourier transform infrared difference spectroscopy of the nicotinic acetylcholine receptor: evidence for specific protein structural changes upon desensitization. Biochemistry. 32, 5448-5454.

Baenziger, J.E., Morris, M.L., Darsaut, T.E., and Ryan, S.E. (2000). Effect of membrane lipid composition on the conformational equilibria of the nicotinic acetylcholine receptor. J Biol Chem. 275, 777-784.

Baier, C.J., Gallegos, C.E., Levi, V., and Barrantes, F.J. (2010). Cholesterol modulation of nicotinic acetylcholine receptor surface mobility. Eur Biophys J. 39, 213-227.

Barrantes, F.J. (2004). Structural basis for lipid modulation of nicotinic acetylcholine receptor function. Brain Res Brain Res Rev. 47, 71-95.

Biedermannova, L., E. Riley, K., Berka, K., Hobza, P., and Vondrasek, J. (2008). Another role of proline: Stabilization interactions in proteins and protein complexes concerning proline and tryptophane. Phys. Chem. Chem. Phys. 10, 6350-6359.

Bocquet, N., Nury, H., Baaden, M., Le Poupon, C., Changeux, J.-P., Delarue, M., and Corringer, P.-J. (2009). X-ray structure of a pentameric ligand-gated ion channel in an apparently open conformation. Nature. 457, 111-114.

Borroni, V., and Barrantes, F.J. (2011). Cholesterol modulates the rate and mechanism of acetylcholine receptor internalization. J Biol Chem. 286, 17122-17132.

Bouzat, C., Gumilar, F., Spitzmaul, G., Wang, H.L., Rayes, D., Hansen, S.B., Taylor, P., and Sine, S.M. (2004). Coupling of agonist binding to channel gating in an ACh-binding protein linked to an ion channel. Nature. 430, 896-900.

Bouzat, C., Roccamo, A.M., Garbus, I., and Barrantes, F.J. (1998). Mutations at lipid-exposed residues of the acetylcholine receptor affect its gating kinetics. Mol Pharmacol. 54, 146-153.

Boyd, N.D., and Cohen, J.B. (1980). Kinetics of binding of [3H]acetylcholine to Torpedo postsynaptic membranes: association and dissociation rate constants by rapid mixing and ultrafiltration. Biochemistry. 19, 5353-5358.

Brannigan, G., Henin, J., Law, R., Eckenhoff, R., and Klein, M.L. (2008). Embedded cholesterol in the nicotinic acetylcholine receptor. Proc Natl Acad Sci U S A.105, 14418-14423.

Burley, S.K., and Petsko, G.A. (1985). Aromatic-aromatic interaction: a mechanism of protein structure stabilization. Science. 229, 23-28.

Carswell, C.L., Sun, J., and Baenziger, J.E. (2015a). Intramembrane aromatic interactions influence the lipid sensitivities of pentameric ligand-gated ion channels. Journal of Biological Chemistry. 290, 2496-507.

Carswell, C.L., Henault, C.M., Murlidaran, S., Therien, J.P., Juranka, P.F., Surujballi, J.A., Brannigan, G., and Baenziger, J.E. (2015b). Role of the Fourth Transmembrane alpha Helix in the Allosteric Modulation of Pentameric Ligand-Gated Ion Channels. Structure. 23, 1655-1664.

Celie, P.H., van Rossum-Fikkert, S.E., van Dijk, W.J., Brejc, K., Smit, A.B., and Sixma, T.K. (2004). Nicotine and carbamylcholine binding to nicotinic acetylcholine receptors as studied in AChBP crystal structures. Neuron. 41, 907-914.

Changeux, J.P., Kasai, M., and Lee, C.Y. (1970). Use of a snake venom toxin to characterize the cholinergic receptor protein. Proc Natl Acad Sci U S A. 67, 1241-127.

Choma, C., Gratkowski, H., Lear, J.D., and DeGrado, W.F. (2000). Asparagine-mediated self-association of a model transmembrane helix. Nat. Struct. Biol. 7, 161-166.

Curran, A.R., and Engelman, D.M. (2003). Sequence motifs, polar interactions and conformational changes in helical membrane proteins. Curr. Opin. Struct. Biol. 13, 412-417.

Cymer, F., Von Heijne, G., and White, S.H. (2015). Mechanisms of integral membrane protein insertion and folding. J. Mol. Biol. 427, 999-1022.

Cymes, G.D., and Grosman, C. (2008). Pore-opening mechanism of the nicotinic acetylcholine receptor evinced by proton transfer. Nat Struct Mol Biol. 15, 389-396.

daCosta, C.J., and Baenziger, J.E. (2013). Gating of pentameric ligand-gated ion channels: structural insights and ambiguities. Structure. 21, 1271-1283.

daCosta, C.J., Dey, L., Therien, J.P.D., and Baenziger, J.E. (2013). A distinct mechanism for activating uncoupled nicotinic acetylcholine receptors. Nat Chem Biol. 9, 701-707.

daCosta, C.J., Michel Sturgeon, R., Hamouda, A.K., Blanton, M.P., and Baenziger, J.E. (2011). Structural characterization and agonist binding to human a4b2 nicotinic receptors. Biochem Biophys Res Commun. 407, 456-460.

daCosta, C.J., Ogrel, A.A., McCardy, E.A., Blanton, M.P., and Baenziger, J.E. (2002). Lipid-protein interactions at the nicotinic acetylcholine receptor. A functional coupling between nicotinic receptors and phosphatidic acid-containing lipid bilayers. J Biol Chem. 277, 201-208.

daCosta, C.J., Wagg, I.D., McKay, M.E., and Baenziger, J.E. (2004). Phosphatidic acid and phosphatidylserine have distinct structural and functional interactions with the nicotinic acetylcholine receptor. J Biol Chem. 279, 14967-14974.

daCosta, C.J.B., and Baenziger, J.E. (2009). A lipid-dependent uncoupled conformation of the acetylcholine receptor. J. Biol. Chem. 284, 17819-17825.

daCosta, C.J.B., Medaglia, S.A., Lavigne, N., Wang, S., Carswell, C.L., and Baenzinger, J.E. (2009). Anionic lipids allosterically modulate multiple nicotinic acetylcholine receptor conformational equilibria. J. Biol. Chem. 284, 33841-33849.

Daeffler, K.N.-., Lester, H.A., and Dougherty, D.A. (2012). Functionally important aromatic-aromatic and sulfur-p interactions in the D2 dopamine receptor. J. Am. Chem. Soc. 134, 14890-14896.

de Almeida, R.F., Loura, L.M., Prieto, M., Watts, A., Fedorov, A., and Barrantes, F.J. (2006). Structure and dynamics of the gammaM4 transmembrane domain of the acetylcholine receptor in lipid bilayers: insights into receptor assembly and function. Mol Membr Biol. 23, 305-315.

de Planque, M.R., and Killian, J.A. (2003). Protein-lipid interactions studied with designed transmembrane peptides: role of hydrophobic matching and interfacial anchoring. Mol Membr Biol. 20, 271-284.

Du, J., Lu, W., Wu, S., Cheng, Y., and Gouaux, E. (2015). Glycine receptor mechanism elucidated by electron cryo-microscopy. Nature. 526, 224-229.

Duret, G., Van Renterghem, C., Weng, Y., Prevost, M., Moraga-Cid, G., Huon, C., Sonner, J.M., and Corringer, P.J. (2011). Functional prokaryotic-eukaryotic chimera from the pentameric ligand-gated ion channel family. Proc Natl Acad Sci U S A. 108, 12143-12148.

Epstein, M., and Racker, E. (1978). Reconstitution of carbamylcholine-dependent sodium ion flux and desensitization of the acetylcholine receptor from Torpedo californica. J Biol Chem. 253, 6660-6662.

Fink, A., Sal-Man, N., Gerber, D., and Shai, Y. (2012). Transmembrane domains interactions within the membrane milieu: principles, advances and challenges. Biochim. Biophys. Acta 1818, 974-983.

Fong, T.M., and McNamee, M.G. (1986). Correlation between acetylcholine receptor function and structural properties of membranes. Biochemistry. 25, 830-40.

Froehner, S.C. (1993). Regulation of ion channel distribution at synapses. Annu. Rev. Neurosci. 16, 347-368.

Gonzalez-Gutierrez, G., Lukk, T., Agarwal, V., Papke, D., Nair, S.K., and Grosman, C. (2012). Mutations that stabilize the open state of the Erwinia chrisanthemi ligand-gated ion channel fail to change the conformation of the pore domain in crystals. Proc Natl Acad Sci U S A. 109, 6331-6336.

Gonzalez-Ros, J.M., Llanillo, M., Paraschos, A., and Martinez-Carrion, M. (1982). Lipid environment of acetylcholine receptor from Torpedo californica. Biochemistry. 21, 3467-3474.

Govind, A.P., Walsh, H., and Green, W.N. (2012). Nicotine-induced upregulation of native neuronal nicotinic receptors is caused by multiple mechanisms. J. Neurosci. 32, 2227-2238.

Grutter, T., de Carvalho, L.P., Dufresne, V., Taly, A., Edelstein, S.J., and Changeux, J.P. (2005). Molecular tuning of fast gating in pentameric ligand-gated ion channels. Proc Natl Acad Sci U S A. 102, 18207-18212.

Haeger, S., Kuzmin, D., Detro-Dassen, S., Lang, N., Kilb, M., Tsetlin, V., Betz, H., Laube, B., and Schmalzing, G. (2010). An intramembrane aromatic network determines pentameric assembly of Cys-loop receptors. Nature Structural and Molecular Biology. 17, 90-98.

Hansen, S.B., Sulzenbacher, G., Huxford, T., Marchot, P., Taylor, P., and Bourne, Y. (2005). Structures of Aplysia AChBP complexes with nicotinic agonists and antagonists reveal distinctive binding interfaces and conformations. EMBO J. 24, 3635-3646.

Hassaine, G., Deluz, C., Grasso, L., Wyss, R., Tol, M.B., Hovius, R., Graff, A., Stahlberg, H., Tomizaki, T., Desmyter, A., et al. (2014). X-ray structure of the mouse serotonin 5-HT3 receptor. Nature. 512, 276-281.

Henault, C.M., Juranka, P.F., and Baenziger, J.E. (2015). The M4 Transmembrane alpha-Helix Contributes Differently to Both the Maturation and Function of Two Prokaryotic Pentameric Ligand-gated Ion Channels. J. Biol. Chem. 290, 25118-25128.

Hénault, C.M., Sun, J., Therien, J.P.D., DaCosta, C.J.B., Carswell, C.L., Labriola, J.M., Juranka, P.F., and Baenziger, J.E. (2015). The role of the M4 lipid-sensor in the folding, trafficking, and allosteric modulation of nicotinic acetylcholine receptors.

Neuropharmacology. 96, 157-168.

Herz, J.M., Johnson, D.A., and Taylor, P. (1987). Interaction of noncompetitive inhibitors with the acetylcholine receptor. The site specificity and spectroscopic properties of ethidium binding. J Biol Chem. 262, 7238-7247.

Herz, J.M., Kolb, S.J., Erlinger, T., and Schmid, E. (1991). Channel permeant cations compete selectively with noncompetitive inhibitors of the nicotinic acetylcholine receptor. J Biol Chem. 266, 16691-16698.

Hibbs, R.E., and Gouaux, E. (2011). Principles of activation and permeation in an anion-selective Cys-loop receptor. Nature. 474, 54-60.

Hilf, R.J., and Dutzler, R. (2009). Structure of a potentially open state of a proton-activated pentameric ligand-gated ion channel. Nature. 457, 115-118.

Hilf, R.J., and Dutzler, R. (2008). X-ray structure of a prokaryotic pentameric ligand-gated ion channel. Nature. 452, 375-379.

Hille, B. (2001). Ion Channels of Excitable Membranes (Sunderland, Massachusetts U.S.A.: Sinauer Associates, Inc).

Holt, A., and Killian, J.A. (2010). Orientation and dynamics of transmembrane peptides: the power of simple models. Eur Biophys J. 39, 609-621.

Huang, L.Y., Catterall, W.A., and Ehrenstein, G. (1978). Selectivity of cations and nonelectrolytes for acetylcholine-activated channels in cultured muscle cells. J Gen Physiol. 71, 397-410.

Huang, X., Chen, H., Michelsen, K., Schneider, S., and Shaffer, P.L. (2015). Crystal structure of human glycine receptor-a3 bound to antagonist strychnine. Nature. 526, 277-280.

Jensen, M.O., and Mouritsen, O.G. (2004). Lipids do influence protein function-the hydrophobic matching hypothesis revisited. Biochim Biophys Acta. 1666, 205-226.

Joh, N.H., Min, A., Faham, S., Whitelegge, J.P., Yang, D., Woods Jr., V.L., and Bowie, J.U. (2008). Modest stabilization by most hydrogen-bonded side-chain interactions in membrane proteins. Nature. 453, 1266-1270.

Johnson, R.M., Hecht, K., and Deber, C.M. (2007). Aromatic and cation-p interactions enhance helix-helix association in a membrane environment. Biochemistry. 46, 9208-9214.

Jones, O.T., and McNamee, M.G. (1988). Annular and nonannular binding sites for cholesterol associated with the nicotinic acetylcholine receptor. Biochemistry. 27, 2364-2374.

Kleiger, G., Grothe, R., Mallick, P., and Eisenberg, D. (2002). GXXXG and AXXXA: Common a-helical interaction motifs in proteins, particularly in extremophiles.

Biochemistry. 41, 5990-5997.

Kreir, M., Farre, C., Beckler, M., George, M., Fertig, N. (2008). Rapid screening of membrane protein activity: electrophysiological analysis of OmpF reconstituted in proteoliposomes. Lab Chip. 8(4), 587-95.

Kucerka, N., Tristram-Nagle, S., and Nagle, J.F. (2005). Structure of fully hydrated fluid phase lipid bilayers with monounsaturated chains. J Membr Biol. 208, 193-202.

Kwolek, U., Kulig, W., Wydro, P., Nowakowska, M., Rog, T., and Kepczynski, M. (2015). Effect of Phosphatidic Acid on Biomembrane: Experimental and Molecular Dynamics Simulations Study. J Phys Chem B. 119, 10042-10051.

Labriola, J.M., Pandhare, A., Jansen, M., Blanton, M.P., Corringer, P.-., and Baenziger, J.E. (2013). Structural sensitivity of a prokaryotic pentameric ligand-gated ion channel to its membrane environment. J. Biol. Chem. 288, 11294-11303.

Laitko, U., Juranka, P.F., and Morris, C.E. (2006). Membrane stretch slows the concerted step prior to opening in a Kv channel. J. Gen. Physiol. 127, 687-701.

Lee, A.G. (2004). How lipids affect the activities of integral membrane proteins. Biochim Biophys Acta. 1666, 62-87.

Lee, W.Y., and Sine, S.M. (2005). Principal pathway coupling agonist binding to channel gating in nicotinic receptors. Nature. 438, 243-247.

Lester, H.A., Dibas, M.I., Dahan, D.S., Leite, J.F., and Dougherty, D.A. (2004). Cys-loop receptors: new twists and turns. Trends Neurosci. 27, 329-336.

Li, L., Lee, Y.H., Pappone, P., Palma, A., and McNamee, M.G. (1992). Site-specific mutations of nicotinic acetylcholine receptor at the lipid-protein interface dramatically alter ion channel gating. Biophys J. 62, 61-63.

Li, P., and Steinbach, J.H. (2010). The neuronal nicotinic alpha4beta2 receptor has a high maximal probability of being open. Br J Pharmacol. 160, 1906-1915.

Lummis, S.C., Beene, D.L., Lee, L.W., Lester, H.A., Broadhurst, R.W., and Dougherty, D.A. (2005). Cis-trans isomerization at a proline opens the pore of a neurotransmitter-gated ion channel. Nature. 438, 248-252.

Lundbaek, J.A., Andersen, O.S., Werge, T., and Nielsen, C. (2003). Cholesterol-induced protein sorting: an analysis of energetic feasibility. Biophys J. 84, 2080-2089.

Methot, N., Demers, C.N., and Baenziger, J.E. (1995). Structure of both the ligand- and lipid-dependent channel-inactive states of the nicotinic acetylcholine receptor probed by FTIR spectroscopy and hydrogen exchange. Biochemistry. 34, 15142-15149.

Miller, P.S., and Aricescu, A.R. (2014). Crystal structure of a human GABAA

receptor. Nature. 512, 270-275.

Mishina, M., Takai, T., Imoto, K., Noda, M., Takahashi, T., Numa, S., Methfessel, C., and Sakmann, B. (1986). Molecular distinction between fetal and adult forms of muscle acetylcholine receptor. Nature. 321, 406-411.

O'Brien, R., Eldefraw, A., and Eldefraw, M. (1972). Isolation of Acetylcholine Receptors. Annu. Rev. Pharmacol. 12, 19.

Ochoa, E.L., Dalziel, A.W., and McNamee, M.G. (1983). Reconstitution of acetylcholine receptor function in lipid vesicles of defined composition. Biochim Biophys Acta. 727, 151-162.

Ramadurai, S., Holt, A., Schafer, L.V., Krasnikov, V.V., Rijkers, D.T.S., Marrink, S.J., Killian, J.A., and Poolman, B. (2010). Influence of hydrophobic mismatch and amino acid composition on the lateral diffusion of transmembrane peptides. Biophys. J. 99, 1447-1454.

Rawicz, W., Olbrich, K.C., McIntosh, T., Needham, D., and Evans, E. (2000). Effect of chain length and unsaturation on elasticity of lipid bilayers. Biophys J. 79, 328-339.

Rienzo, M., Lummis, S.C.R., and Dougherty, D.A. (2014). Structural requirements in the transmembrane domain of GLIC revealed by incorporation of noncanonical histidine analogs. Chem. Biol. 21, 1700-1706.

Ryan, S.E., and Baenziger, J.E. (1999). A structure-based approach to nicotinic receptor pharmacology. Mol Pharmacol. 55, 348-55.

Ryan, S.E., Demers, C.N., Chew, J.P., and Baenziger, J.E. (1996). Structural effects of neutral and anionic lipids on the nicotinic acetylcholine receptor. An infrared difference spectroscopy study. J Biol Chem. 271, 24590-24597.

Ryan, S.E., Hill, D.G., and Baenziger, J.E. (2002). Dissecting the chemistry of nicotinic receptor-ligand interactions with infrared difference spectroscopy. J Biol Chem. 277, 10420-10426.

Sakmann, B., and Brenner, H.R. (1978). Change in synaptic channel gating during neuromuscular development. Nature. 276, 401-402.

Sauguet, L., Poitevin, F., Murail, S., Van Renterghem, C., Moraga-Cid, G., Malherbe, L., Thompson, A.W., Koehl, P., Corringer, P.J., Baaden, M., and Delarue, M. (2013). Structural basis for ion permeation mechanism in pentameric ligand-gated ion channels. EMBO J. 32(5), 728-741.

Schiebler, W., and Hucho, F. (1978). Membranes rich in acetylcholine receptor: characterization and reconstitution to excitable membranes from exogenous lipids. Eur J Biochem. 85, 55-63.

Shen, X.M., Deymeer, F., Sine, S.M., and Engel, A.G. (2006). Slow-channel mutation in acetylcholine receptor alphaM4 domain and its efficient knockdown. Ann Neurol. 60, 128-136.

Sine, S.M., and Engel, A.G. (2006). Recent advances in Cys-loop receptor structure and function. Nature. 440, 448-455.

Smit, A.B., Brejc, K., Syed, N., and Sixma, T.K. (2003). Structure and function of AChBP, homologue of the ligand-binding domain of the nicotinic acetylcholine receptor. Ann N Y Acad Sci. 998, 81-92.

Smit, A.B., Syed, N.I., Schaap, D., van Minnen, J., Klumperman, J., Kits, K.S., Lodder, H., van der Schors, R. C., van Elk, R., Sorgedrager, B., et al. (2001). A glia-derived acetylcholine-binding protein that modulates synaptic transmission. Nature. 411, 261-268.

Sobel, A., Weber, M., and Changeux, J.P. (1977). Large-scale purification of the acetylcholine-receptor protein in its membrane-bound and detergent-extracted forms from Torpedo marmorata electric organ. Eur J Biochem. 80, 215-224.

Sturgeon, R.M., and Baenziger, J.E. (2010). Cations mediate interactions between the nicotinic acetylcholine receptor and anionic lipids. Biophys J. 98, 989-998.

Sunshine, C., and McNamee, M.G. (1994). Lipid modulation of nicotinic acetylcholine receptor function: the role of membrane lipid composition and fluidity. Biochim Biophys Acta. 1191, 59-64.

Sunshine, C., and McNamee, M.G. (1992). Lipid modulation of nicotinic acetylcholine receptor function: the role of neutral and negatively charged lipids. Biochim Biophys Acta. 1108, 240-246.

Tamamizu, S., Guzman, G.R., Santiago, J., Rojas, L.V., McNamee, M.G., and Lasalde-Dominicci, J.A. (2000). Functional effects of periodic tryptophan substitutions in the alpha M4 transmembrane domain of the Torpedo californica nicotinic acetylcholine receptor. Biochemistry. 39, 4666-4673.

Tasneem, A., Iyer, L.M., Jakobsson, E., and Aravind, L. (2005). Identification of the prokaryotic ligand-gated ion channels and their implications for the mechanisms and origins of animal Cys-loop ion channels. Genome Biol. 6, R4.

Tobimatsu, T., Fujita, Y., Fukuda, K., Tanaka, K., Mori, Y., Konno, T., Mishina, M., and Numa, S. (1987). Effects of substitution of putative transmembrane segments on nicotinic acetylcholine receptor function. FEBS Lett. 222, 56-62.

Unwin, N. (2005). Refined structure of the nicotinic acetylcholine receptor at 4 Åresolution. J. Mol. Biol. 346, 967-989.

Vallejo, Y.F., Buisson, B., Bertrand, D., and Green, W.N. (2005). Chronic nicotine

exposure upregulates nicotinic receptors by a novel mechanism. J Neurosci. 25, 5563-5572.

Wang, H.L., Cheng, X., and Sine, S.M. (2012). Intramembrane proton binding site linked to activation of bacterial pentameric ion channel. J Biol Chem. 287, 6482-6489.

Waters, M.L. (2002). Aromatic interactions in model systems. Curr. Opin. Chem. Biol. 6, 736-741.

Weill, C.L., McNamee, M.G., and Karlin, A. (1974). Affinity-labeling of purified acetylcholine receptor from Torpedo californica. Biochem Biophys Res Commun. 61, 997-1003.

Wootten, D., Simms, J., Miller, L.J., Christopoulos, A., and Sexton, P.M. (2013). Polar transmembrane interactions drive formation of ligand-specific and signal pathway-biased family B G protein-coupled receptor conformations. Proc. Natl. Acad. Sci. U. S. A. 110, 5211-5216.

Xiu, X., Hanek, A.P., Wang, J., Lester, H.A., and Dougherty, D.A. (2005). A unified view of the role of electrostatic interactions in modulating the gating of Cys loop receptors. J. Biol. Chem. 280, 41655-41666.

Zhou, F.X., Cocco, M.J., Russ, W.P., Brunger, A.T., and Engelman, D.M. (2000). Interhelical hydrogen bonding drives strong interactions in membrane proteins. Nat. Struct. Biol. 7, 154-160.

Zimmermann, I., and Dutzler, R. (2011). Ligand activation of the prokaryotic pentameric ligand-gated ion channel ELIC. PLoS Biol. 9, e1001101.

# Chapter 7

## Curriculum Vitae

## Education

| | |
|---|---|
| Fall 2012-<br>Fall 2016 | Master's in Science, Biochemistry<br>University of Ottawa – Ottawa, Ontario, Canada |
| Fall 2008-<br>Winter 2012 | Honour's Bachelor of Science, with Specialization in Biochemistry<br>University of Ottawa – Ottawa, Ontario, Canada |

## Research Experience

| | |
|---|---|
| Fall 2012-<br>Fall 2016 | Master's in Science: Biochemistry<br>Thesis Topic: The Role of Transmembrane Domain Inter-Helix Chemistry in the Function of pLGICs |
| Summer<br>2012 | Summer Research Student<br>Continuation of 2011 Summer Research Project |
| Fall 2011-<br>Winter 2012 | Undergraduate Honour's Research Project<br>Continuation of 2011 Summer Research Project |
| Summer<br>2011 | Summer Research Student<br>Research Project: Conformational Transition-State Stabilization of the Acetylcholine Receptor by Membrane Hydrophobic Thickness. |

## Scholarships and Awards

| | |
|---|---|
| 2014 | 1st place Protein Engineering Canada Poster Presentation |
| 2013 | University of Ottawa – Biochemistry Travel Award (Philadelphia, PA**)** |
| 2013 | University of Ottawa – Faculty of Graduate and Postdoctoral Studies Conference Travel Grant (Philadelphia, PA**)** |
| 2008 | University of Ottawa Admission Scholarship |

## Publications

Papers published or *in press* in refereed journals:

- Baenziger, J.E., Domville, J.A., and **Therien, J.P.D.** (2016). *The role of cholesterol in activation and coupling of nicotinic acetylcholine receptors.* Current topics in membranes. In press.

- Carswell, C.L., Hénault, C.M., Murlidaran, S., **Therien, J.P.D.**, Juranka, P.J., Surujballi, J.A., Brannigan, G., and Baenziger, J.E. (2015). *Role of the transmembrane α-helix, M4, in the potentiation of pentameric ligand-gated ion channels.* Structure. Sep 1;23(9):1655-64.

- Baenziger, J.E., Hénault, C.M., **Therien, J.P.D.**, and Sun, J. (2015). *Nicotinic acetylcholine receptor-lipid interactions: mechanistic insight and biological function.* Biochim Biophys Acta. Sep;1848(9):1806-17.

- Hénault, C.M., Sun, J., **Therien, J.P.D.**, daCosta, C.J.B., Carswell, C.L., Labriola, J., Juranka, P.J., and Baenziger, J.E. (2015). *The role of the M4 lipid-sensor in the folding, trafficking, and allosteric modulation of nicotinic acetylcholine receptors.* Neuropharm. Sep;96(Pt B):157-68.

- daCosta, C.J.B., Dey, L., **Therien, J.P.D.**, and Baenziger, J.E. (2013). *A distinct mechanisms for activating uncoupled nicotinic acetylcholine receptors.* Nat Chem Biol. Nov;9(11):701-7.

Papers in preparation:

- **Therien, J.P.D.**, and Baenziger, J.E. (2016). *Two distinct transmembrane domain archetypes for pentameric ligand-gated ion channels.* In preparation.

**Non Refereed Contributions**

- **J.P. Daniel Therien** and John E. Baenziger. *The Role of Transmembrane Domain Inter-Helix Chemistry in the Function of Pentameric Ligand-Gated Ion Channels.* University of Ottawa BMI seminar day. Ottawa, Ontario, Canada. March 8th, 2016 – Seminar.

- **J.P. Daniel Therien,** Camille M. Hénault, Peter F. Juranka, Julian A. Surujballi, and John E. Baenziger. *The role of intramembrane interactions in the gating of a pentameric ligand-gated ion channel.* Biophysical Society of Canada 1st meeting. Waterloo, Ontario, Canada. June 18th, 2015 – Poster

- **J.P. Daniel Therien,** Peter F. Juranka, and John E. Baenziger. *The role of intramembrane chemistry in the gating of a pentameric ligand-gated ion channel.* University of Ottawa BMI graduate poster day. Ottawa, Ontario, Canada. May 14th, 2015 – Poster

- **J.P. Daniel Therien,** Peter F. Juranka, and John E. Baenziger. *The role of intramembrane chemistry in the gating of a pentameric ligand-gated ion channel.* Protein Engineering Canada. Ottawa, Ontario, Canada. June 21st, 2014 – Poster

- **J.P. Daniel Therien**, Peter F. Juranka, and John E. Baenziger. *The role of intramembrane chemistry in the gating of a pentameric ligand-gated ion channel.* University of Ottawa BMI seminar day. Ottawa, Ontario, Canada. March 7th, 2014 – Seminar.

- **J.P. Daniel Therien**, Lopamudra Dey, Corrie J.B. daCosta, and John E. Baenziger. *A Novel mechanism for activating uncoupled nicotinic acetylcholine receptors.* University of Ottawa BMI graduate poster day. Ottawa, Ontario, Canada. May 16th, 2013 – Poster.

- **J.P. Daniel Therien**, Lopamudra Dey, Corrie J.B. daCosta, and John E. Baenziger. *Effect of membrane hydrophobic thickness on the uncoupling of binding/gating in the nicotinic acetylcholine receptor.* Biophysical Society 57th Annual Meeting. Philadelphia, Pennsylvania, USA. February 6th, 2013 – Poster.

- **J.P. Daniel Therien**, and John E. Baenziger. *Conformational transition-state stabilization of the acetylcholine receptor by membrane hydrophobic thickness.* University of Ottawa Undergraduate Research Poster Day. Ottawa, Ontario, Canada. March 23rd, 2012 – Poster.

## Teaching Experience

| | |
|---|---|
| Fall 2014 | University of Ottawa – Teaching Assistant for CHM1511/1711 Labs – Demonstrator and Evaluator |
| Winter 2014 | University of Ottawa – Teaching Assistant for BCH2333/2733 Labs – Demonstrator and Evaluator |

## Graduate Coursework

| | |
|---|---|
| Fall 2013 | BCH8101: Physical and Chemical Methods in Biochemistry |
| Winter 2013 | CMM8350: Ion Channels – Cellular and Molecular Aspects of Membrane Function |

## Skills

### Computer Programs

- MS Office (Word/Excel/PowerPoint) (Advanced)
- PyMol (Advanced)
- GraphPad – Prism (Advanced)
- Adobe Photoshop/Illustrator (Intermediate)
- BLAST/ExPASy (Intermediate)

### Lab Techniques

- PCR/Mutagenesis/Ligation
- DNA and cRNA preparation
- Molecular Cloning
- Protein Purification
- Agarose and Acrylamide Gel Electrophoresis
- Electrophysiology
- FT-IR
- Fluorescence Spectroscopy
- TLC/Lipid Extraction